Unclassified

$\mathcal{M}c$

TURBULENT MIXING AND BURNING OF COAXIAL STREAMS INSIDE A DUCT OF ARBITRARY SHAPE

C. E. Peters

ARO, Inc.

January 1969

ROCKET TEST FACILITY
ARNOLD ENGINEERING DEVELOPMENT CENTER
AIR FORCE SYSTEMS COMMAND
ARNOLD AIR FORCE STATION, TENNESSEE

Unclassified

NOTICES

TURBULENT MIXING AND BURNING OF COAXIAL STREAMS INSIDE A DUCT OF ARBITRARY SHAPE

C. E. Peters

ARO, Inc.

FOREWORD

The research reported herein was jointly sponsored by the Arnold Engineering Development Center (AEDC), Air Force Systems Command (AFSC), Arnold Air Force Station, Tennessee, under Program Element 65402234 and by the Air Force Office of Aerospace Research, Arlington, Virginia, under Project 6952, Program Element 6144501F.

The research was conducted by ARO, Inc. (a subsidiary of Sverdrup and Parcel and Associates, Inc.), contract operator of AEDC under Contract F40600-69-C-0001. The work was conducted under ARO Project Nos. RW5717 and RW5802 in the Research Branch of the Rocket Test Facility (RTF), and the manuscript was submitted for publication as partial results of this research effort on October 31, 1968.

The author wishes to acknowledge the assistance of the members of Central Computer Operations, ARO, Inc. Mr. F. C. Loper made many helpful suggestions on the mathematical analysis. Mr. W. J. Phares not only contributed to the mathematical analysis, but also programmed the system of equations for numerical solution.

This material has been accepted by the University of Brussels (Université Libre de Bruxelles) as partial fulfillment of the requirements for the degree of Doctor of Applied Science.

This technical report has been reviewed and is approved.

Marion L. Laster
Research Division
Directorate of Plans
   and Technology

Edward R. Feicht
Colonel, USAF
Director of Plans
   and Technology

ABSTRACT

A theoretical investigation of the ducted turbulent mixing of coaxial streams is presented. The effects of equilibrium chemical reactions in the mixing layer are included in the analysis. In Part I, the theory is developed for ducted mixing systems in which the inviscid portions of the flow are assumed to be one-dimensional. The integral method is used, and the mixing zone velocity profiles are assumed to be similar. Turbulent Prandtl and Lewis numbers are assumed to be unity, and the turbulent shear stress along one control surface in the mixing layer is computed by use of a semi-empirical model for the eddy viscosity. The theory is formulated to include the downstream regime where the mixing layer extends across the entire duct. The system of integral equations is transformed into a form suitable for numerical solution by standard methods. In Part II, the theory is extended to include the influence of a nonuniform supersonic inviscid core flow. A technique is developed for coupling the numerical solution of the inviscid core flow (from the method of characteristics) with the solution of the integral equations for the mixing layer. The theory is correlated with low speed experiments, with supersonic air-air ejector experiments and with experiments on ducted rocket-air mixing. The correlations show that the theory gives satisfactory results for the performance of ducted rocket-air mixing systems which are representative of air augmented rockets.

CONTENTS

PART I

DUCTED MIXING WITH ONE-DIMENSIONAL INVISCID

CORE FLOW (1-D CORE THEORY)

CONTENTS
(Continued)

PART II

DUCTED MIXING THEORY WITH TWO—DIMENSIONAL
INVISCID CORE FLOW (2-D CORE THEORY)

CONTENTS
(Continued)

CONTENTS
(Continued)

LIST OF FIGURES

LIST OF FIGURES

(Continued)

LIST OF FIGURES
(Continued)

LIST OF FIGURES
(Continued)

LIST OF SYMBOLS

b	Mixing zone width
$\lvert B \rvert$	Determinant in equation for db/dx (Section VII)
c	Mixing length constant
c_p	Specific heat
C_k	Mass fraction of element k
$\overline{C}$	Mass fraction of elements from primary stream
C_1, $C_2 \ldots$	Constants in duct wall equation
Ch	Choking parameter (defined by Eq. 105 — Section XVII)
D	Diameter
$\lvert D \rvert$	Coefficient determinant of system of equations
F_1, $F_2 \ldots$	Coefficients in system of differential equations
F_d	Mixing duct thrust (defined by Eq. 104 — Section XVII)
F_n	Vacuum thrust of primary nozzle
G_1, $G_2 \ldots$	Coefficients in system of differential equations
H	Static enthalpy
H_1, $H_2 \ldots$	Coefficients in system of differential equations
H_o	Total, or stagnation, enthalpy
k	Constant in eddy viscosity equation (Section VI)
k_o	Incompressible eddy viscosity constant
k_∞	Asymptotic eddy viscosity constant (at large Mach number)
ℓ	Mixing length
L	Length of mixing duct

LIST OF SYMBOLS
(Continued)

m_k	Mass fraction of molecular species k
M	Mach number
M_u	Effective average Mach number at duct exit (Section XVII)
O/F	Rocket oxidizer—fuel mass ratio
p	Static pressure
p_b	Back pressure
p_o	Total, or stagnation, pressure
p_o'	Pitot pressure
$|P|$	Determinant in equation for dp_w/dx (Section VII)
Q	Species conservation parameter (defined by eq. 27, Section V)
r	Radial coordinate
r_n	Radius of primary nozzle exit
R	Gas constant (universal gas constant/molecular weight)
$|R|$	Determinant in equation for dr_i/dx (Section VII)
T	Static temperature
T_o	Total, or stagnation, temperature
u	Axial velocity component
u_{max}	Maximum velocity in mixing layer
u_{min}	Minimum velocity in mixing layer
$|U_c|$	Determinant in equation for du_c/dx (Section VII)
$|U_w|$	Determinant in equation for du_w/dx (Section VII)
v	Transverse or radial velocity component
V	Magnitude of the total velocity vector

LIST OF SYMBOLS
(Continued)

w_a Initial mass flow of secondary stream

w_j Initial mass flow of primary stream

x Axial coordinate

x_c Length of inviscid core

x_e Length parameter in duct wall equation (Appendix I)

Δx Integration step size

y Transverse coordinate (two-dimensional), mixing zone coordinate

α Mach angle

γ Ratio of specific heats

δ^* Boundary layer displacement thickness

ϵ Turbulent eddy viscosity

θ Flow angle

ρ Density

σ Similarity parameter for two-dimensional mixing

τ Turbulent shear stress

Subscripts

1   Mixing duct inlet

I,II,III   First, second, third mixing regimes

a   Inviscid secondary flow

c   Centerline

i   Inner mixing zone boundary

j   Inviscid primary flow

m   Half radius control surface in mixing zone

n   Primary nozzle exit

w   Duct wall

SECTION I
INTRODUCTION

Ducted turbulent mixing of coaxial streams occurs in many devices of practical interest. Typical examples are the jet pump (or air-air ejector) and composite propulsion systems such as the air augmented rocket (Refs. 1, 2). For propulsive applications one must consider the possibility that exothermic chemical reactions will occur in the mixing layer.

The basic objective of this research is to develop a theory to describe the ducted turbulent mixing of coaxial streams, including chemical reactions. Emphasis has been placed on relatively long mixing systems in which the mixing layer may extend over most or all of the duct cross section at the duct exit plane. The duct pressure distribution will be strongly influenced by the thick mixing layers, and will be very different from the inviscid pressure distribution. In other words, this may be considered a "strong viscous interaction" problem.

Consider the mixing system shown schematically in Fig. 1, in which the primary and secondary fluids are specified. The specific objective of this work is to predict the secondary mass flow rate, w_a, and the duct wall pressure distribution if the following parameters are prescribed:

1. Geometry
2. Primary (central) stream initial conditions
3. Secondary stream stagnation pressure, p_{oa}, and stagnation temperature, T_{oa}
4. Back pressure, p_b

Three distinct flow regimes are shown in the mixing flow field of Fig. 1. In the first regime, turbulent mixing occurs between the inviscid secondary flow and the

1

Secondary Stream
Stagnation Conditions
P_{oa}, T_{oa}

Inviscid Secondary
Flow

Inviscid
Core
Flow

Duct Wall
$r_w = f(x)$

p_b

① 1

$w_a \longrightarrow$

Turbulent Mixing Zone

p_{oj}

T_{oj}

First
Regime

Second
Regime

Third
Regime
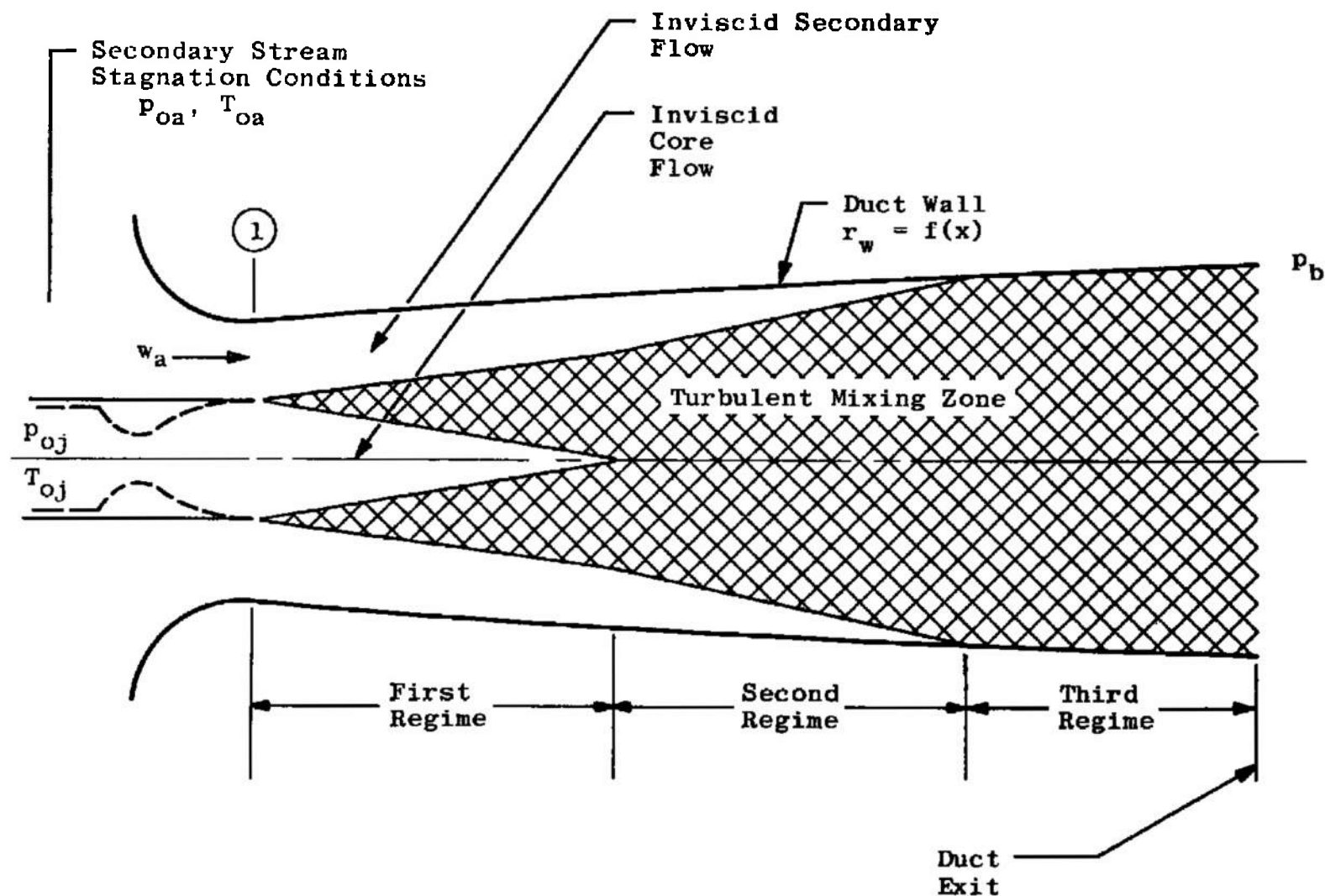
Duct
Exit

Fig. 1 Schematic of Ducted Mixing System

core of inviscid primary flow. In the second regime, the
inviscid core has been dissipated, but a region of inviscid
secondary flow exists near the duct wall. The third regime
occurs after the mixing layer has spread to the duct wall,
and the flow is entirely turbulent. The mixing is essen-
tially free turbulent in nature in the first and second
regimes, although not isobaric.

Several modes of operation are possible for a
ducted mixing system when the primary stream is initially
supersonic and the secondary stream is initially subsonic.
These operating modes are distinguished by the factor which
limits the secondary mass flow rate, w_a. The "upstream
choking" mode occurs when the back pressure is relatively
low, and the secondary stream static pressure is low
relative to the primary flow (Fig. 2a). The primary stream
expands, causing the secondary flow to choke at some station
near the inlet of the mixing duct, and the secondary flow
is supersonic downstream of the choking station. Fabri and
Paulon (Ref. 3) called this mode the "supersonic regime" in
their work on air-air ejectors. As the secondary stream
stagnation pressure is increased, the choking station will
move upstream. If the secondary stagnation pressure is
increased sufficiently the choking station will be fixed at
the initial section, with the primary nozzle either correctly
expanded or overexpanded. Fabri and Paulon called this
limiting case of the upstream choking mode the "saturated
supersonic regime." The secondary stream minimum area is
a function only of the geometry, and the mass flow, w_a, is
directly proportional to p_{oa} in this limiting case.

The "downstream choking" mode (Fig. 2b) is en-
countered when the back pressure is low, and w_a is limited
by choking of the flow at or near the duct exit. The
secondary flow is subsonic throughout the duct. This mode

3
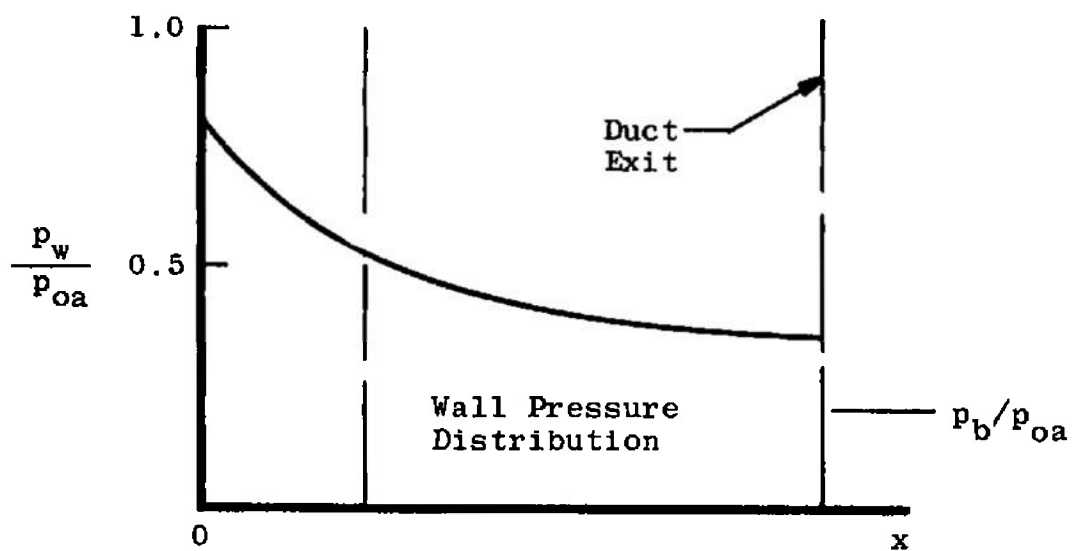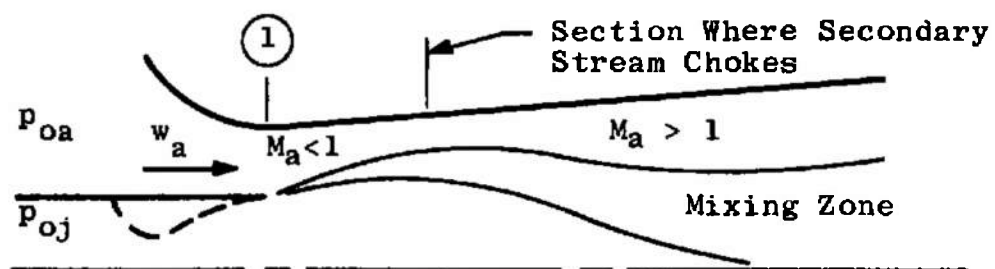
a. Upstream Choking Mode

Fig. 2 Operational Modes of a Ducted Mixing System
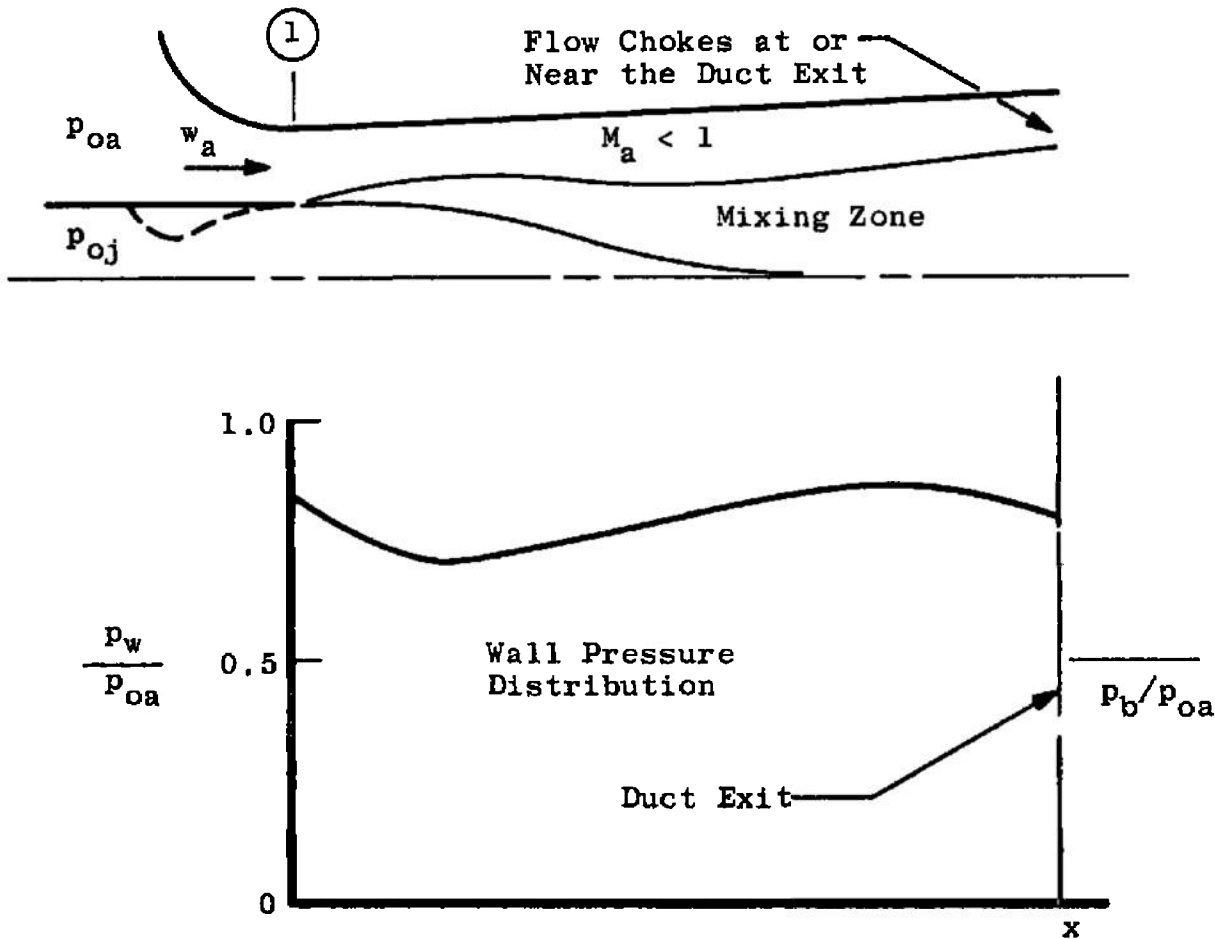
b. Downstream Choking Mode

Fig. 2 Continued
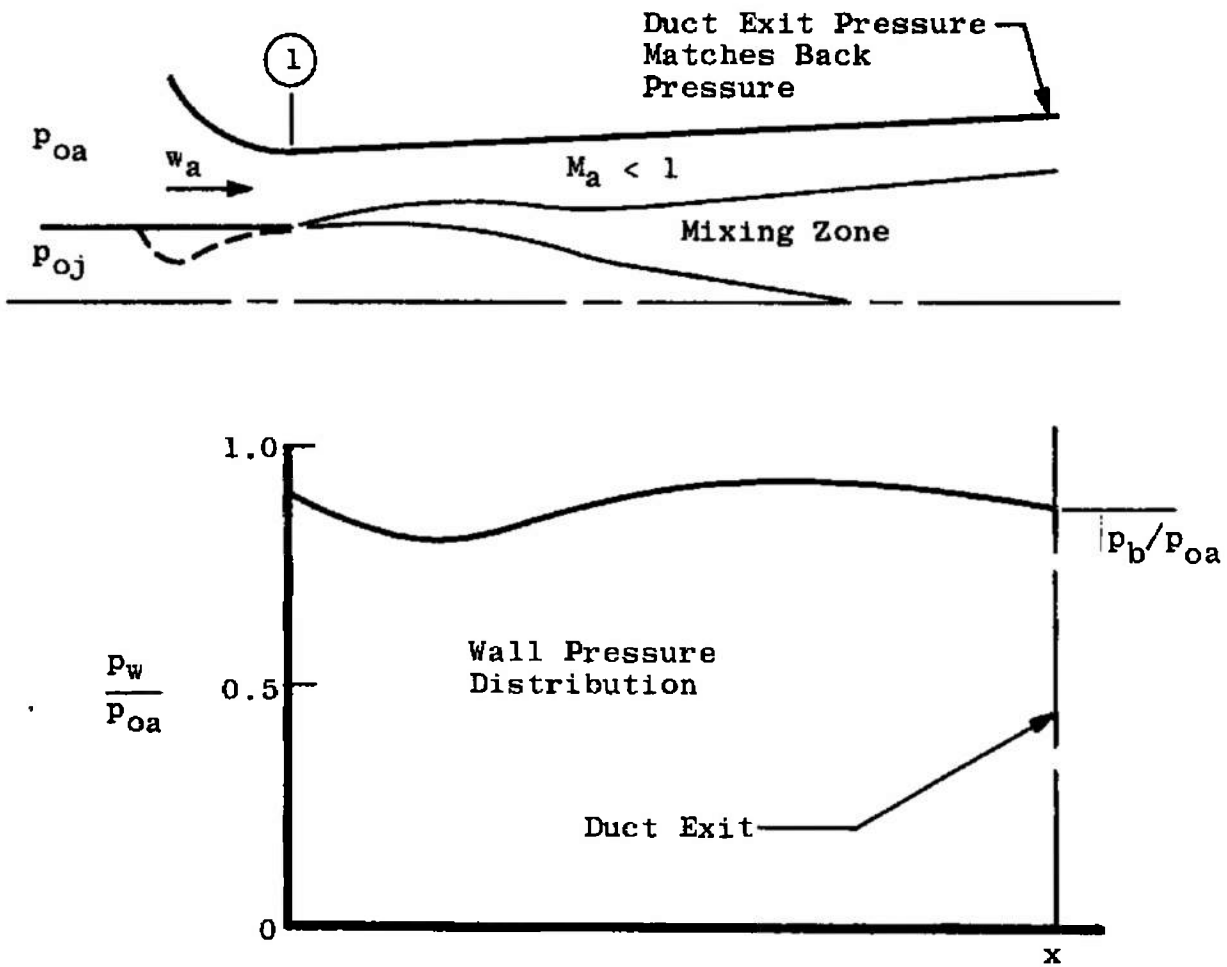
c. Back Pressure Dependent Mode

Fig. 2 Concluded

will probably not occur in a cylindrical or divergent mixing
duct unless the primary and secondary fluids have greatly
different densities, or unless chemical reactions occur in
the mixing process. The downstream choking mode is impor-
tant for certain propulsive applications.

The "back pressure dependent" mode of operation
(Fig. 2c) occurs when the back pressure, p_b, is sufficiently
high to unchoke the duct flow. The secondary flow is subsonic
throughout the duct, and the duct exit pressure exactly
matches the back pressure. Fabri and Paulon called this mode
the "mixed regime" and it is commonly encountered in jet
pump applications.

If it is to be considered adequate, a theory for
the mixing duct flow must be capable of predicting the per-
formance in each of the operational modes shown in Fig. 2.

It should be noted that certain limiting cases of
ducted mixing can be successfully analyzed by application of
one-dimensional theoretical concepts (Ref. 3, for example).
If the mixing duct is relatively long and of constant cross
section, and the system is operating in the back pressure
dependent mode, then the performance can be predicted by
assuming that the flow is fully mixed and uniform at the duct
exit. If the initial conditions are specified, then overall
conservation equations for momentum, mass flow and energy
can be solved for the one-dimensional flow conditions at the
duct exit. This one-dimensional theory gives no information
about the duct length required to achieve complete mixing
because the equations include no characteristic length
scale. Also, the one-dimensional approach is not applicable
to mixing ducts of variable cross section because the unknown
axial wall pressure forces cannot be predicted. The detailed
mixing duct flow must be treated in order to compute the un-
known wall pressure integral in variable area configurations.

Some limited success has been achieved in analyzing constant area ejector systems operating in the upstream choking mode by application of "quasi-one-dimensional" concepts. Fabri and Paulon (Ref. 3) and Kochendorfer and Rousso (Ref. 4) have used such quasi-one-dimensional approaches. Viscous effects are neglected, and again, no characteristic length appears in the equations. The analysis is limited to mixing ducts of constant cross sectional area. The primary stream is assumed to expand isentropically and one-dimensionally, while the secondary stream contracts. Fabri and Paulon assumed that the outer stream is isentropic and that $M_a = 1$ at the choking section. Solution of the combined momentum equation for both streams makes it unnecessary to assume that the primary and secondary pressures are equal at the choking section. Kochendorfer and Rousso formulated their analysis somewhat differently. They assumed that $M_a = 1$ and that the primary and secondary pressures are equal at the choking section. The combined stream momentum equation was used to define the secondary stream total pressure at the choking section.

The key assumption in these quasi-one-dimensional approaches is that the area of the primary stream at the choking section is the same as the one-dimensional isentropic area at the same static pressure. This assumption is approximately true when the primary nozzle flow is nearly uniform and not too highly underexpanded, but can be seriously in error in many practical cases. The neglect of viscous effects is less serious for supersonic ejectors with relatively large secondary flows. For this case, Chow and Addy (Ref. 5) have shown that viscous effects are small. It should be noted, however, that viscous effects are important for an air-air ejector operating with low or zero secondary flow rates.

The quasi-one-dimensional theories are simple to apply and give good engineering results for many constant area ejector configurations. These theories, however, are too limited in scope for application to many ejector problems.

In Part I of this report, a theoretical model is developed for the ducted mixing system, based on the integral form of the steady boundary layer equations. Both the inviscid primary and secondary streams are assumed to be one-dimensional. The mixing zone chemistry is assumed to be either frozen or in equilibrium. The turbulent shear along one control surface in the mixing layer is computed by means of a semi-empirical function for the eddy viscosity. This theory, hereafter called the "1-D Core Theory," agrees well with experimental results for subsonic mixing flows, but is inadequate when the primary stream is supersonic and non-uniform.

In Part II of this report, the first regime theory is extended to include treatment of the inviscid core flow with the irrotational method of characteristics (This theory will be called the "2-D Core Theory."). Inclusion of the method of characteristics greatly complicates the solution; however, the modified theory can be applied to supersonic primary flows which are initially nonuniform (conical primary nozzles, for example), or to cases where the primary nozzle is underexpanded.

It should be noted that the 2-D Core Theory differs from the 1-D Core Theory only in the first regime in which there is an inviscid core of primary flow (Fig. 1). The two theories are identical in the second and third regimes, i.e., after the inviscid core has been dissipated.

Most of the comparisons with experimental results have been made with the 2-D Core Theory. The 1-D Core Theory has been correlated only with some low speed experimental results, both to establish the empirical incompressible eddy

viscosity constants and to establish the validity of the theory for low speed flows.

Many assumptions have been made in the analytical model developed during this investigation. Some of these assumptions are necessary because the current knowledge of turbulent flow processes is very meager, even for flow configurations much less complex than the one considered here. Other assumptions have been made to render the analytical model tractable from a mathematical point of view. Recognizing the many simplifications in the theoretical model, it is essential that its validity be established by detailed comparisons with experiment in the flow regime of interest. Extensive experiments have been made by the author and his co-workers at AEDC on a ducted mixing system in which the primary flow was the exhaust from a fuel-rich rocket (Refs. 6, 7). The secondary stream was room temperature air, and various mixing duct configurations were used so that all of the operating modes shown in Fig. 2 were encountered. Correlations of the 2-D Core Theory with these rocket-air mixing experiments, as well as with experimental results for air-air ejectors, are discussed in Sections XVI and XVII.

SECTION II
SUMMARY OF ANALYTICAL APPROACHES FOR TURBULENT MIXING

The purpose of this section is to give a brief sur-
vey of the various methods which have been used in the analysis
of free turbulent mixing, and to discuss the methods in view
of the current state of experimental knowledge. A complete
review of the extensive mixing literature is not intended;
the objective is to mention the various analytical methods
so that the approach taken in this investigation can be viewed
in historical perspective. More detailed information on the
earlier work in this field can be found in the excellent
monograph of Abramovich (Ref. 8) and in Refs. 9—11.

The analysis of free turbulent mixing is neces-
sarily semi—empirical because no fundamental quantitative
flow model for turbulence is currently available. Numerous
experimental investigations, however, have established cer-
tain approximations which provide reasonably accurate predic-
tions of the mean flow field, at least for relatively simple
flow configurations. All of the analytical approaches have
incorporated the simplification that the complex fluctuating
turbulent flow field can be replaced with an equivalent steady
flow. The fluctuating nature of the flow is usually treated
by use of "apparent" turbulent transport properties which
are analogous to molecular transport properties in laminar
flow. The usual boundary layer approximations have been
used in most analyses. Most of the existing analyses have
been made for isobaric flow, i.e., jets, wakes and mixing
layers surrounded by uniform inviscid streams of large ex-
tent.

1. Low Speed Mixing (Constant Density)

Models for turbulent shear — In 1925 Prandtl
formulated his famous mixing length theory for turbulent

shear. He hypothesized that the mean value of the fluctuating velocity component in the turbulent field is equal to the product of the local mean velocity gradient times a characteristic mixing length, ℓ. The mixing length is proportional to the local width of the mixing layer for free mixing (ℓ = cb), and is assumed to be constant across the layer. A small element of fluid is assumed to conserve its axial velocity while moving transversely over the mixing length. The turbulent shear stress (Reynolds stress) in the axial direction is

$$\tau = -\rho \overline{u'v'} = \rho c^2 b^2 \left| \frac{\partial u}{\partial y} \right| \frac{\partial u}{\partial y}$$

where c is an empirical constant, u is the mean axial velocity, ρ is the density, b is the width of the mixing layer and u' and v' are the local components of the fluctuating velocity.

Taylor's vorticity transport theory is based on a similar mixing length concept, with the vorticity of a fluid element being conserved over the mixing length. Both Prandtl's and Taylor's theories assume that the eddy length scale, ℓ, is much less than the local width of the mixing layer. Taylor's vorticity transport theory results in the same expression for turbulent shear as Prandtl's mixing length theory for two-dimensional mixing. Because of its complexity in all but the simplest flows, Taylor's theory has been used much less frequently than the Prandtl mixing length theory.

The Boussinesq concept of an "apparent" or "eddy" viscosity has proven to be very useful in the analysis of free mixing problems. The axial shear stress is

$$\tau = -\rho \overline{u'v'} = \rho \epsilon \frac{\partial u}{\partial y}$$

where ϵ is the eddy kinematic viscosity. The eddy viscosity is not a fluid property, but is related to the dynamics of the particular problem.

Prandtl's mixing length theory gives the following relation for the eddy viscosity:

$$\epsilon = c^2 b^2 \left| \frac{\partial u}{\partial y} \right|$$

Thus, Prandtl's mixing length theory states that the eddy viscosity varies with $\left| \partial u / \partial y \right|$ across the mixing layer.

In 1942 Prandtl proposed another model for the turbulent eddy viscosity, based on the assumption that $\overline{v' \ell}$ (equivalent to ϵ) is related to the local mean velocity gradient across the mixing layer. This model, which implies that the turbulent eddy scale is of the same order as the mixing zone width, yields the following expression for the eddy viscosity:

$$\epsilon = k b \left(u_{max} - u_{min} \right)$$

k is an empirical constant, u_{max} is the maximum velocity in the mixing layer and u_{min} is the minimum velocity in the layer. The eddy viscosity is assumed to be constant across the mixing layer, or a function of only the axial coordinate. This Prandtl eddy viscosity model has been widely applied to a variety of free mixing problems because of its mathematical simplicity, and because the results agree fairly well with experiment for many flow configurations.

Methods of solution – The two most widely used analytical techniques for low speed mixing have been (1) finding similarity solutions to the boundary layer equations, and (2) the von Kármán integral method.

The early attempts to solve free mixing problems were primarily limited to finding similarity solutions. Using the Prandtl mixing length theory for turbulent shear, Tollmein (Ref. 12) found solutions for (1) the two-dimensional mixing layer between a semi-infinite stream and a medium at rest, (2) the two-dimensional jet flowing into a medium at rest, and (3) the axisymmetric jet flowing into a medium at rest.

Goertler (Ref. 13) applied the Prandtl eddy viscosity model to the two-dimensional mixing layer problem, and obtained solutions which correlated well with the experimental results of Reichardt (Ref. 14).

Early experiments on fully developed low speed mixing zones and jets showed clearly that the mean velocity profiles exhibit shape similarity, i.e., all profiles can be made approximately congruent if suitably normalized. These early experiments also indicated that the width of the fully developed mixing layer increases linearly with axial distance, x. This linear relation between b and x is inherent in the analyses of Tollmein and Goertler. Tollmein assumed that $\ell = cx$, with the proportionality constant relating b and x being absorbed into the empirical constant, c. Similarly, Goertler assumed that $\epsilon = kx\,(u_{max}-u_{min})$.

The experimental observation that the fully developed velocity profiles are approximately similar has led to the widespread use of the von Kármán integral method for the solution of free mixing problems. In the integral method the velocity profile shape is prescribed, usually based on prior experimental information, and the boundary layer equations are satisfied only on the average across the mixing layer. It is a well known characteristic of the integral method that the overall results are relatively in-

sensitive to the profile shape chosen, as long as the shape is approximately correct.

Kuethe (Ref. 15) was the first to use the integral method for the solution of free mixing problems. He obtained solutions for the two-dimensional mixing layer between two streams flowing at different velocities. Later, Squire and Trouncer (Ref. 16) applied the integral method to the solution of the axisymmetric two stream mixing problem.

The solutions of Kuethe and of Squire and Trouncer were obtained by using the Prandtl mixing length theory to compute the turbulent shear in the mixing layer. As the integral method is usually applied, with the shear evaluated at one fixed point in the normalized velocity profile, Prandtl's mixing length and eddy viscosity theories give identical results. Both theories give the same functional form for the characteristic shear, i.e., proportional to $(u_{max} - u_{min})^2$.

Mixing with finite secondary velocities - It has been seen that Prandtl's theories for turbulent shear have been applied to mixing with finite secondary velocities, even though the experiments which guided Prandtl's formulation of these theories were made only with zero secondary velocity. Both theories predict that the mixing rate decreases rapidly as the velocity ratio, u_{min}/u_{max}, is increased, and that no mixing at all occurs when $u_{max} = u_{min}$. Experiments, however, have shown that the mixing rate of species is quite large when $u_{max} = u_{min}$ (Ref. 17). Fejer, et al. (Ref. 17) give an excellent discussion of this problem of coaxial stream mixing when the secondary velocity is relatively large compared to the primary velocity.

Forstall and Shapiro (Ref. 18) made a series of experiments on coaxial stream mixing in the range of secondary-primary velocity ratios from 0.2 to 0.5. It was found that

the analysis of Squire and Trouncer, based on mixing length theory, predicted the experimental results fairly well at the lower velocity ratios, but deviated considerably from the experimental results at a velocity ratio of 0.5.

In general, the Prandtl theories for turbulent transport should be applied with caution when the secondary-primary velocity ratio exceeds about 0.3.

Heat and mass transfer – Forstall and Shapiro investigated the mass transfer in their experiments by use of a tracer gas in the primary field. They also summarized the results of other investigators on heat and mass transfer in free turbulent mixing. In general, heat and mass diffuse at the same rate (unity turbulent Lewis number), but faster than does momentum. The average value of the turbulent Prandtl (and Schmidt) number is approximately 0.7 for low speed mixing.

2. Variable Density Mixing

The Prandtl theories for turbulent shear give reasonably good results for nearly constant density mixing, as long as the secondary velocity is small relative to the primary velocity. When the mixing is accompanied by large density gradients in the layer, the current state of knowledge is much less satisfactory.

Large transverse density gradients in the mixing zone may be caused by:

1. Large difference in the inviscid stream Mach numbers (compressibility effect).

2. Large difference in the temperature and/or compositions of the inviscid streams.

3. Exothermic chemical reactions in the mixing zones.

All of these factors occur simultaneously in the most complex cases of interest.

The influence of density gradients on the free turbulent eddy viscosity is currently a source of speculation. Those who apply Prandtl's low speed shear theories directly to variable density mixing problems assume that the density gradient has no influence on the eddy viscosity distribution in the mixing layer. At the other extreme are those who use the compressibility transformation technique, which implies a large influence of density on the eddy viscosity. The reason for the uncertainty is that the computed velocity profiles are relatively insensitive to the distribution of eddy viscosity across the mixing layer. Consequently, it is very difficult to determine the eddy viscosity distributions from mean flow measurements in variable density mixing experiments. Unfortunately, very precise measurements in a mixing system with very large density gradients have not yet appeared in the literature.

Because of the insensitivity of the mean flow profiles to the eddy viscosity model chosen, greatly different theories have predicted mean flow profiles which agree fairly well with the available experimental profiles. The empirical constants in the eddy viscosity model, however, usually must be adjusted to correlate the experimental growth rate of the mixing layer.

Methods of solution — The various techniques for analyzing variable density mixing include (1) numerical solutions of the boundary layer equations, (2) compressibility transformations, (3) linearized solutions of the boundary layer equations, and (4) integral methods.

Vasiliu (Ref. 19) obtained numerical solutions for the problem of the mixing and combustion layer along the boundary between a supersonic rocket plume and surrounding

air stream. The axial pressure gradient was prescribed from a prior inviscid analysis, and finite rate chemistry was included in the mixing analysis. The eddy viscosity was assumed to be a function of only the streamwise coordinate, and non-unity (but constant) turbulent Prandtl and Lewis numbers could be used. Such solutions are a tribute to modern computer technology, but unfortunately the current uncertainty about turbulent transport properties makes it doubtful whether this approach is any more rewarding than simpler methods. The current knowledge about chemical reaction rates in turbulent flows is even poorer than that about turbulent transport. After the knowledge about turbulent transport and chemical reaction rates has progressed, the numerical technique will undoubtedly become the most powerful approach for free mixing problems.

Mager (Ref. 20) proposed a compressibility transformation of the boundary layer equations which is the turbulent counterpart of the Howarth transformation for laminar flow. Ting and Libby (Ref. 21) applied Mager's transformation to free turbulent mixing and derived an expression for the eddy viscosity. Libby (Ref. 22) analyzed isobaric coaxial jet mixing, including equilibrium chemical reactions, with the compressibility transformation technique. The corresponding incompressible solutions were obtained from linearized equations incorporating the Prandtl eddy viscosity model. The turbulent Prandtl and Lewis numbers were assumed to be unity. A reference density appears in the transformation, and this must be chosen arbitrarily because the theory offers no guidance on this subject.

The compressibility transformation predicts the largest distortion of the incompressible velocity profile shape of any of the methods in current use. The available experimental results, although limited, do not tend to sub-

stantiate the profile distortion predicted by the compressibility transformation (Ref. 23, for example). In fact, Peters (Ref. 24) used this experimental observation that the velocity profile shape is apparently invariant to develop a speculative model for the variable density eddy viscosity.

Kleinstein (Ref. 25) presented a linearized solution of the compressible boundary layer equations for isobaric coaxial stream mixing. He assumed that the product $\rho\epsilon$ is a function of only the axial coordinate. One is inclined to prefer Kleinstein's solution over the compressibility transformation solution because it predicts less distortion of the incompressible profile shapes.

Because the mixing zone velocity profiles are insensitive to transverse density gradients, the integral method is useful for analyzing variable density mixing problems. The normalized profile shape is usually assumed to be the same as the constant density profile shape. One advantage of the integral method is that it is relatively easy to include the effects of streamwise pressure gradients.

Korst, et al. (Ref. 26) have used the integral technique quite successfully to analyze the two-dimensional compressible mixing layer, with application to the flow past back steps. Warren (Ref. 27) and Donaldson and Gray (Ref. 28) have used the integral method to analyze the variable density mixing of an axisymmetric jet with a quiescent medium. Donaldson and Gray also proposed a simple compressibility correction to the Prandtl eddy viscosity model, based on a characteristic Mach number in the mixing layer.

Heat and mass transfer — As is the case for the eddy viscosity, the relative rates of transport for heat, mass and momentum are not well understood for variable

density mixing. Alpinieri (Ref. 29) and Zakkay, et al.
(Ref. 30) made a series of experiments on nonreactive co-
axial stream mixing. The outer stream was either subsonic
or supersonic air, and the jet fluid was either hydrogen,
helium, argon or carbon dioxide. In addition to showing that
the mixing rate is not zero when the streams have equal
velocities, these experiments indicated that heat and mass
tend to diffuse faster than momentum.

Zakkay, et al. evaluated the centerline values of
the turbulent Schmidt and Lewis numbers for their various
experiments, and found a great deal of scatter in the re-
sults. Most of the Schmidt numbers fell between 0.4 and 2.0.
Somewhat less scatter was observed for the Lewis number
results, with most of the data falling between 0.5 and 1.2.
These results show that it is extremely questionable whether
the relative transport of momentum, heat, and mass can be
accurately represented by constant values of the Prandtl
(or Schmidt) and Lewis numbers. No experimental results
have come to the attention of the author on the relative
rates of transport of momentum, heat and mass for mixing
with simultaneous chemical reactions.

3. Ducted Coaxial Stream Mixing

When the two streams mix inside a duct, the axial
pressure gradient is not prescribed, but must be computed
as an additional unknown parameter in the flow field solu-
tion.

Mikhail (Ref. 31) used the integral method to
analyze the low speed flow in a constant area jet pump. He
assumed that the mixing zone velocity profile could be
represented by a cosine function, and used Prandtl's mixing
length theory to evaluate the shear along one control sur-
face in the mixing zone.

For ducted mixing with large density gradients, relatively few analyses have come to the attention of the author.* Emmons (Ref. 32) treated the flow in the mixing duct of an air augmented rocket by numerical solution of the boundary layer equations. Finite rate chemistry was considered in the mixing layer, although with a highly simplified reaction model. The eddy viscosity was assumed to be a function of only the streamwise coordinate. Emmons' paper is very brief and it is not clear how he treated the axial pressure gradients. He apparently assumed the inviscid portions of the flow to be one-dimensional, although this point is also unclear.

Peters, et al. (Ref. 6) used the integral method to analyze ducted coaxial stream mixing with equilibrium chemical reactions. The turbulent Prandtl and Lewis numbers were assumed to be unity, and the normalized mixing zone velocity profile was assumed to be a cosine function. Rather than characterizing the growth rate of the mixing zone with a shear stress evaluated along a control surface in the zone, the equation of Abramovich (Ref. 33) was used to calculate the growth rate. The assumption that the inviscid portions of the flow were one-dimensional limited the validity and applicability of the theory for supersonic mixing, although the predicted mixing zone profiles agreed fairly well with experimental profiles. Another limitation of the theory was the use of the Abramovich mixing zone growth rate equation, which is strictly applicable only to isobaric mixing.

The analysis presented in this report may be considered an extension and refinement of the theory of Ref. 6.

---

* Edelman and Fortune (Ref. 47) recently presented a boundary layer type analysis (negligible lateral pressure gradients) for ducted coaxial stream mixing. The viscous layer is computed by finite difference methods, and finite rate chemistry is included in the computations. Either the duct pressure distribution or the duct shape can be prescribed.

4. Ducted Mixing With Nonuniform Inviscid Core

For certain classes of problems in ejectors and propulsion systems, it is essential that the nonuniform nature of the inviscid core flow be considered. For example, a supersonic ejector system having a conical nozzle and operating in the "upstream choking" mode (Section I) cannot be satisfactorily analyzed if the inviscid core flow is assumed to be one-dimensional. The amount of pluming of the supersonic primary stream depends on the detailed flow profile at the primary nozzle exit.

Addy (Ref. 34) and Chow and Addy (Ref. 5) have analyzed the flow in an axisymmetric ejector system. The secondary flow was assumed to be one-dimensional and the primary stream was treated with the method of characteristics. The inviscid flow field was first computed, then the effects of mixing were obtained by superimposing the two-dimensional mixing profiles of Korst and Chow (Ref. 35) on the inviscid boundary. Chow and Addy obtained excellent agreement between their analysis and their air-air ejector experiments. The superposition technique gives good results for the air-air ejector operating in the upstream choking mode because the effect of mixing is relatively small*.

Chow and Addy clearly point out that their solution is valid only for flows with relatively weak viscous interaction. They suggest that their solution can be improved by successive viscous corrections to the inviscid

---

* The discussion here is limited to cases in which the secondary flow is large enough so that the mixing zone does not impinge on the duct wall. For zero and low flow rates, the mixing zone impinges on the wall and viscous effects are very important. Chow and Addy analyzed these low secondary flow cases by using a base pressure analysis which included effects of base bleed.

solution, but that the superposition technique is limited to
flows with thin mixing layers, i.e., approximately two-
dimensional mixing. Another limitation of the superposition
technique in general is that the mixing profiles are com-
puted with the assumption that there are no transverse
pressure gradients, but then are superimposed onto a flow
which has strong radial pressure gradients.

To be valid in the downstream portion of the flow
field, as well as to be self consistent in the upstream
portion, the inviscid flow field and the mixing layer must
be computed simultaneously. The simultaneous solution of
the inviscid core flow (with the method of characteristics),
the mixing layer and the secondary inviscid flow is the
subject of Part II of this report (2-D Core Theory).

SECTION III
GENERAL DISCUSSION OF METHODS USED IN THE ANALYSIS

The purpose of this section is to outline the principal assumptions and techniques used in this investigation.

1. Outline of Principal Assumptions

As pointed out in Section II, the analysis of free turbulent mixing is necessarily approximate, and a number of assumptions is required to provide a complete mathematical representation of the problem. These assumptions, as well as others which have been made for mathematical convenience, are listed below. The more critical or questionable assumptions are discussed briefly.

(1) The flow is axisymmetric.

(2) All gases obey the perfect gas law.

(3) The usual assumptions used in the analysis of turbulent boundary layers are assumed to be applicable. The most important of these assumptions is that the radial pressure gradients in the mixing layer are negligible. The neglect of radial pressure gradients has yielded good results for low speed free mixing problems (Ref. 8), but may not be valid when the mixing layer is wholly or partly supersonic. Nevertheless, this assumption has been widely applied in the analysis of high speed mixing layers. It is not intended that the neglect of radial pressure gradients be justified, but rather that the assumption be clearly noted.

(4) The inviscid portion of the secondary flow is assumed to be one-dimensional and isentropic. This assumption is quite valid when the secondary flow

is subsonic and the radii of curvature of the
streamlines are large with respect to the radius
of the flow passage. This mixing theory is also
applied to cases in which the secondary flow
accelerates into the low supersonic range (Ma < 1.3).
The one-dimensional assumption will be less valid
for these supersonic cases, but this is not con-
sidered a serious defect in the analysis compared
to some of the more questionable assumptions.

(5) The inviscid portion of the primary flow (inviscid
core) is assumed to be one-dimensional and isen-
tropic for the 1-D Core Theory (Part I). Again,
this assumption will be quite valid for subsonic
primary flows. For supersonic primary flows, this
assumption will be approximately correct only if
the primary flow is initially uniform and the whole
process is nearly isobaric.

(6) The inviscid core flow is assumed to be isen-
tropic for the 2-D Core Theory (Part II). This
region of the flow is treated with the irrota-
tional method of characteristics. For primary
nozzles which provide uniform or conical flow, it
is well known that the shock waves in the free jet
are weak in the near field, but become more signi-
ficant in the far field (several primary nozzle
radii downstream). Some of the mixing configurations
considered in this investigation are relatively long,
and it is to be expected that neglecting the shock
waves in the flow will cause some deviation from
experiment.

(7) The mixing layer is assumed to be completely tur-
bulent, and the boundary layer thicknesses at the

initiation of the free mixing layer are assumed to be negligible. The first of these assumptions implies that transition from laminar to turbulent flow occurs well upstream of the initial section of the mixing duct. The assumption that the initial boundary layers are thin is reasonably valid in this analysis because the major interest is in the region many initial boundary layer thicknesses downstream from the mixing duct entrance.

(8) The finite thickness of the nozzle lip separating the primary and secondary flows is assumed to be negligible.

(9) The viscous effects at the duct wall are assumed to be negligible. In one correlation of the flow in a low speed jet pump (Section IX) the duct is approximately 10 diameters long and the wall boundary layer effects are significant. In that one case the wall viscous effects were computed by use of an approximate displacement thickness correction to the duct contour.

(10) The shape of the normalized velocity profiles in the mixing layer is assumed to be similar at all axial locations, and to be represented by a cosine function.

(11) The turbulent Prandtl and Lewis numbers in the mixing layer are assumed to be unity.

(12) For mixing with simultaneous chemical reactions, the reactions are assumed to be in equilibrium. The current knowledge of reaction chemistry in turbulent flows is insufficient to allow a theoretical verification of this assumption; its validity can only be checked by comparison of the theory with experiment.

(13) The eddy viscosity at the half-velocity point in the mixing layer is assumed to be given by the Prandtl eddy viscosity equation, with the effect of variable density treated by a modification of the correction suggested by Donaldson and Gray. This eddy viscosity model is discussed further in Section VI.

(14) In the third regime, where the turbulent region extends across the entire duct (Fig. 1), the free mixing concepts of shear and profile shape similarity are assumed to be applicable. Mikhail (Ref. 31) found that the cosine profile was a reasonably good representation of the third regime velocity profiles in his low speed jet pump configuration. It is realized that the third regime flow will eventually become a fully developed duct flow in which wall effects predominate. However, this analysis is not intended for application to more than 1 or 2 duct diameters downstream into the third regime. The validity of free turbulent shear relations in the upstream portion of the third regime can only be established by comparison of theory and experiment.

These assumptions, along with others that are mentioned in the text, sufficiently define the ducted mixing problem so that flow field solutions can be obtained by application of the integral method.

2. Outline of Analytical Developments - 1-D Core Theory

Section IV presents the derivation of three basic integral equations for the ducted mixing problem. These integral equations, which are derived from the

continuity equation and the axial boundary layer momentum equation, are:

(1) A continuity equation for the entire flow.

(2) A momentum equation for the entire flow.

(3) A momentum equation for the portion of the flow between the duct centerline and a control surface located halfway across the mixing layer.

A term representing the turbulent shear stress appears in the last equation.

Section V presents the equations for the mixing zone velocity, and for relating the mixing zone temperature and density to the velocity. The method of treating the mixing zone chemistry is presented.

Section VI presents the model used for the turbulent eddy viscosity. A modification of the density correction suggested by Donaldson and Gray is developed. The range of applicability of the eddy viscosity model is discussed.

Section VII presents the method of transforming the set of three basic differential—integral equations (derived in Section IV) into a set of three first order ordinary differential equations for three variables which fully define the flow. All of the auxiliary functions which are needed to compute the coefficients of these differential equations are presented in Appendix I. The resulting system of equations is solved by standard numerical techniques.

Section VIII presents a brief discussion of the numerical aspects of the solution, from the point of view of the engineering results.

3. Outline of Analytical Developments – 2-D Core Theory

Section X presents the derivation of three basic integral equations. These equations differ from the 1–D Core Theory equations in that the integrals do not include the inviscid core; the influence of the inviscid core appears in terms of the boundary conditions for the integral equations.

Section XI presents the equations used to represent the flow in the mixing layer. With a few exceptions, the mixing zone parameters are determined in the same way as in the 1–D Core Theory.

Section XII presents the transformation of the three basic differential–integral equations (derived in Section X) into a set of ordinary differential equations suitable for numerical solution by conventional techniques. All of the auxiliary functions required to compute the coefficients are presented in Appendix II.

Section XIII presents the method of characteristics solution for the inviscid core flow. The key technique for coupling the method of characteristics solution to the system of integral equations is discussed.

Section XIV presents a brief discussion of the numerical aspects of the 2–D Core Theory solutions.

Section XV presents the methods used to obtain solutions for ducted mixing systems operating in (1) the "downstream choking" mode, (2) the "back pressure dependent" mode, and (3) the "upstream choking" mode. In all cases, the solutions are obtained by iteration of the initial static pressure.

Appendix III presents a listing of computer program inputs and printout variables for both the 1–D Core Theory and 2–D Core Theory programs.

PART I
DUCTED MIXING WITH ONE-DIMENSIONAL INVISCID CORE FLOW
(1-D CORE THEORY)

SECTION IV
DEVELOPMENT OF BASIC DIFFERENTIAL – INTEGRAL EQUATIONS

In this section a set of three basic differential-integral equations[*] is derived from the boundary layer equations. The three equations are (1) a continuity equation for the entire flow, (2) a momentum equation for the entire flow, and (3) a momentum equation for the portion of the flow between the duct centerline and an arbitrary control surface.

1. Integration of Boundary Layer Equations

The axial momentum equation for axisymmetric flow is:

$$\rho u r \frac{\partial u}{\partial x} + \rho v r \frac{\partial u}{\partial r} = \frac{\partial}{\partial r}(\tau r) - r \frac{\partial P}{\partial x} \tag{1}$$

The continuity equation is:

$$\frac{\partial}{\partial x}(\rho u r) + \frac{\partial}{\partial r}(\rho v r) = 0 \tag{2}$$

The pressure is a function of only the axial coordinate, and is equal to the wall pressure, p_w. After multiplying each term by dr, eq. (1) is integrated between the arbitrarily selected lower and upper limits, r_1 and r_2:

$$\int_{r_1}^{r_2} \rho u r \frac{\partial u}{\partial x} dr + \int_{r_1}^{r_2} \rho v r \frac{\partial u}{\partial r} dr = \tau_2 r_2 - \tau_1 r_1 - \frac{dP_w}{dx} \int_{r_1}^{r_2} r\, dr \tag{3}$$

---

[*]The term "differential-integral equations" is used to denote the integral form of the boundary layer differential equations. These equations contain terms of the type $\frac{d}{dx}\int_{r_1}^{r_2} \rho u r\, dr$

Now consider the second term of eq. (3). Integrating by parts:

$$\int_{r_1}^{r_2} \rho v r \frac{\partial u}{\partial r} dr = \left[\rho v u r\right]_{r_1}^{r_2} - \int_{r_1}^{r_2} u \frac{\partial}{\partial r}(\rho v r) dr \tag{4}$$

Noting that $\partial/\partial r (\rho v r) = -\partial/\partial x (\rho u r)$ from eq. (2), eq. (4) is substituted into eq. (3):

$$\int_{r_1}^{r_2} \rho u r \frac{\partial u}{\partial x} dr + \rho_2 v_2 u_2 r_2 - \rho_1 v_1 u_1 r_1 + \int_{r_1}^{r_2} u \frac{\partial}{\partial x}(\rho u r) dr =$$

$$\tau_2 r_2 - \tau_1 r_1 - \frac{d P_w}{dx} \int_{r_1}^{r_2} r \, dr$$

Combining terms:

$$\int_{r_1}^{r_2} \left[\rho u r \frac{\partial u}{\partial x} + u \frac{\partial}{\partial x}(\rho u r)\right] dr + \rho_2 v_2 u_2 r_2 - \rho_1 v_1 u_1 r_1 =$$

$$\tau_2 r_2 - \tau_1 r_1 - \frac{d P_w}{dx} \int_{r_1}^{r_2} r \, dr$$

or

$$\int_{r_1}^{r_2} \frac{\partial}{\partial x}(\rho u^2) r \, dr + \rho_2 v_2 u_2 r_2 - \rho_1 v_1 u_1 r_1 = \tau_2 r_2 - \tau_1 r_1$$

$$- \frac{d P_w}{dx} \int_{r_1}^{r_2} r \, dr \tag{5}$$

Now let $r_1 = 0$ and $r_2 = r_w$, and note that $\tau_w = 0$:

$$\int_0^{r_w} \frac{\partial}{\partial x}(\rho u^2) r \, dr + \rho_w v_w u_w r_w = -\frac{d P_w}{dx} \frac{r_w^2}{2} \tag{6}$$

31

Integrating the continuity equation (eq. 2):

$$\rho v r = - \int_0^r \frac{\partial}{\partial x}(\rho u r)\, dr$$

Thus

$$\rho_w v_w r_w = - \int_0^{r_w} \frac{\partial}{\partial x}(\rho u r)\, dr \qquad (7)$$

Substituting eq. (7) into eq. (6):

$$\int_0^{r_w} \frac{\partial}{\partial x}(\rho u^2) r\, dr - u_w \int_0^{r_w} \frac{\partial}{\partial x}(\rho u) r\, dr = -\frac{dp_w}{dx}\frac{r_w^2}{2} \qquad (8)$$

To provide a second momentum equation, eq. (5) is evaluated with $r_1 = 0$ and $r_2 = r_m$, the arbitrary position in the mixing zone where $u = u_m$:

$$\int_0^{r_m} \frac{\partial}{\partial x}(\rho u^2) r\, dr - u_m \int_0^{r_m} \frac{\partial}{\partial x}(\rho u) r\, dr = \tau_m r_m - \frac{dp_w}{dx}\frac{r_m^2}{2} \qquad (9)$$

Equations (7), (8), and (9) are the three basic integral equations, i.e., a continuity equation for the entire flow, a momentum equation for the entire flow and a momentum equation for the interior portion of the flow between $r = 0$ and $r = r_m$.

Applying Leibnitz' rule for differentiating an integral (Ref. 36) to eq. (7):

$$\rho_w v_w r_w = -\frac{d}{dx} \int_0^{r_w} \rho u r\, dr + \rho_w u_w r_w \frac{dr_w}{dx}$$

Because the wall is a streamline in the flow field, $v_w = u_w\, dr_w/dx$, and the continuity equation becomes:

$$\frac{d}{dx}\int_0^{r_w} \rho u \, r \, dr = 0 \tag{10}$$

Similarly, applying Leibnitz' rule to eq. (8) gives:

$$\frac{d}{dx}\int_0^{r_w} \rho u^2 r \, dr - \rho_w u_w^2 r_w \frac{dr_w}{dx} - u_w \frac{d}{dx}\int_0^{r_w} \rho u \, r \, dr$$

$$+ u_w \left(\rho_w u_w r_w \frac{dr_w}{dx}\right) = -\frac{dp_w}{dx}\frac{r_w^2}{2}$$

or

$$\frac{d}{dx}\int_0^{r_w} \rho u^2 r \, dr = -\frac{dp_w}{dx}\frac{r_w^2}{2} \tag{11}$$

Applying Leibnitz' rule to eq. (9) gives

$$\frac{d}{dx}\int_0^{r_m} \rho u^2 r \, dr - \rho_m u_m^2 r_m \frac{dr_m}{dx} - u_m \frac{d}{dx}\int_0^{r_m} \rho u \, r \, dr$$

$$+ u_m \left(\rho_m u_m r_m \frac{dr_m}{dx}\right) = \tau_m r_m - \frac{dp_w}{dx}\frac{r_m^2}{2}$$

or

$$\frac{d}{dx}\int_0^{r_m} \rho u^2 r \, dr - u_m \frac{d}{dx}\int_0^{r_m} \rho u \, r \, dr = \tau_m r_m - \frac{dp_w}{dx}\frac{r_m^2}{2} \tag{12}$$

Equations (10), (11) and (12) are the working forms of the three basic integral equations.

2. First Regime Differential—Integral Equations

Referring to the schematic shown in Fig. 3, the mixing layer in the first regime is bounded on either side by a region of one—dimensional isentropic flow. The radius of the mixing zone control surface, r_m, is taken to be half the radial distance across the mixing zone, i.e., $r_m = r_i + b/2$. The integrals appearing in eqs. (10), (11) and (12) can be divided into parts corresponding to the various regions of the flow. Thus the following equations are obtained.

Continuity Equation

$$\frac{d}{dx}\left[\rho_j u_j \frac{r_i^2}{2}\right] + \frac{d}{dx}\int_{r_i}^{r_i+b}\rho u r\, dr + \frac{d}{dx}\left[\rho_a u_a \frac{r_w^2 - (r_i+b)^2}{2}\right] = 0 \tag{13}$$

Total Momentum Equation

$$\frac{d}{dx}\left[\rho_j u_j^2 \frac{r_i^2}{2}\right] + \frac{d}{dx}\int_{r_i}^{r_i+b}\rho u^2 r\, dr + \frac{d}{dx}\left[\rho_a u_a^2 \frac{r_w^2 - (r_i+b)^2}{2}\right]$$
$$= -\frac{dp_w}{dx}\frac{r_w^2}{2} \tag{14}$$

Half—Radius Momentum Equation

$$\frac{d}{dx}\left[\rho_j u_j^2 \frac{r_i^2}{2}\right] + \frac{d}{dx}\int_{r_i}^{r_i+b/2}\rho u^2 r\, dr - u_m \frac{d}{dx}\left[\rho_j u_j \frac{r_i^2}{2}\right]$$
$$- u_m \int_{r_i}^{r_i+b/2}\rho u r\, dr = \tau_m(r_i + b/2) - \frac{dp_w}{dx}\frac{(r_i+b/2)^2}{2} \tag{15}$$
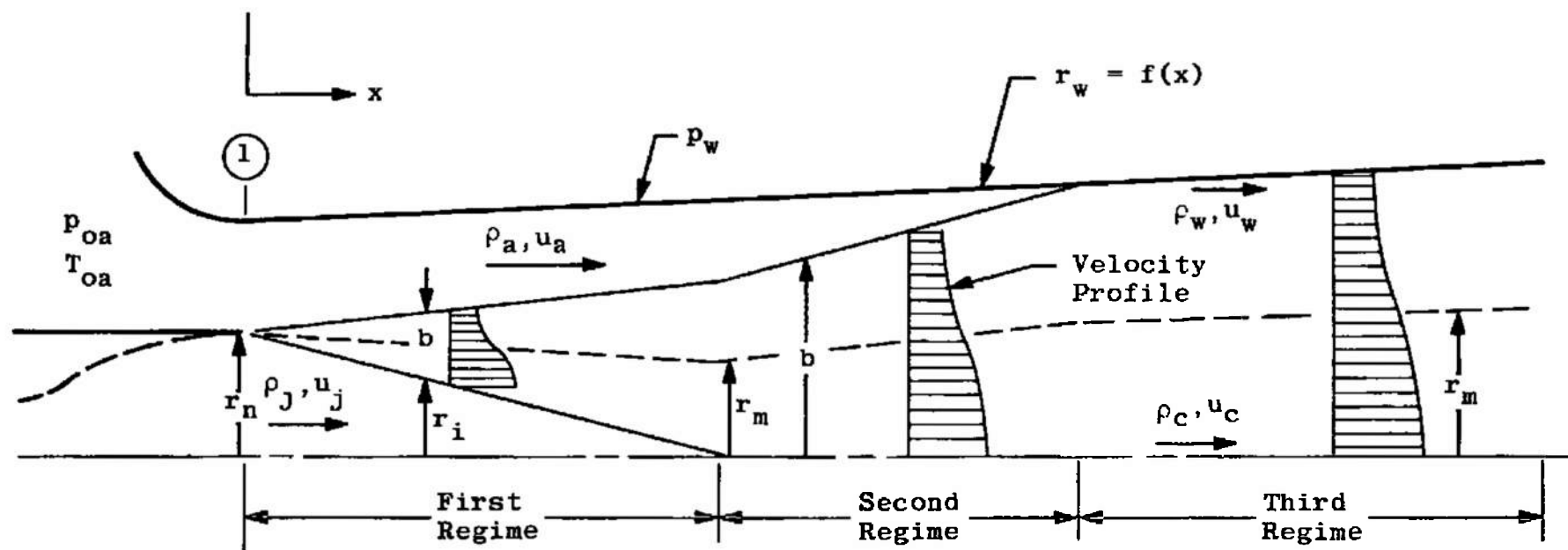
Fig. 3 Nomenclature for Integral Analysis (1-D Core Theory)

3. Second Regime Differential-Integral Equations

In the second regime (Fig. 3) the mixing zone extends to the centerline ($r_i = 0$), but a region of one-dimensional isentropic flow exists outside the mixing layer. In this regime, $r_m = b/2$, and the following equations are obtained.

Continuity Equation

$$\frac{d}{dx}\int_0^b \rho u r\, dr + \frac{d}{dx}\left[\rho_a u_a \frac{r_w^2 - b^2}{2}\right] = 0 \tag{16}$$

Total Momentum Equation

$$\frac{d}{dx}\int_0^b \rho u^2 r\, dr + \frac{d}{dx}\left[\rho_a u_a^2 \frac{r_w^2 - b^2}{2}\right] = -\frac{dp_w}{dx}\frac{r_w^2}{2} \tag{17}$$

Half-Radius Momentum Equation

$$\frac{d}{dx}\int_0^{b/2} \rho u^2 r\, dr - u_m \frac{d}{dx}\int_0^{b/2} \rho u r\, dr = \tau_m \frac{b}{2} - \frac{dp_w}{dx}\frac{b^2}{8} \tag{18}$$

4. Third Regime Differential-Integral Equations

In the third regime (Fig. 3) the mixing zone extends across the entire duct, thus $r_i = 0$, $b = r_w$ and $r_m = r_{w/2}$. The integral terms in eqs. (10), (11) and (12) only include the mixing layer, and the following equations are obtained.

Continuity Equation

$$\frac{d}{dx}\int_0^{r_w} \rho u r\, dr = 0 \tag{19}$$

Total Momentum Equation

$$\frac{d}{dx} \int_0^{r_w} \rho u^2 r \, dr = -\frac{dP_w}{dx} \frac{r_w^2}{2} \tag{20}$$

Half–Radius Momentum Equation

$$\frac{d}{dx} \int_0^{r_w/2} \rho u^2 r \, dr - u_m \frac{d}{dx} \int_0^{r_w/2} \rho u r \, dr = \tau_m \frac{r_w}{2}$$

$$- \frac{dP_w}{dx} \frac{r_w^2}{8} \tag{21}$$

SECTION V
MIXING ZONE PROFILES

A set of three basic differential—integral equations was developed in Section IV for each of the three mixing regimes. Solution of these differential—integral equations requires that ρ and u in the mixing layer be defined in terms of the other variables of the problem. The following development of the relations for the density and velocity distributions is essentially the same as that of Peters, et al. (Ref. 6).

1. Relation Between Velocity, Composition and Enthalpy

The axisymmetric boundary layer equations for momentum, energy and conservation of elemental species, with unity turbulent Prandtl and Lewis numbers, are (Ref. 22):

Momentum Equation

$$\rho u r \frac{\partial u}{\partial x} + \rho v r \frac{\partial u}{\partial r} = \frac{\partial}{\partial r}\left(\rho \epsilon r \frac{\partial u}{\partial r}\right) - r \frac{\partial P}{\partial x} \tag{22}$$

Energy Equation

$$\rho u r \frac{\partial H_0}{\partial x} + \rho v r \frac{\partial H_0}{\partial r} = \frac{\partial}{\partial r}\left(\rho \epsilon r \frac{\partial H_0}{\partial r}\right) \tag{23}$$

Conservation of Elemental Species

$$\rho u r \frac{\partial C_k}{\partial x} + \rho v r \frac{\partial C_k}{\partial r} = \frac{\partial}{\partial r}\left(\rho \epsilon r \frac{\partial C_k}{\partial r}\right) \tag{24}$$

These equations are the steady laminar boundary layer equations with the laminar transport properties replaced by the corresponding effective turbulent values. For free turbulent mixing, the turbulent transport is normally an order of magnitude or more larger than the molecular

transport; therefore, the molecular transport coefficients are neglected.

For application to flows with chemical reaction, it is important to note that C_k is defined as the local mass fraction of the element k, and H_o is defined as the stagnation enthalpy, including chemical heats of formation. As Libby has shown (Ref. 22), these definitions for C_k and H_o remove the usual formation terms from the energy and species equations. For chemically frozen flow, C_k can be interpreted as the local mass fraction of the molecular species k, and H_o can be defined with the usual definition of enthalpy, i.e., $\int_o^{T_o} c_p \, dT$

Now consider the case of isobaric mixing of an initially uniform jet with a surrounding uniform infinite stream. The dp/dx term in eq. (22) is zero, and eqs. (22), (23) and (24) are identical in form. The initial and boundary conditions for all variables are similar, and the following linear relation is obtained between u, H_o and C_k:

$$\frac{u - u_a}{u_j - u_a} = \frac{H_o - H_{oa}}{H_{oj} - H_{oa}} = \frac{C_k - C_{ka}}{C_{kj} - C_{ka}} \tag{25}$$

The subscript "a" refers to the outer stream and "j" to the inviscid jet. H_o and C_k are related to u by eq. (25) for isobaric mixing, and if these variables also define the density, ρ, then the solution of the momentum equation completely defines the flow field.

Equation (25) is also assumed to be valid for mixing with axial pressure gradients. Note, however, that the inviscid reference velocities, u_a and u_j, are pressure dependent. The assumption that eq. (25) is valid for flows with axial pressure gradients is made conditionally. If

eq. (25) is valid, then the computed total flux of any elemental species should be the same at all axial stations in the flow field. In the ducted mixing case, this species conservation may be expressed as

$$\int_0^{r_w} \rho u C_k r \, dr = constant \tag{26}$$

If the integral of eq. (26) does remain approximately constant throughout a flow field computation, then the use of eq. (25) is justified, at least for an integral method. In other words, the solution of the integrated momentum equation is also a satisfactory solution of the integrated species and energy equations.

Because the transport coefficients for all species are the same, the composition at any point in the mixing zone may be considered a simple two component mixture. This composition may be characterized by the single parameter $\bar{C}$, which is defined as the mass fraction of elements originating in the central stream (thus $\bar{C}_j = 1$, $\bar{C}_a = 0$). Equation (25) becomes

$$\frac{u - u_a}{u_j - u_a} = \frac{H_o - H_{oa}}{H_{oj} - H_{oa}} = \bar{C} \tag{25a}$$

Considering eq. (26), a species conservation parameter, Q, is now defined in terms of $\bar{C}$,

$$Q = \frac{2\pi}{w_j} \int_0^{r_w} \rho u \bar{C} r \, dr \tag{27}$$

where w_j is the initial mass flow of the jet. If eq. (25a) is correct, then the computed value of Q will be equal to unity throughout the flow field.

The theoretical variation of Q for a ducted rocket-air mixing system is discussed in Section XVII.

2. Mixing Zone Velocity Profiles

It is assumed that the mixing zone velocity profiles are similar and can be represented by a cosine function:

$$\frac{u - u_{min}}{u_{max} - u_{min}} = \frac{1}{2}\left[1 + \cos \pi\left(\frac{r - r_i}{b}\right)\right] \tag{28}$$

In the first regime (Fig. 3) the velocity profile equation is

$$\frac{u - u_a}{u_j - u_a} = \frac{1}{2}\left[1 + \cos \pi\left(\frac{r - r_i}{b}\right)\right] \tag{28a}$$

It has been assumed that the radial pressure gradients in the mixing zone are negligible, and that the inviscid secondary and primary flows are one-dimensional. It follows then that the pressure across the entire duct at any axial station is p_w, with p_w being a function only of x. The inviscid stream velocities, u_j and u_a, are isentropic functions of only p_w, therefore eq. (28a) defines u in terms of p_w, r_1, and b.

In the second regime the velocity profile equation is

$$\frac{u - u_a}{u_c - u_a} = \frac{1}{2}\left[1 + \cos \pi\left(\frac{r}{b}\right)\right] \tag{28b}$$

where u_c is the centerline velocity (Fig. 3). In the third regime the velocity profile equation is

$$\frac{u - u_w}{u_c - u_w} = \frac{1}{2}\left[1 + \cos \pi\left(\frac{r}{r_w}\right)\right] \tag{28c}$$

where u_w is the velocity at the duct wall.

Note that the composition profiles are determined from these velocity profile equations (eqs. 28a–c) and eq. (25a).

Velocity along the half–radius control surface – The cosine velocity profile gives the result that the velocity at the half–radius point in the profile is the average of the inviscid stream velocities. In the first regime the velocity, u_m, is given by

$$u_m = \frac{1}{2}\left(u_j + u_a\right)$$ (29a)

In the second regime

$$u_m = \frac{1}{2}\left(u_c + u_a\right)$$ (29b)

In the third regime

$$u_m = \frac{1}{2}\left(u_c + u_w\right)$$ (29c)

3. Mixing Zone Density

The mixing zone density is given by the perfect gas law,

$$\rho = P/RT$$ (30)

where T is the static temperature and R is the gas constant, defined as the universal gas constant divided by the molecular weight of the gas.

The method cf determining the mixing zone temperatures and gas constants is discussed in the next two sections for the cases of equilibrium and frozen chemistry, respectively.

4. Equilibrium Mixing Zone Chemistry

For rocket–air mixing, the mixing zone chemistry is assumed to be in equilibrium, i.e., the chemical reaction

rates are assumed to be very fast with respect to a characteristic time for the flow. The temperatures and gas properties in the mixing zone must be computed by application of the concepts of equilibrium chemistry. If the mixing were isobaric, then the mixing zone temperatures and gas properties would be unique functions of $\overline{C}$ for any given problem. In the case of ducted mixing, the pressure will not be constant in any given problem, and in principle, the mixing zone temperatures and compositions will continuously shift to the equilibrium condition at the local pressure. To treat this chemistry problem rigorously, one would need to incorporate an equilibrium chemistry computation into the flow field solution. Rather than resort to this complication, the mixing zone chemistry is treated by an approximate but acceptably accurate technique.

The equilibrium mixing zone temperatures and compositions are determined, as a function of $\overline{C}$, with an exterior calculation for representative values of p_w, u_j and u_a^*. A hypothetical mixing zone total temperature is then defined, and it is assumed that this total temperature, as well as the corresponding gas properties, is invariant throughout the flow field. This technique implies that the gases are in chemical equilibrium at the representative values of p_w, u_j and u_a, but that the flow is effectively frozen for deviations from the selected representative condition. The validity of this technique has been checked for the conditions of the rocket—air mixing experiments of Refs. 6 and 7, and the error in the mixing zone density profile was found to be negligible.

Once the jet and secondary flow stagnation conditions are specified, the choice of a representative value for p_w completely defines the static enthalpy, H,

---

* The assumption of an equilibrium primary stream expansion process is used to relate u_j to p_w.

from eq. (25a) and the energy equation:

$$H = H_0 - u^2/2 \tag{31}$$

H, $\bar{C}$ and p_w completely define the chemical problem if the elemental compositions of the inviscid streams are known. The temperature and molecular composition can then be computed with a standard equilibrium chemistry computer program. For hydrogen—oxygen—nitrogen or hydrocarbon—oxygen—nitrogen systems, the technique presented in the Appendix of Ref. 6 may also be used to compute the equilibrium temperatures and composition. A calculation procedure was presented in Ref. 6 with which the tabulated equilibrium properties for hydrogen—air and hydrocarbon—air systems (Refs. 37 and 38) can be used to compute the equilibrium properties for systems in which the nitrogen-oxygen mole ratio differs from 3.76 (mole ratio for standard air). That technique of Ref. 6 was used in this investigation.

The equilibrium chemistry computations yield the static temperature, the molecular composition and the molecular weight as a function of $\bar{C}$. The local gas constant, R, is determined from the molecular weight, and the mixture specific heat is given by the relation

$$C_p = \sum m_k C_{pk} \tag{32}$$

where m_k is the mass fraction of molecular species k and c_{pk} is the specific heat of species k at the static temperature. The specific heats, c_{pk}, are tabulated in standard gas tables (Ref. 39, for example). The local velocity, u, is determined by $\bar{C}$ (from eq. 25a and the representative values of u_a and u_j), and the hypothetical mixing zone total temperature is defined by use of the energy equation:

$$T_0 = T + u^2/2c_p \tag{33}$$

A typical set of curves relating T_o, c_p and R to $\bar{C}$ is shown in Fig. 4 for the experimental conditions of Refs. 6 and 7. The corresponding frozen distributions of T_o, c_p and R are also shown in Fig. 4.

5. Frozen Mixing Zone Chemistry

For frozen mixing, two methods of determining the T_o, c_p and R distributions are presented. The first method is used when the specific heats of the constituent gases may be assumed to be constant and independent of temperature. The second method is used when the specific heats of the gases are considered to vary with temperature. When the temperatures of the inviscid streams are greatly different the second method should be used, but the first is adequate for mixing of streams having relatively low temperatures, such as mixing in the usual air—air ejector.

Constant specific heats — The mixing zone total enthalpy, H_o, is determined from eq. (25a) as a function of $\bar{C}$, where $H_{oa} = c_{pa} T_{oa}$ and $H_{oj} = c_{pj} T_{oj}$. The local specific heat is given by

$$c_p = \bar{C} c_{pj} + \left(1 - \bar{C}\right) c_{pa} \tag{34}$$

The local gas constant is given by

$$R = \bar{C} R_j + \left(1 - \bar{C}\right) R_a \tag{35}$$

The local mixing zone stagnation temperature is given by

$$T_o = H_o / c_p \tag{36}$$

Variable specific heats — The local mixing zone molecular composition is determined as a function of $\bar{C}$ from the relation

$$m_k = \bar{C} m_{kj} + \left(1 - \bar{C}\right) m_{ka} \tag{37}$$

Within the figure:

Total Temperature Ratio, T_o/T_{oa}

Equilibrium
Chemistry

Frozen Mixing

Air

Hydrogen-Oxygen Rocket
(Gaseous Propellants)
$O/F = 3.2$
$T_{oa} = 530^oR$ (294^oK)
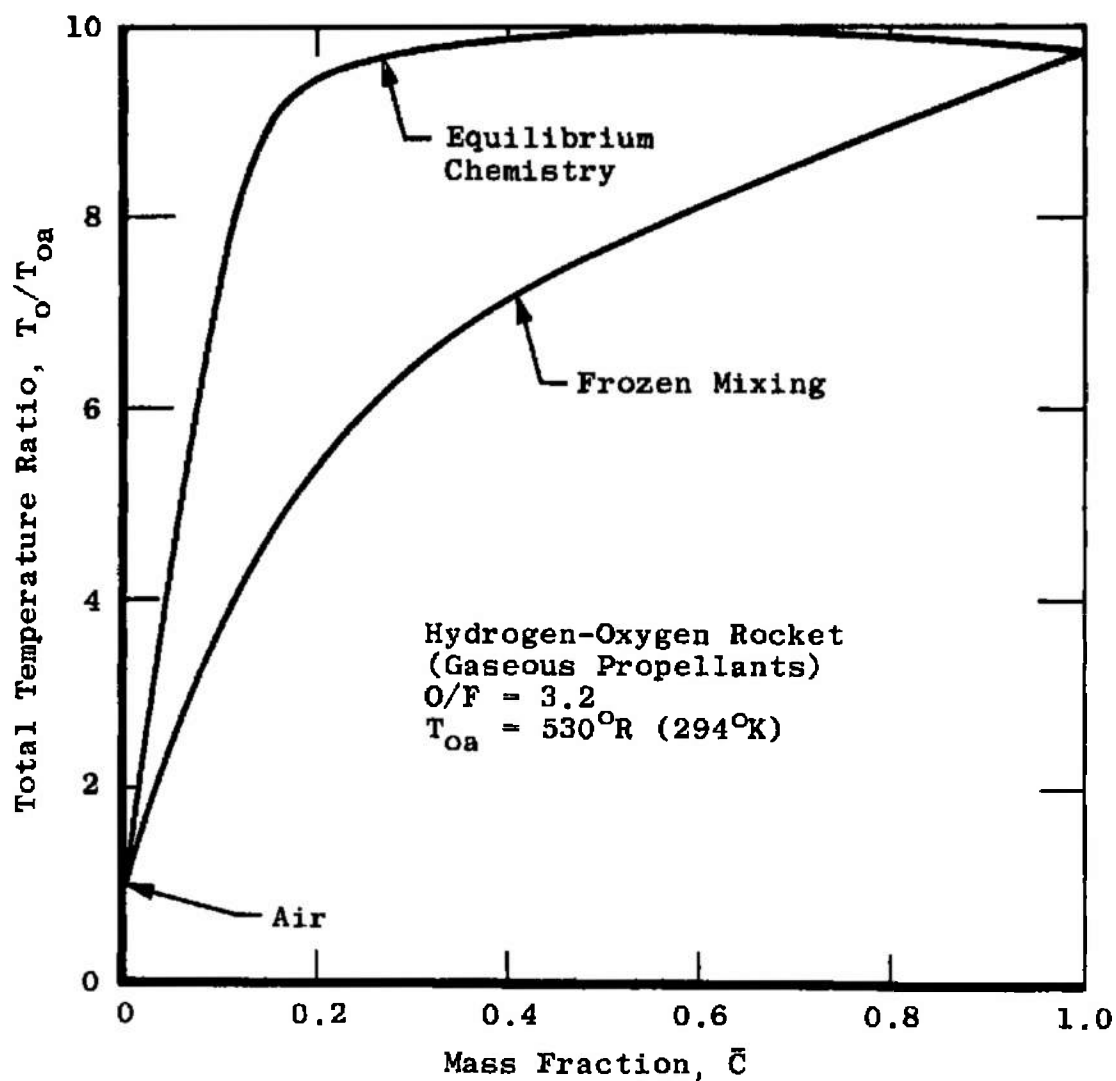
Mass Fraction, $\bar{C}$

a. Total Temperature
Fig. 4 Mixing Zone Properties for Rocket-Air Mixing

b. Specific Heat
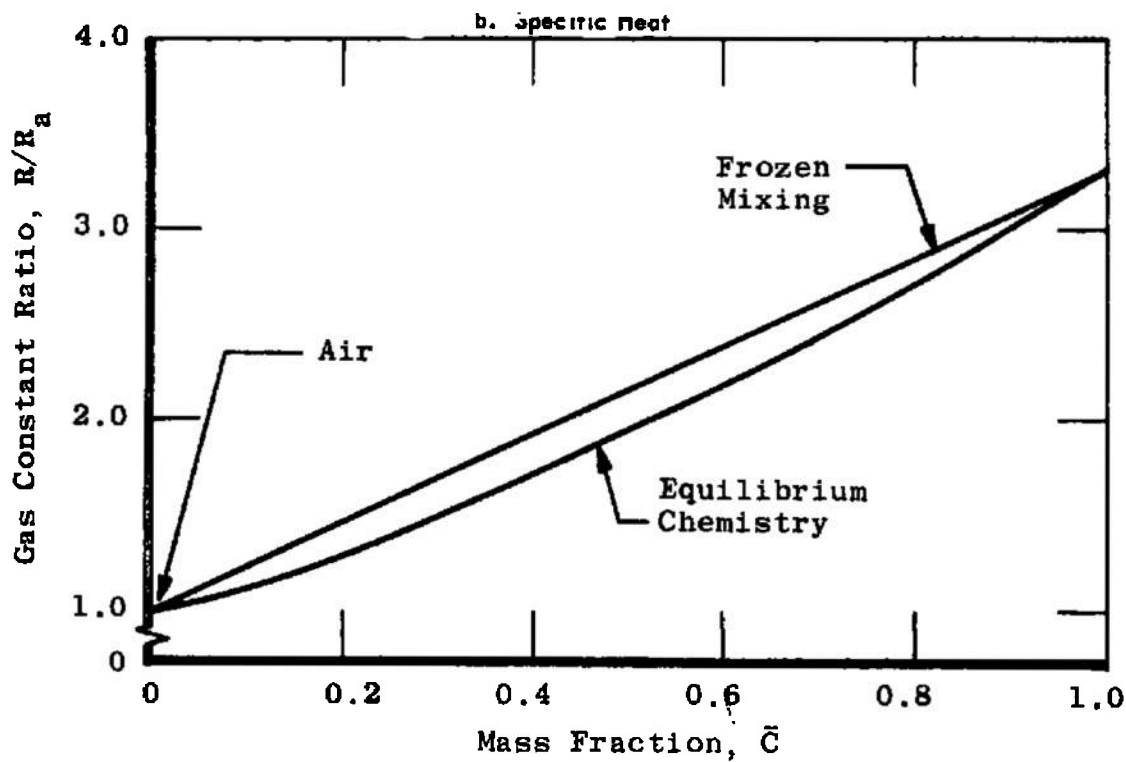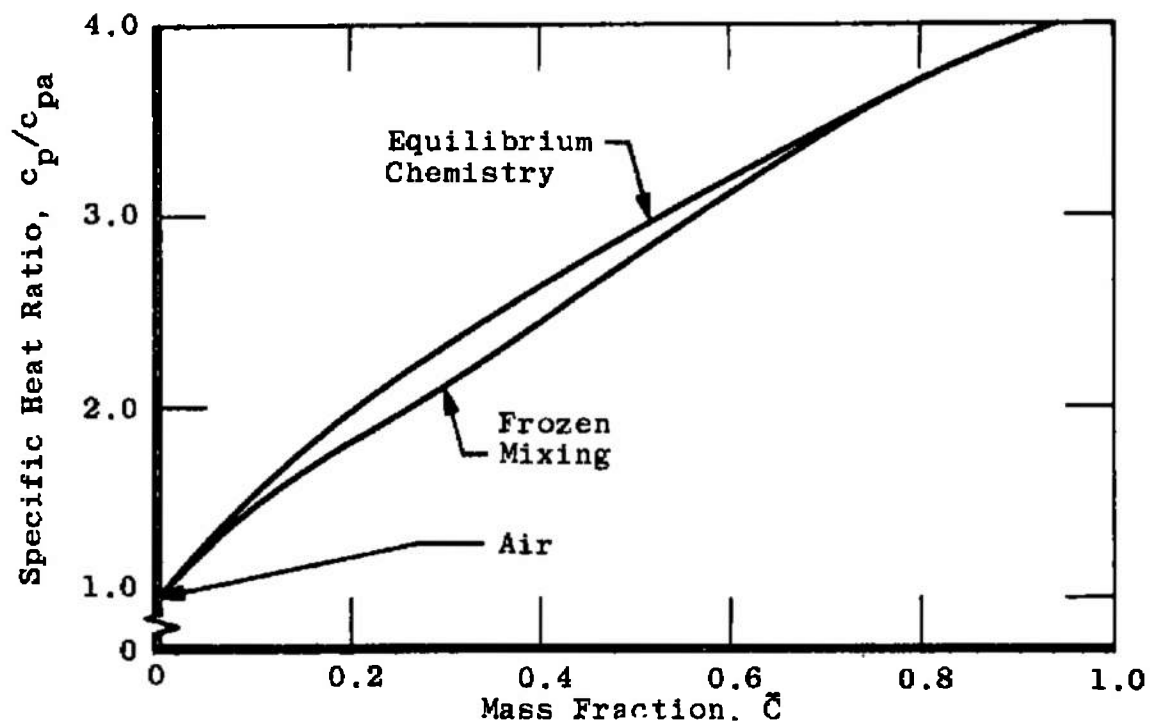
c. Gas Constant

Fig. 4 Concluded

where m_k is the mass fraction of molecular species k. The local gas constant, R, is given by eq. (35), but an iterative process must be used to determine T_o and c_p. The stagnation enthalpy, H_o, is given by eq. (25a), and the static enthalpy, is computed from eq. (31), along with a representative u vs. $\bar{C}$ function (same procedure as for equilibrium chemistry). The local static temperature is determined by trial of various values of T until the following equation is satisfied:

$$H = \sum m_k H_k \tag{38}$$

The values of H_k are obtained from standard tabulated gas tables (Ref. 39, for example). After T is determined the mixture specific heat is obtained from eq. (32), with the c_{pk}'s taken from the gas tables at T. The hypothetical total temperature is then determined from eq. (33).

The resulting T_o, c_p and R functions of $\bar{C}$ are assumed to be invariant in the flow field computation. This procedure, which is basically the same as used for equilibrium chemistry, assumes that the variation of the specific heats is negligible for the range of temperatures that a given mixture undergoes in the flow field. This procedure is exact for isobaric mixing, as is true for equilibrium chemistry.

The frozen distributions shown in Fig. 4 were computed by taking into account the variation of the specific heats with temperature.

SECTION VI
TURBULENT EDDY VISCOSITY

As is usual with the integral method, the turbulent shear is evaluated at only one position in the mixing zone, in this case at the half radius control surface, r_m (Fig. 3). This turbulent shear stress, τ_m, is determined by the equation

$$\tau_m = \rho_m \epsilon_m \left. \frac{\partial u}{\partial r} \right|_m \tag{39}$$

where ϵ_m is the eddy viscosity.

Eddy viscosity model — The semi-empirical model for the eddy viscosity which is used in this investigation is the Prandtl incompressible model

$$\epsilon_m = k\, b \left(u_{max} - u_{min} \right) \tag{40}$$

with the empirical constant, k, corrected for the influence of variable density in the mixing layer. The variable density correction used is a modification of the correction suggested by Donaldson and Gray (Ref. 28) for the mixing of an axisymmetric jet flowing into a quiescent medium. Their analytical model was an integral method similar to the model reported herein, and the turbulent shear stress was evaluated along a control surface, r_m (x), where the velocity was $u_m = \frac{1}{2} u_{max}$.

Donaldson and Gray evaluated the value of k (using the Prandtl eddy viscosity model) at various axial stations in the flow field for several different experiments. They found that the influence of density gradients in the mixing layer could be generalized if k is taken to be a function of only the local Mach number, M_m, at the control surface, r_m. For their cases of interest, with zero secondary velocity,

they found an influence of the nozzle lip geometry on the
computed values of k. For flows which issue from a nozzle
in a large plate (causing the induced secondary flow to be
initially radial) the computed values of k were, in general,
somewhat larger than for nozzle geometries in which the
induced secondary flow was nearly axial. When plotted
against M_m, the values of k for both configurations tend
to decrease quite quickly with increasing M_m, then to
become nearly constant for larger values of M_m.

The two curves which Donaldson and Gray faired
through the data (for sharp and blunt nozzle lips) can be
approximated quite well by an exponential function of M_m,
with the "half-decay" of k occurring at $M_m \simeq 0.45$. If k_o
is the value at $M_m = 0$, and k_∞ the asymptotic value at
large M_m, this exponential function can be written as

$$\frac{k - k_\infty}{k_0 - k_\infty} = \exp\left(-3.42\, M_m^2\right) \tag{41}$$

Donaldson and Gray evaluated k in both the core
region of the jet (first regime) and the developed region
(second regime). The absolute values which they computed
for k in the core region appear to be in error. Experience
in correlating a similar integral method with low speed
experiments has shown that the core region (first regime)
values of k are smaller than the developed region values by
a factor of 1.5 - 1.6. Donaldson and Gray, on the other hand,
found the same values of k in both regions of the flow.
Their developed region values of k appear to be approxi-
mately correct, so their core region values are too high

by a factor of 1.5 - 1.6[*]. The reason for this discrepancy is not clear, although it may be related to the momentum correction which Donaldson and Gray used to account for initial boundary layers in the jet.

The procedure which has been used in this investigation is to assume that eq. (41) correctly expresses the effect of density gradients, but to evaluate k_o and k_∞ by correlating the present integral theory with experimental results. The 1-D Core Theory was correlated with various low speed experiments (Section IX) and the values of k_o in the first and second regimes were found to be approximately 0.007 and 0.011, respectively.

The 2-D Core Theory (Part II) was correlated with several experiments for rocket-air mixing (Refs. 6 and 7) in which M_m varied from approximately 1.5 to 1.8. These values of M_m are higher than any reported by Donaldson and Gray, so the results for k are taken to be k_∞. It was found that the rocket-air mixing could be satisfactorily correlated if k_∞/k_o was taken to be 0.66. Substituting this value into eq. (41), one obtains

$$k/k_o = 0.66 + 0.34 \exp\left(-3.42 M_m^2\right) \tag{42}$$

This equation is shown in Fig. 5, along with the results from Warren's experiments, the only experiments with sharp lip nozzles which Donaldson and Gray considered.

---

[*] Because of different definitions for the characteristic length and velocity scales in the Prandtl eddy viscosity model, Donaldson and Gray's values of k are about 4 times larger than the corresponding values used in this investigation.
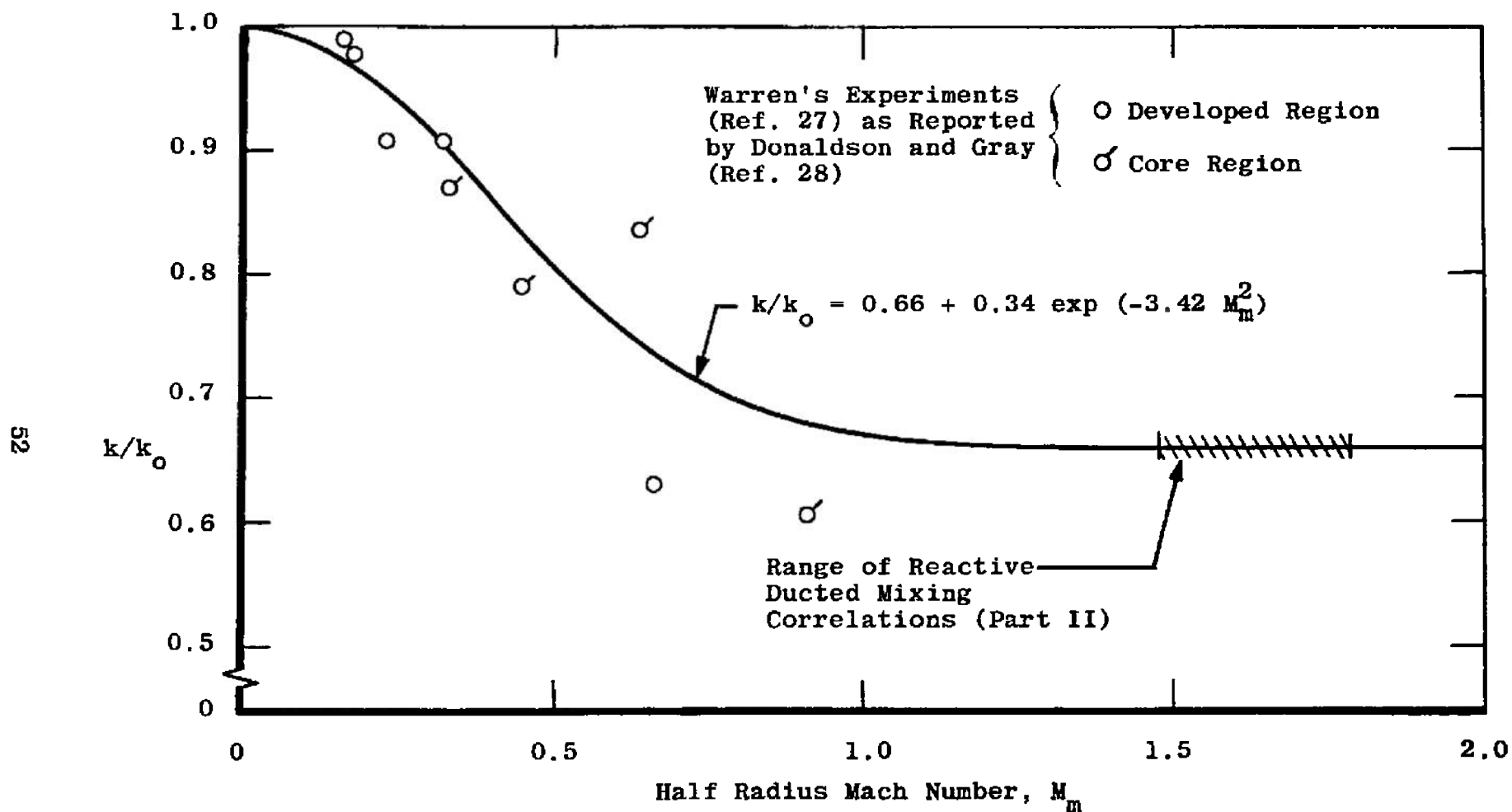
Fig. 5 Variable Density Correction to the Eddy Viscosity Constant

All of the computations presented in this report were made using eq. (42), along with k_{oI} = 0.007 (first regime) and $k_{oII, III}$ = 0.011 (second and third regimes).

As was pointed out in Section II, the Prandtl eddy viscosity model (eq. 40) is questionable for two stream mixing when u_a/u_j is greater than 0.3. The greatest interest in this investigation has been in correlating the rocket-air mixing experiments of Refs. 6 and 7. In those experiments, the value of u_a/u_j did not exceed 0.1. The 2-D Core Theory is also correlated with supersonic air-air ejector experiments in Part II, and u_a/u_j exceeded 0.5 in some of those experiments. It is to be expected that the predicted mixing zone growth rate will be too small for these air-air ejectors, however, the influence of mixing on the performance of supersonic air-air ejectors is known to be small (in the upstream choking mode of operation). Consequently, the use of the Prandtl eddy viscosity model should not cause serious errors in the overall results.

Turbulent shear stress — Differentiating the velocity profile equations from Section V, the velocity gradient at r_m is found to be:

First regime

$$\left.\frac{\partial u}{\partial r}\right|_m = \frac{\pi}{2}\frac{(u_a - u_j)}{b} \tag{43a}$$

Second regime

$$\left.\frac{\partial u}{\partial r}\right|_m = \frac{\pi}{2}\frac{(u_a - u_c)}{b} \tag{43b}$$

Third regime

$$\left.\frac{\partial u}{\partial r}\right|_m = \frac{\pi}{2}\frac{(u_w - u_c)}{r_w} \tag{43c}$$

Substituting eqs. (40) and (43) into eq. (39), one obtains the following equations for the shear stress at r_m:

First regime

$$\tau_m = \frac{\pi}{2} k_I P_m (u_a - u_j) \left| (u_a - u_j) \right|$$ (44a)

Second regime

$$\tau_m = \frac{\pi}{2} k_{II} P_m (u_a - u_c) \left| (u_a - u_c) \right|$$ (44b)

Third regime

$$\tau_m = \frac{\pi}{2} k_{III} P_m (u_w - u_c) \left| (u_w - u_c) \right|$$ (44c)

SECTION VII
TRANSFORMATION OF DIFFERENTIAL–INTEGRAL EQUATIONS

A system of three basic differential–integral equations was derived in Section IV for each of the three mixing regimes. In this section, the system of differential–integral equations will be transformed into a form suitable for solution with conventional numerical techniques. The transformation technique used is essentially the same as that suggested by Phares and Loper (Ref. 40).

1. First Regime Transformation

The three first regime differential–integral equations which were derived in Section IV are as follows:

Continuity Equation

$$\frac{d}{dx}\left[\rho_j u_j \frac{r_i^2}{2}\right] + \frac{d}{dx}\int_{r_i}^{r_i+b} \rho u r\, dr + \frac{d}{dx}\left[\rho_a u_a \frac{r_w^2-(r_i+b)^2}{2}\right] = 0 \quad (13)$$

Total Momentum Equation

$$\frac{d}{dx}\left[\rho_j u_j^2 \frac{r_i^2}{2}\right] + \frac{d}{dx}\int_{r_i}^{r_i+b} \rho u^2 r\, dr + \frac{d}{dx}\left[\rho_a u_a^2 \frac{r_w^2-(r_i+b)^2}{2}\right] = -\frac{dP_w}{dx}\frac{r_w^2}{2}$$

$$(14)$$

Half–Radius Momentum Equation

$$\frac{d}{dx}\left[\rho_j u_j^2 \frac{r_i^2}{2}\right] + \frac{d}{dx}\int_{r_i}^{r_i+b/2} \rho u^2 r\, dr - u_m \frac{d}{dx}\left[\rho_j u_j \frac{r_i^2}{2}\right] \quad (15)$$

$$-u_m \frac{d}{dx}\int_{r_i}^{r_i+b/2} \rho u r\, dr = \tau_m\left(r_i+b/2\right) - \frac{dP_w}{dx}\frac{\left(r_i+b/2\right)^2}{2}$$

Sufficient information about the terms in eqs. (13) through (15) was developed in Sections V and VI so that the

55

mixing problem can be defined in terms of three flow field variables which are functions of only the axial coordinate, x. The variables chosen in the first regime are (1) the wall pressure, p_w, (2) the radius of the inner boundary of the mixing zone, r_i, and (3) the width of the mixing zone, b. The objective here is to transform eqs. (13) through (15) into three equations of the form

$$A_1 \frac{d p_w}{dx} + A_2 \frac{d r_i}{dx} + A_3 \frac{d b}{dx} = A_4 \tag{45}$$

which may easily be solved by standard numerical procedures.

First apply Leibnitz' rule to eqs. (13) through (15):
The continuity equation becomes

$$\frac{d}{dx}\left[\rho_j u_j \frac{r_i^2}{2}\right] + \int_{r_i}^{r_i+b} \frac{\partial}{\partial x}(\rho u) r \, dr + \rho_a u_a (r_i+b)\left(\frac{d r_i}{dx} + \frac{d b}{dx}\right)$$

$$- \rho_j u_j r_i \frac{d r_i}{dx} + \frac{d}{dx}\left[\rho_a u_a \frac{r_w^2 - (r_i+b)^2}{2}\right] = 0 \tag{46}$$

The total momentum equation becomes

$$\frac{d}{dx}\left[\rho_j u_j^2 \frac{r_i^2}{2}\right] + \int_{r_i}^{r_i+b} \frac{\partial}{\partial x}(\rho u^2) r \, dr + \rho_a u_a^2 (r_i+b)\left(\frac{d r_i}{dx} + \frac{d b}{dx}\right)$$

$$- \rho_j u_j^2 r_i \frac{d r_i}{dx} + \frac{d}{dx}\left[\rho_a u_a^2 \frac{r_w^2 - (r_i+b)^2}{2}\right] = -\frac{d p_w}{dx}\frac{r_w^2}{2} \tag{47}$$

The half-radius momentum equation becomes

$$\frac{d}{dx}\left[\rho_j u_j^2 \frac{r_i^2}{2}\right] + \int_{r_i}^{r_i+b/2} \frac{\partial}{\partial x}(\rho u^2) r \, dr - u_m \int_{r_i}^{r_i+b/2} \frac{\partial}{\partial x}(\rho u) r \, dr$$

$$+ (u_m - u_j)\rho_j u_j r_i \frac{d r_i}{dx} = \tau_m (r_i + b/2) - \frac{d p_w}{dx}\frac{(r_i + b/2)^2}{2} \tag{48}$$

The first regime mixing zone profiles are expressed in terms of the variable $y = \left(\dfrac{r-r_i}{b}\right)$ (Section V); therefore, change the variable of integration in the integral terms from r to y, using the relations

$$\int_{r_i}^{r_i+b} (\ )\, r\, dr = b^2 \int_0^1 (\ )\, y\, dy + b\, r_i \int_0^1 (\ )\, dy \qquad (49)$$

and

$$\int_{r_i}^{r_i+b/2} (\ )\, r\, dr = b^2 \int_0^{1/2} (\ )\, y\, dy + b\, r_i \int_0^{1/2} (\ )\, dy \qquad (50)$$

Equations (46) – (48) become:

$$\frac{d}{dx}\left[\rho_j u_j \frac{r_i^2}{2}\right] + b^2 \int_0^1 \frac{\partial}{\partial x}(\rho u)\, y\, dy + b\, r_i \int_0^1 \frac{\partial}{\partial x}(\rho u)\, dy - \rho_j u_j r_i \frac{dr_i}{dx}$$

$$+ \rho_a u_a (r_i+b)\left(\frac{dr_i}{dx} + \frac{db}{dx}\right) + \frac{d}{dx}\left[\rho_a u_a \frac{r_w^2 - (r_i+b)^2}{2}\right] = 0 \qquad (46a)$$

$$\frac{d}{dx}\left[\rho_j u_j^2 \frac{r_i^2}{2}\right] + b^2 \int_0^1 \frac{\partial}{\partial x}(\rho u^2)\, y\, dy + b\, r_i \int_0^1 \frac{\partial}{\partial x}(\rho u^2)\, dy - \rho_j u_j^2 r_i \frac{dr_i}{dx}$$

$$+ \rho_a u_a^2 (r_i+b)\left(\frac{dr_i}{dx} + \frac{db}{dx}\right) + \frac{d}{dx}\left[\rho_a u_a^2 \frac{r_w^2 - (r_i+b)^2}{2}\right]$$

$$= -\frac{dP_w}{dx}\frac{r_w^2}{2} \qquad (47a)$$

$$\frac{d}{dx}\left[\rho_j u_j^2 \frac{r_i^2}{2}\right] + b^2 \int_0^{1/2} \frac{\partial}{\partial x}(\rho u^2)\, y\, dy + b\, r_i \int_0^{1/2} \frac{\partial}{\partial x}(\rho u^2)\, dy$$

$$- u_m b^2 \int_0^{1/2} \frac{\partial}{\partial x}(\rho u)\, y\, dy - u_m b\, r_i \int_0^{1/2} \frac{\partial}{\partial x}(\rho u)\, dy + (u_m - u_j)\rho_j u_j r_i \frac{dr_i}{dx}$$

$$= \tau_m (r_i + b/2) - \frac{dP_w}{dx}\frac{(r_i + b/2)^2}{2} \qquad (48a)$$

57

The inviscid stream parameters $(\rho_j, u_j, \rho_a, u_a)$ are isentropic functions of only p_w, and the non-integral terms of eqs. (46a) – (48a) can be expressed directly in terms of the flow field variables (x, p_w, r_i, b).

The integrands of the integral terms of eqs. (46a) – (48a) are $\partial/\partial x\ (\rho u)$ and $\partial/\partial x\ (\rho u^2)$, and these integrands must now be expressed in terms of the variables (x, p_w, r_i, b). The parameters ρ and u are actually functions of (x, r), however, assume for the moment that ρ and u are functions of the independent variables (x, r, p_w, r_i, b). Then one can write

$$\rho(x,r) = \bar{\rho}(x, r, p_w, r_i, b)$$

and

$$u(x,r) = \bar{u}(x, r, p_w, r_i, b)$$

where $\rho = \bar{\rho}$ and $u = \bar{u}$, the only difference being the variables which are considered independent. Application of the chain rule for differentiation of composite functions gives

$$\frac{\partial \rho}{\partial x} = \frac{\partial \bar{\rho}}{\partial x} + \frac{\partial \bar{\rho}}{\partial p_w}\frac{dp_w}{dx} + \frac{\partial \bar{\rho}}{\partial r_i}\frac{dr_i}{dx} + \frac{\partial \bar{\rho}}{\partial b}\frac{db}{dx} \tag{51}$$

and

$$\frac{\partial u}{\partial x} = \frac{\partial \bar{u}}{\partial x} + \frac{\partial \bar{u}}{\partial p_w}\frac{dp_w}{dx} + \frac{\partial \bar{u}}{\partial r_i}\frac{dr_i}{dx} + \frac{\partial \bar{u}}{\partial b}\frac{db}{dx} \tag{52}$$

Applying eqs. (51) and (52) to the integrands $\partial/\partial x\ (\rho u)$ and $\partial/\partial x\ (\rho u^2)$, one obtains

$$\frac{\partial}{\partial x}(\rho u) = \rho\frac{\partial u}{\partial x} + u\frac{\partial \rho}{\partial x} = \left(\rho\frac{\partial \bar{u}}{\partial x} + u\frac{\partial \bar{\rho}}{\partial x}\right) + \frac{dp_w}{dx}\left(\rho\frac{\partial \bar{u}}{\partial p_w} + u\frac{\partial \bar{\rho}}{\partial p_w}\right)$$

$$+ \frac{dr_i}{dx}\left(\rho\frac{\partial \bar{u}}{\partial r_i} + u\frac{\partial \bar{\rho}}{\partial r_i}\right) + \frac{db}{dx}\left(\rho\frac{\partial \bar{u}}{\partial b} + u\frac{\partial \bar{\rho}}{\partial b}\right) \tag{53}$$

and

$$\frac{\partial}{\partial x}(\rho u^2) = 2\rho u \frac{\partial u}{\partial x} + u^2 \frac{\partial \rho}{\partial x} = \left(2\rho u \frac{\partial \bar{u}}{\partial x} + u^2 \frac{\partial \bar{\rho}}{\partial x}\right)$$
$$+ \frac{dP_w}{dx}\left(2\rho u \frac{\partial \bar{u}}{\partial P_w} + u^2 \frac{\partial \bar{\rho}}{\partial P_w}\right) + \frac{dr_i}{dx}\left(2\rho u \frac{\partial \bar{u}}{\partial r_i} + u^2 \frac{\partial \bar{\rho}}{\partial r_i}\right)$$
$$+ \frac{db}{dx}\left(2\rho u \frac{\partial \bar{u}}{\partial b} + u^2 \frac{\partial \bar{\rho}}{\partial b}\right) \quad (54)$$

Substituting eqs. (53) and (54) into eqs. (46a) through (48a), one obtains after expansion of the non-integral terms and considerable rearrangement:

Continuity equation:

$$F_1 \frac{dP_w}{dx} + F_2 \frac{dr_i}{dx} + F_3 \frac{db}{dx} = F_4 \quad (55)$$

Total momentum equation

$$G_1 \frac{dP_w}{dx} + G_2 \frac{dr_i}{dx} + G_3 \frac{db}{dx} = G_4 \quad (56)$$

Half-radius momentum equation

$$H_1 \frac{dP_w}{dx} + H_2 \frac{dr_i}{dx} + H_3 \frac{db}{dx} = H_4 \quad (57)$$

The coefficients of eqs. (55) - (57) are given by the following equations:

$$F_1 = b^2 \int_0^1 \left(\rho \frac{\partial \bar{u}}{\partial P_w} + u \frac{\partial \bar{\rho}}{\partial P_w}\right) y \, dy + b r_i \int_0^1 \left(\rho \frac{\partial \bar{u}}{\partial P_w} + u \frac{\partial \bar{\rho}}{\partial P_w}\right) dy$$
$$+ u_j \frac{r_i^2}{2} \frac{dP_j}{dP_w} + \rho_j \frac{r_i^2}{2} \frac{du_j}{dP_w} + \frac{u_a}{2}\left[r_w^2 - (r_i + b)^2\right]\frac{d\rho_a}{dP_w}$$
$$+ \frac{\rho_a}{2}\left[r_w^2 - (r_i + b)^2\right]\frac{du_a}{dP_w}$$

$$(55a)$$

$$F_2 = b^2 \int_0^1 \left(\rho \frac{\partial \bar{u}}{\partial r_i} + u \frac{\partial \bar{\rho}}{\partial r_i} \right) y \, dy + b r_i \int_0^1 \left(\rho \frac{\partial \bar{u}}{\partial r_i} + u \frac{\partial \bar{\rho}}{\partial r_i} \right) dy \quad \text{(55b)}$$

$$F_3 = b^2 \int_0^1 \left(\rho \frac{\partial \bar{u}}{\partial b} + u \frac{\partial \bar{\rho}}{\partial b} \right) y \, dy + b r_i \int_0^1 \left(\rho \frac{\partial \bar{u}}{\partial b} + u \frac{\partial \bar{\rho}}{\partial b} \right) dy \quad \text{(55c)}$$

$$F_4 = -b^2 \int_0^1 \left(\rho \frac{\partial \bar{u}}{\partial x} + u \frac{\partial \bar{\rho}}{\partial x} \right) y \, dy - b r_i \int_0^1 \left(\rho \frac{\partial \bar{u}}{\partial x} + u \frac{\partial \bar{\rho}}{\partial x} \right) dy$$

$$- \rho_a u_a r_w \frac{d r_w}{d x} \quad \text{(55d)}$$

$$G_1 = b^2 \int_0^1 \left(2\rho u \frac{\partial \bar{u}}{\partial P_w} + u^2 \frac{\partial \bar{\rho}}{\partial P_w} \right) y \, dy + b r_i \int_0^1 \left(2\rho u \frac{\partial \bar{u}}{\partial P_w} + u^2 \frac{\partial \bar{\rho}}{\partial P_w} \right) dy$$

$$+ \frac{r_w^2}{2} + \rho_j u_j r_i^2 \frac{d u_j}{d P_w} + u_j^2 \frac{r_i^2}{2} \frac{d \rho_j}{d P_w}$$

$$+ \frac{u_a^2}{2} \left[r_w^2 - (r_i + b)^2 \right] \frac{d \rho_a}{d P_w} + \rho_a u_a \left[r_w^2 - (r_i + b)^2 \right] \frac{d u_a}{d P_w} \quad \text{(56a)}$$

$$G_2 = b^2 \int_0^1 \left(2\rho u \frac{\partial \bar{u}}{\partial r_i} + u^2 \frac{\partial \bar{\rho}}{\partial r_i} \right) y \, dy + b r_i \int_0^1 \left(2\rho u \frac{\partial \bar{u}}{\partial r_i} + u^2 \frac{\partial \bar{\rho}}{\partial r_i} \right) dy \quad \text{(56b)}$$

$$G_3 = b^2 \int_0^1 \left(2\rho u \frac{\partial \bar{u}}{\partial b} + u^2 \frac{\partial \bar{\rho}}{\partial b} \right) y \, dy + b r_i \int_0^1 \left(2\rho u \frac{\partial \bar{u}}{\partial b} + u^2 \frac{\partial \bar{\rho}}{\partial b} \right) dy \quad \text{(56c)}$$

$$G_4 = -b^2 \int_0^1 \left(2\rho u \frac{\partial \bar{u}}{\partial x} + u^2 \frac{\partial \bar{\rho}}{\partial x} \right) y \, dy$$

$$- b r_i \int_0^1 \left(2\rho u \frac{\partial \bar{u}}{\partial x} + u^2 \frac{\partial \bar{\rho}}{\partial x} \right) dy - \rho_a u_a^2 r_w \frac{d r_w}{d x}$$

$$\text{(56d)}$$

$$H_1 = b^2 \int_0^{1/2} \left(2\rho u \frac{\partial \bar{u}}{\partial P_w} + u^2 \frac{\partial \bar{P}}{\partial P_w}\right) y \, dy + b r_i \int_0^{1/2} \left(2\rho u \frac{\partial \bar{u}}{\partial P_w} + u^2 \frac{\partial \bar{P}}{\partial P_w}\right) dy$$

$$- u_m b^2 \int_0^{1/2} \left(\rho \frac{\partial \bar{u}}{\partial P_w} + u \frac{\partial \bar{P}}{\partial P_w}\right) y \, dy - u_m b r_i \int_0^{1/2} \left(\rho \frac{\partial \bar{u}}{\partial P_w} + u \frac{\partial \bar{P}}{\partial P_w}\right) dy$$

$$+ \frac{(r_i + b/2)^2}{2} + (u_j - u_m) u_j \frac{r_i^2}{2} \frac{dP_j}{dP_w} + (2u_j - u_m) P_j \frac{r_i^2}{2} \frac{du_j}{dP_w}$$

(57a)

$$H_2 = b^2 \int_0^{1/2} \left(2\rho u \frac{\partial \bar{u}}{\partial r_i} + u^2 \frac{\partial \bar{P}}{\partial r_i}\right) y \, dy + b r_i \int_0^{1/2} \left(2\rho u \frac{\partial \bar{u}}{\partial r_i} + u^2 \frac{\partial \bar{P}}{\partial r_i}\right) dy$$

$$- u_m b^2 \int_0^{1/2} \left(\rho \frac{\partial \bar{u}}{\partial r_i} + u \frac{\partial \bar{P}}{\partial r_i}\right) y \, dy - u_m b r_i \int_0^{1/2} \left(\rho \frac{\partial \bar{u}}{\partial r_i} + u \frac{\partial \bar{P}}{\partial r_i}\right) dy$$

(57b)

$$H_3 = b^2 \int_0^{1/2} \left(2\rho u \frac{\partial \bar{u}}{\partial b} + u^2 \frac{\partial \bar{P}}{\partial b}\right) y \, dy + b r_i \int_0^{1/2} \left(2\rho u \frac{\partial \bar{u}}{\partial b} + u^2 \frac{\partial \bar{P}}{\partial b}\right) dy$$

$$- u_m b^2 \int_0^{1/2} \left(\rho \frac{\partial \bar{u}}{\partial b} + u \frac{\partial \bar{P}}{\partial b}\right) y \, dy - u_m b r_i \int_0^{1/2} \left(\rho \frac{\partial \bar{u}}{\partial b} + u \frac{\partial \bar{P}}{\partial b}\right) dy$$

(57c)

$$H_4 = -b^2 \int_0^{1/2} \left(2\rho u \frac{\partial \bar{u}}{\partial x} + u^2 \frac{\partial \bar{P}}{\partial x}\right) y \, dy - b r_i \int_0^{1/2} \left(2\rho u \frac{\partial \bar{u}}{\partial x} + u^2 \frac{\partial \bar{P}}{\partial x}\right) dy$$

$$+ u_m b^2 \int_0^{1/2} \left(\rho \frac{\partial \bar{u}}{\partial x} + u \frac{\partial \bar{P}}{\partial x}\right) y \, dy + u_m b r_i \int_0^{1/2} \left(\rho \frac{\partial \bar{u}}{\partial x} + u \frac{\partial \bar{P}}{\partial x}\right) dy$$

$$+ \tau_m \left(r_i + b/2\right)$$

(57d)

All of the auxiliary equations required to evaluate the coefficients F, G and H are presented in Appendix I.

Equations (55) – (57) are linear in the derivatives dp_w/dx, dr_1/dx and db/dx, therefore these equations can be solved for the derivatives by application of Cramer's rule, as long as the determinant of the coefficients is not zero:

$$\frac{dp_w}{dx} = \frac{|P|}{|D|} \tag{58}$$

$$\frac{dr_i}{dx} = \frac{|R|}{|D|} \tag{59}$$

$$\frac{db}{dx} = \frac{|B|}{|D|} \tag{60}$$

where the determinants are:

$$|D| = \begin{vmatrix} F_1 & F_2 & F_3 \\ G_1 & G_2 & G_3 \\ H_1 & H_2 & H_3 \end{vmatrix} \quad \text{(coefficient determinant)}$$

$$|P| = \begin{vmatrix} F_4 & F_2 & F_3 \\ G_4 & G_2 & G_3 \\ H_4 & H_2 & H_3 \end{vmatrix}$$

$$|B| = \begin{vmatrix} F_1 & F_2 & F_4 \\ G_1 & G_2 & G_4 \\ H_1 & H_2 & H_4 \end{vmatrix}$$

$$|R| = \begin{vmatrix} F_1 & F_4 & F_3 \\ G_1 & G_4 & G_3 \\ H_1 & H_4 & H_3 \end{vmatrix}$$

Equations (58) – (60) can be numerically integrated with standard techniques for prescribed initial conditions. The numerical technique used in this investigation was the well known Runge–Kutta method (Ref. 41).

2. Second Regime Transformation

The three second regime equations which were derived in Section IV are as follows:

Continuity equation

$$\frac{d}{dx}\int_{0}^{b}\rho u\, r\, dr + \frac{d}{dx}\left[\rho_a u_a \frac{r_w^2 - b^2}{2}\right] = 0 \tag{16}$$

Total momentum equation

$$\frac{d}{dx}\int_{0}^{b}\rho u^2 r\, dr + \frac{d}{dx}\left[\rho_a u_a^2 \frac{r_w^2 - b^2}{2}\right] = -\frac{dp_w}{dx}\frac{r_w^2}{2} \tag{17}$$

Half-radius momentum equation

$$\frac{d}{dx}\int_{0}^{b/2}\rho u^2 r\, dr - u_m \frac{d}{dx}\int_{0}^{b/2}\rho u\, r\, dr = \tau_m \, b/2 - \frac{dp_w}{dx}\frac{b^2}{8} \tag{18}$$

In the second regime $r_i = 0$, and the three flow field variables are chosen to be p_w, the centerline velocity u_c, and b. The mixing zone coordinate in the second regime is $y = \frac{r}{b}$, therefore

$$\int_{0}^{b}(\ )\, r\, dr = b^2 \int_{0}^{1}(\ )\, y\, dy \tag{61}$$

and

$$\int_{0}^{b/2}(\ )\, r\, dr = b^2 \int_{0}^{1/2}(\ )\, y\, dy \tag{62}$$

Equations (16) — (18) are transformed in the same way as the first regime equations, with the exceptions that the variable u_c is substituted for r_i, and eqs. (61) and (62) are used in place of eqs. (49) and (50). One obtains the following system of equations for the derivatives dp_w/dx, du_c/dx, db/dx:

Continuity equation

$$F_1 \frac{dP_W}{dx} + F_2 \frac{dU_c}{dx} + F_3 \frac{db}{dx} = F_4 \tag{63}$$

Total momentum equation

$$G_1 \frac{dP_W}{dx} + G_2 \frac{dU_c}{dx} + G_3 \frac{db}{dx} = G_4 \tag{64}$$

Half-radius momentum equation

$$H_1 \frac{dP_W}{dx} + H_2 \frac{dU_c}{dx} + H_3 \frac{db}{dx} = H_4 \tag{65}$$

The coefficients of eqs. (63) — (65) are given by the following equations:

$$F_1 = b^2 \int_0^1 \left(\rho \frac{\partial \bar{u}}{\partial P_W} + u \frac{\partial \bar{\rho}}{\partial P_W} \right) y \, dy + \frac{U_a}{2}\left(r_w^2 - b^2\right)\frac{dP_a}{dP_W}$$
$$+ \frac{P_a}{2}\left(r_w^2 - b^2\right)\frac{dU_a}{dP_W} \tag{63a}$$

$$F_2 = b^2 \int_0^1 \left(\rho \frac{\partial \bar{u}}{\partial u_c} + u \frac{\partial \bar{\rho}}{\partial u_c} \right) y \, dy \tag{63b}$$

$$F_3 = b^2 \int_0^1 \left(\rho \frac{\partial \bar{u}}{\partial b} + u \frac{\partial \bar{\rho}}{\partial b} \right) y \, dy \tag{63c}$$

$$F_4 = -b^2 \int_0^1 \left(\rho \frac{\partial \bar{u}}{\partial x} + u \frac{\partial \bar{\rho}}{\partial x} \right) y \, dy - P_a U_a r_w \frac{dr_w}{dx} \tag{63d}$$

$$G_1 = b^2 \int_0^1 \left(2\rho u \frac{\partial \bar{u}}{\partial P_W} + u^2 \frac{\partial \bar{\rho}}{\partial P_W} \right) y \, dy + r_w^2/2$$
$$+ P_a U_a \left(r_w^2 - b^2\right)\frac{dU_a}{dP_W} + \frac{U_a^2}{2}\left(r_w^2 - b^2\right)\frac{dP_a}{dP_W} \tag{64a}$$

64

$$G_2 = b^2 \int_0^1 \left(2\rho u \frac{\partial \bar{u}}{\partial u_c} + u^2 \frac{\partial \bar{\rho}}{\partial u_c} \right) y \, dy \tag{64b}$$

$$G_3 = b^2 \int_0^1 \left(2\rho u \frac{\partial \bar{u}}{\partial b} + u^2 \frac{\partial \bar{\rho}}{\partial b} \right) y \, dy \tag{64c}$$

$$G_4 = -b^2 \int_0^1 \left(2\rho u \frac{\partial \bar{u}}{\partial x} + u^2 \frac{\partial \bar{\rho}}{\partial x} \right) y \, dy$$
$$- \rho_a u_a^2 r_w \frac{d r_w}{dx} \tag{64d}$$

$$H_1 = b^2 \int_0^{1/2} \left(2\rho u \frac{\partial \bar{u}}{\partial P_w} + u^2 \frac{\partial \bar{\rho}}{\partial P_w} \right) y \, dy$$
$$- u_m b^2 \int_0^{1/2} \left(\rho \frac{\partial \bar{u}}{\partial P_w} + u \frac{\partial \bar{\rho}}{\partial P_w} \right) y \, dy + b^2/8 \tag{65a}$$

$$H_2 = b^2 \int_0^{1/2} \left(2\rho u \frac{\partial \bar{u}}{\partial u_c} + u^2 \frac{\partial \bar{\rho}}{\partial u_c} \right) y \, dy$$
$$- u_m b^2 \int_0^{1/2} \left(\rho \frac{\partial \bar{u}}{\partial u_c} + u \frac{\partial \bar{\rho}}{\partial u_c} \right) y \, dy \tag{65b}$$

$$H_3 = b^2 \int_0^{1/2} \left(2\rho u \frac{\partial \bar{u}}{\partial b} + u^2 \frac{\partial \bar{\rho}}{\partial b} \right) y \, dy$$
$$- u_m b^2 \int_0^{1/2} \left(\rho \frac{\partial \bar{u}}{\partial b} + u \frac{\partial \bar{\rho}}{\partial b} \right) y \, dy \tag{65c}$$

$$H_4 = -b^2 \int_0^{1/2} \left(2\rho u \frac{\partial \bar{u}}{\partial x} + u^2 \frac{\partial \bar{\rho}}{\partial x} \right) y \, dy$$
$$+ u_m b^2 \int_0^{1/2} \left(\rho \frac{\partial \bar{u}}{\partial x} + u \frac{\partial \bar{\rho}}{\partial x} \right) y \, dy + \tau_m \frac{b}{2} \tag{65d}$$

All of the auxiliary equations required to evaluate the coefficients F, G and H are presented in Appendix I.

Equations (63) – (65) can be solved for the derivatives of dp_w/dx, du_c/dx and db/dx in the same way as in the first regime, except that eq. (59) is replaced by

$$\frac{d u_c}{d x} = \frac{|U_c|}{|D|} \tag{66}$$

where

$$|U_c| = \begin{vmatrix} F_1 & F_4 & F_3 \\ G_1 & G_4 & G_3 \\ H_1 & H_4 & H_3 \end{vmatrix}$$

3. Third Regime Transformation

The three third regime integral equations which were derived in Section IV are as follows:

Continuity equation

$$\frac{d}{dx} \int_0^{r_w} \rho u r \, dr = 0 \tag{19}$$

Total momentum equation

$$\frac{d}{dx} \int_0^{r_w} \rho u^2 r \, dr = -\frac{d p_w}{dx} \frac{r_w^2}{2} \tag{20}$$

Half–radius momentum equation

$$\frac{d}{dx} \int_0^{r_w/2} \rho u^2 r \, dr - u_m \frac{d}{dx} \int_0^{r_w/2} \rho u r \, dr = \tau_m \frac{r_w}{2} - \frac{d p_w}{dx} \frac{r_w^2}{8} \tag{21}$$

In the third regime $b = r_w$, and the three flow variables are chosen to be (p_w, u_c and u_w). The mixing zone coordinate is $y = \dfrac{r}{r_w}$, therefore

$$\int_0^{r_w} (\ ) r \, dr = r_w{}^2 \int_0^1 (\ ) y \, dy \qquad\qquad (67)$$

and

$$\int_0^{r_w/2} (\ ) r \, dr = r_w{}^2 \int_0^{1/2} (\ ) y \, dy \qquad\qquad (68)$$

Equations (19) – (21) are transformed in the same way as the first regime equations, with the exceptions that the variables r_1 and b are replaced by the centerline velocity, u_c, and the wall velocity, u_w; eqs. (67) and (68) are used instead of eqs. (49) and (50). One obtains the following system of equations for the derivatives dp_w/dx, du_c/dx and du_w/dx:

Continuity equation

$$F_1 \frac{dp_w}{dx} + F_2 \frac{du_c}{dx} + F_3 \frac{du_w}{dx} = F_4 \qquad\qquad (69)$$

Total momentum equation

$$G_1 \frac{dp_w}{dx} + G_2 \frac{du_c}{dx} + G_3 \frac{du_w}{dx} = G_4 \qquad\qquad (70)$$

Half-radius momentum equation

$$H_1 \frac{dp_w}{dx} + H_2 \frac{du_c}{dx} + H_3 \frac{du_w}{dx} = H_4 \qquad\qquad (71)$$

The coefficients of eqs. (69) – (71) are given by the following equations:

$$F_1 = r_w{}^2 \int_0^1 \left(\rho \frac{\partial \bar{u}}{\partial p_w} + u \frac{\partial \bar{\rho}}{\partial p_w} \right) y \, dy \qquad\qquad (69a)$$

$$F_2 = r_w{}^2 \int_0^1 \left(\rho \frac{\partial \bar{u}}{\partial u_c} + u \frac{\partial \bar{\rho}}{\partial u_c} \right) y \, dy \qquad\qquad (69b)$$

$$F_3 = r_w^2 \int_0^1 \left(\rho \frac{\partial \bar{u}}{\partial u_w} + u \frac{\partial \bar{\rho}}{\partial u_w} \right) y \, dy \tag{69c}$$

$$F_4 = -r_w^2 \int_0^1 \left(\rho \frac{\partial \bar{u}}{\partial x} + u \frac{\partial \bar{\rho}}{\partial x} \right) y \, dy - \rho_w u_w r_w \frac{dr_w}{dx} \tag{69d}$$

$$G_1 = r_w^2 \int_0^1 \left(2\rho u \frac{\partial \bar{u}}{\partial \rho_w} + u^2 \frac{\partial \bar{\rho}}{\partial \rho_w} \right) y \, dy + \frac{r_w^2}{2} \tag{70a}$$

$$G_2 = r_w^2 \int_0^1 \left(2\rho u \frac{\partial \bar{u}}{\partial u_c} + u^2 \frac{\partial \bar{\rho}}{\partial u_c} \right) y \, dy \tag{70b}$$

$$G_3 = r_w^2 \int_0^1 \left(2\rho u \frac{\partial \bar{u}}{\partial u_w} + u^2 \frac{\partial \bar{\rho}}{\partial u_w} \right) y \, dy \tag{70c}$$

$$G_4 = -r_w^2 \int_0^1 \left(2\rho u \frac{\partial \bar{u}}{\partial x} + u^2 \frac{\partial \bar{\rho}}{\partial x} \right) y \, dy$$
$$- \rho_w u_w^2 r_w \frac{dr_w}{dx} \tag{70d}$$

$$H_1 = r_w^2 \int_0^{1/2} \left(2\rho u \frac{\partial \bar{u}}{\partial \rho_w} + u^2 \frac{\partial \bar{\rho}}{\partial \rho_w} \right) y \, dy$$
$$- u_m r_w^2 \int_0^{1/2} \left(\rho \frac{\partial \bar{u}}{\partial \rho_w} + u \frac{\partial \bar{\rho}}{\partial \rho_w} \right) y \, dy + \frac{r_w^2}{8} \tag{71a}$$

$$H_2 = r_w^2 \int_0^{1/2} \left(2\rho u \frac{\partial \bar{u}}{\partial u_c} + u^2 \frac{\partial \bar{\rho}}{\partial u_c} \right) y \, dy$$
$$- u_m r_w^2 \int_0^{1/2} \left(\rho \frac{\partial \bar{u}}{\partial u_c} + u \frac{\partial \bar{\rho}}{\partial u_c} \right) y \, dy \tag{71b}$$

$$H_3 = r_w^2 \int_0^{1/2} \left(2\rho u \frac{\partial \bar{u}}{\partial u_w} + u^2 \frac{\partial \bar{\rho}}{\partial u_w} \right) y \, dy$$

$$- u_m r_w^2 \int_0^{1/2} \left(\rho \frac{\partial \bar{u}}{\partial u_w} + u \frac{\partial \bar{\rho}}{\partial u_w} \right) y \, dy \tag{71c}$$

$$H_4 = -r_w^2 \int_0^{1/2} \left(2\rho u \frac{\partial \bar{u}}{\partial x} + u^2 \frac{\partial \bar{\rho}}{\partial x} \right) y \, dy$$

$$+ u_m r_w^2 \int_0^{1/2} \left(\rho \frac{\partial \bar{u}}{\partial x} + u \frac{\partial \bar{\rho}}{\partial x} \right) y \, dy + \tau_m r_w / 2 \tag{71d}$$

All of the auxiliary functions required to evaluate the coefficients F, G and H are presented in Appendix I.

Equations (69) — (71) can be solved for the derivatives dp_w/dx, du_c/dx and du_w/dx in the same way as in the first regime, except that eq. (59) is replaced by eq. (66), and eq. (60) is replaced by

$$\frac{d u_w}{d x} = \frac{|U_w|}{|D|} \tag{72}$$

where

$$|U_w| = \begin{vmatrix} F_1 & F_2 & F_4 \\ G_1 & G_2 & G_4 \\ H_1 & H_2 & H_4 \end{vmatrix}$$

SECTION VIII
NUMERICAL CONSIDERATIONS

The system of linear differential equations developed in Section VII, with the coefficients evaluated using the equations of Appendix I, was solved by conventional numerical procedures. The computer program is quite lengthy and the details will not be given here. The purpose of this section is to give a brief discussion of the numerical solution from the point of view of the engineering results.

Numerical precision - The integral terms appearing in the coefficients F, G and H (Section VII) are evaluated by means of a sixteen point Gaussian quadrature formula. No improvement in the solutions was found when the integrations were made with a 32 point quadrature formula.

The axial step size, Δx, for the Runge-Kutta integrations of the set of differential equations is an input to the program. The solutions have been found insensitive to Δx, and the step size is chosen primarily for convenience in defining the solution. Typically, Δx is chosen to be 0.3 - 1.0 times the primary nozzle radius, r_n.

Computation time - The numerical solutions were obtained by use of an IBM-360/50 digital computer. A typical problem is solved in 30 to 40 axial steps, requiring a computation time of approximately 2 minutes.

Program inputs and printout - The input parameters and parameters which are printed out are given in Appendix III.

SECTION IX
CORRELATION OF 1-D CORE THEORY WITH EXPERIMENTS

"Most of the correlations between theory and experiment have been made with the 2-D Core Theory (Part II). The 1-D Core Theory has been correlated with low speed air-air experiments in order to establish the incompressible values of the eddy viscosity constants (Section VI) and to establish the validity of the theory for constant density flows.

1. Low Speed Isobaric Mixing Experiments

Forstall and Shapiro (Ref. 18) made a series of coaxial mixing experiments with u_a/u_j = 0.2, 0.25 and 0.5. The experimental configuration was ducted, but the duct was sufficiently large in diameter so that the induced axial pressure gradients were negligible. Only the first and second mixing regimes were observed in these experiments. The experimental lengths of the inviscid core (length of the first regime) are shown in Fig. 6 along with the core lengths predicted by the 1-D Core Theory with k_{oI} = 0.007. Also shown in Fig. 6 is the experimental inviscid core length from the zero secondary velocity experiments of Corrsin and Uberoi (Ref. 42). The experimental inviscid core lengths were obtained by using the accepted procedure of plotting the second regime centerline velocity ratio, $(u_c - u_a)/(u_j - u_a)$ vs. x on a log-log plot and then extrapolating the distribution back to the axial position where $(u_c - u_a)/(u_j - u_a)$ equals one. Referring to Fig. 6, it is seen that the theoretical core length is smaller than the experimental value at low secondary velocity, but that the agreement is satisfactory at velocity ratios of 0.2 and 0.25. The theoretical core length is approximately 25 per cent larger than the experimental value at u_a/u_j = 0.5.
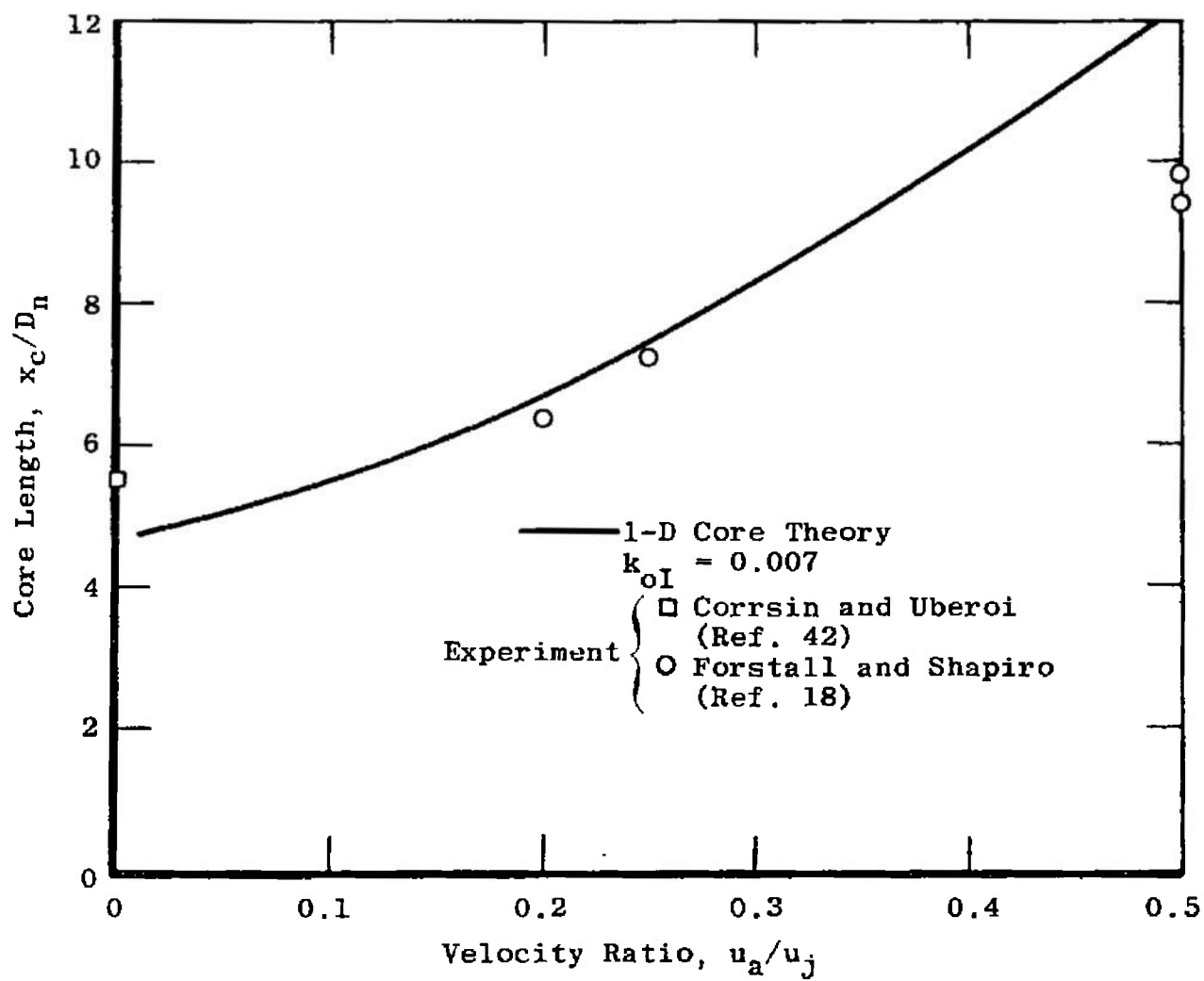
71

Fig. 6 Inviscid Core Lengths for Low Speed Mixing

As discussed in Sections II and VI, this deviation from experiment at velocity ratios larger than about 0.3 is normal for the Prandtl eddy viscosity model.

The axial distribution of the centerline velocity ratio, $(u_c - u_a)/(u_j - u_a)$, is shown in Figs. 7a — d for the Corrsin and Uberoi experiment and for the experiments of Forstall and Shapiro. The theoretical distribution shown in Fig. 7a was computed at $u_a/u_j = 0.01$ because the theory, as currently formulated, cannot be used when the secondary velocity is zero[*]. Referring to Figs. 7a — d, the theory with $k_{oII} = 0.011$ predicts a somewhat excessive rate of decay for the centerline velocity ratio for $u_a/u_j \approx 0$, but the agreement is better for velocity ratios of 0.2 and 0.25. As was the case in the first regime, the predicted rate of mixing in the second regime for $u_a/u_j = 0.5$ (Fig. 7d) is considerably less than shown by the experiment.

One other aspect of the value for k_{oI} should be noted. In the first regime the mixing is initially two-dimensional in nature. One would expect, therefore, that k_{oI} should be approximately the same value as obtained from two-dimensional experiments. Experimental two-dimensional mixing data for zero secondary velocity are usually correlated with the error function profile (Ref. 26),

$$u/u_j = \frac{1}{2}\left[1 + erf\left(\sigma \frac{y}{x}\right)\right]$$

---

[*] The Corrsin and Uberoi experiment was made without a duct. The theoretical curve of Fig. 7a was computed by assuming that the process was ducted, but the duct diameter chosen for the computation was large enough so that the resulting axial pressure gradients were negligible.
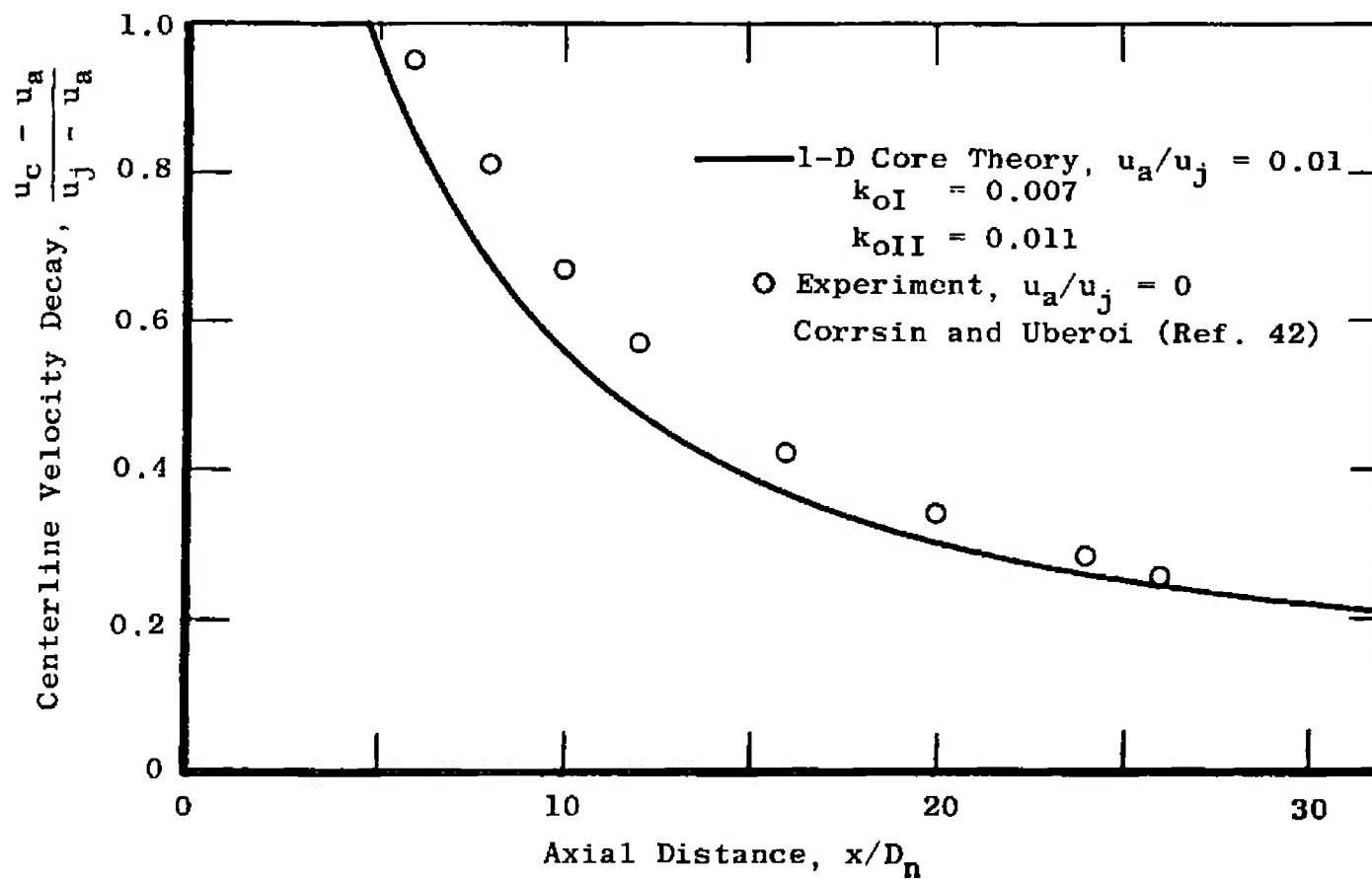
a. $u_a/u_j = 0$

Fig. 7 Centerline Velocity Decay for Low Speed Mixing
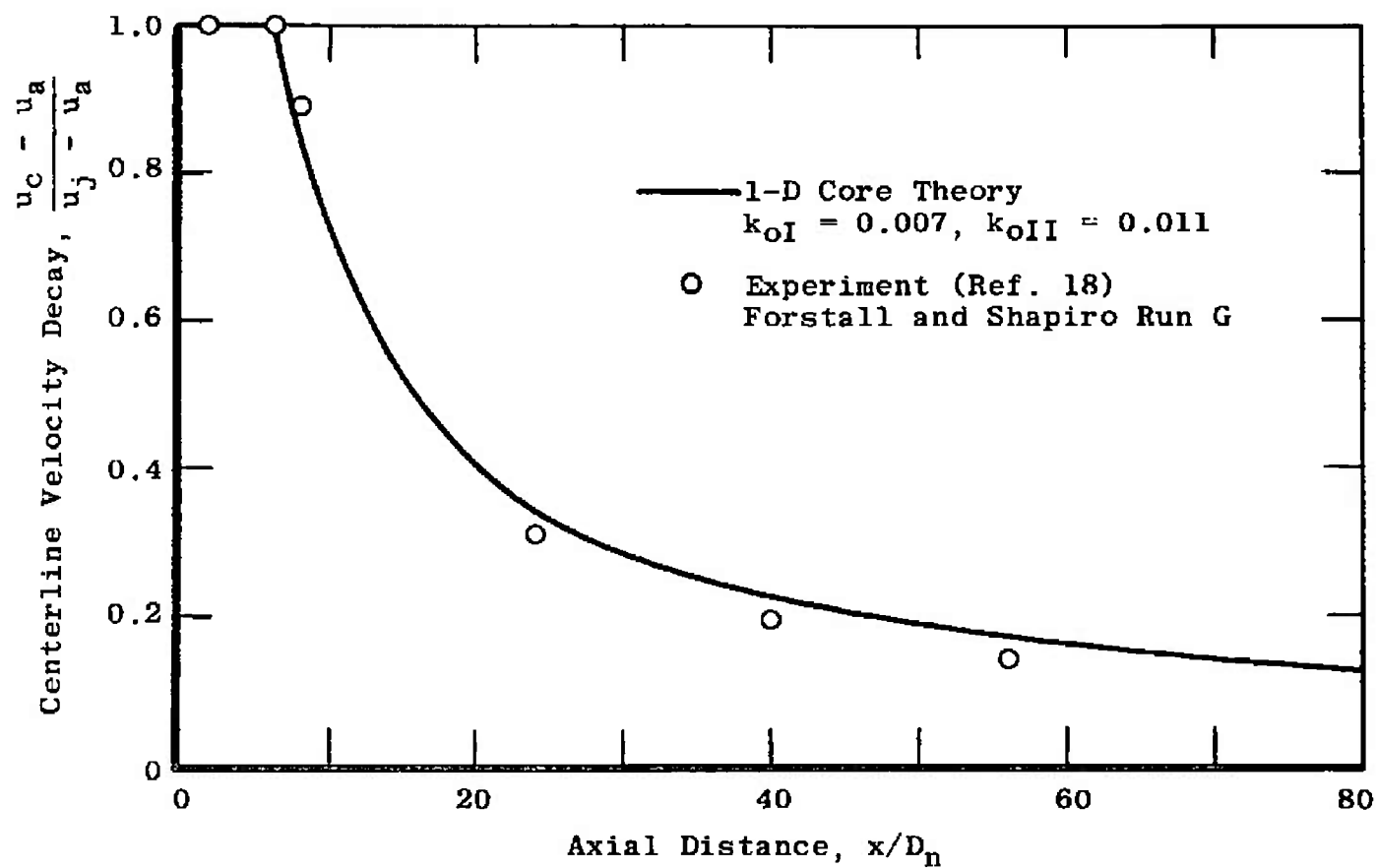
b. $u_a/u_j = 0.2$
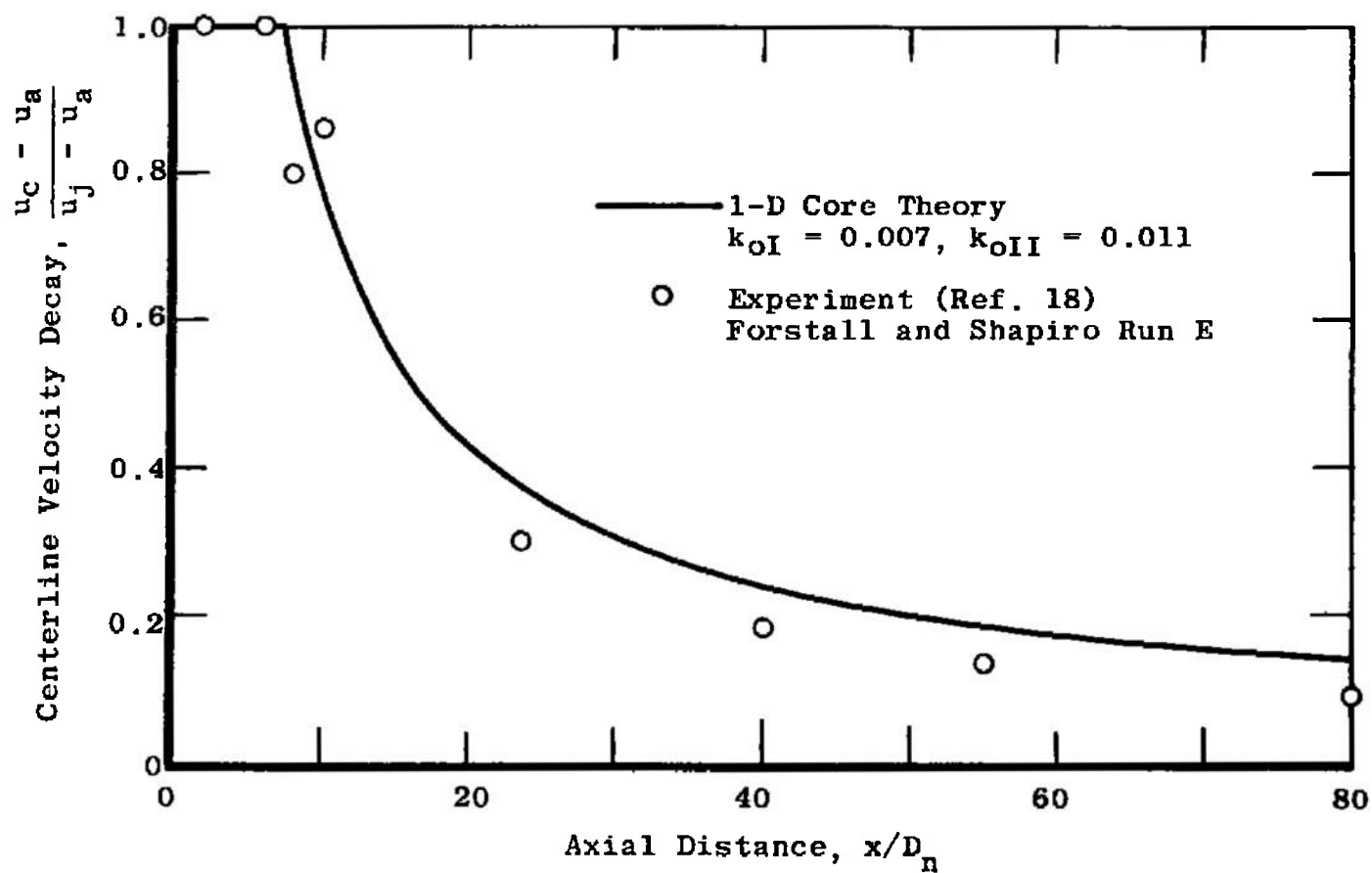
Fig. 7 Continued

c. $u_a/u_j - 0.25$

Fig. 7 Continued
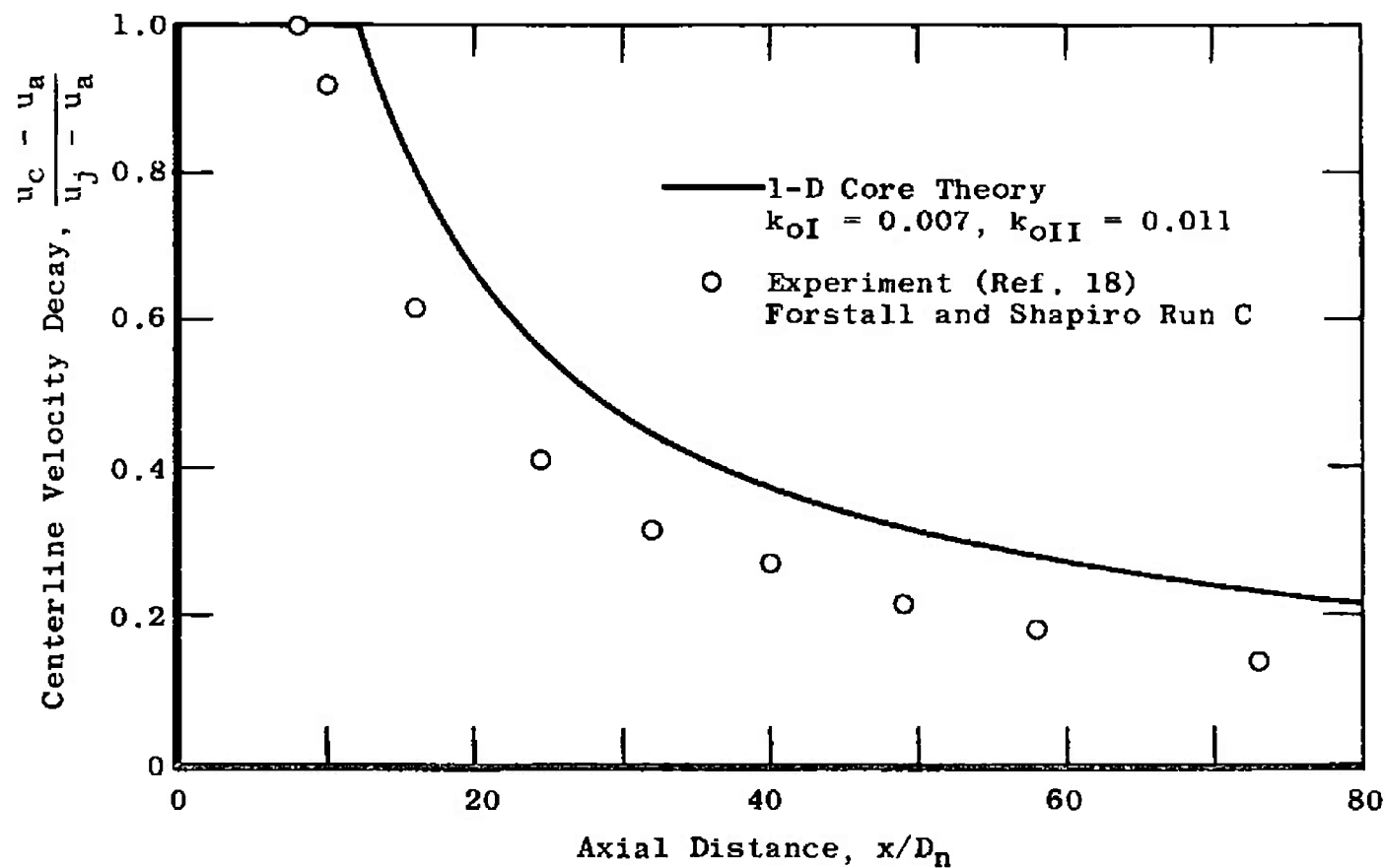
d. $u_a/u_j = 0.5$

Fig. 7 Concluded

where the similarity constant, σ, is inversely proportional to the rate of growth of the mixing layer. The accepted incompressible value for σ is 12. A certain value for σ also implies a certain value for the rate of change with x of the velocity gradient at the half-velocity position in the mixing zone. Computations have shown that the same rate of change of the velocity gradient at the half-velocity position is obtained for the error function profile with $\sigma = 12$ and for the cosine profile with $k_{oI} \approx 0.007$. This result, therefore, tends to substantiate the value of k_{oI} which was used to correlate the 1-D Core Theory with coaxial mixing experiments.

2. Low Speed Jet Pump Experiment

Mikhail (Ref. 31) reported experiments on a low speed jet pump with a cylindrical mixing duct. The apparatus is shown schematically in Fig. 8 along with the initial conditions for the case considered here. Both the primary and secondary streams were unheated air.

The experimental duct pressure distribution is shown in Fig. 9 along with the results of the 1-D Core Theory. All three mixing regimes are encountered in this configuration. The influence of the wall boundary layer on the axial pressure distribution is considerable in this long mixing duct. An approximate linear variation of the wall boundary layer displacement thickness, δ^*, was used to correct the duct contour for the effect of the boundary layer. This wall boundary layer correction, although quite approximate, causes the theoretical pressure distribution to agree satisfactorily with the experiment.

The centerline velocity distribution for the jet pump is shown in Fig. 10. The wall boundary correction is shown to have a relatively small influence on the center-

Secondary Flow
From Atmosphere

$r_n/r_w = 0.26$

Valve for Regulating
Back Pressure

①

$\rightarrow$ $u_{a1} = 48$ ft./sec.

$\rightarrow$ $u_{j1} = 240$ ft./sec.

Cylindrical Mixing Duct
$D_w = 4$ in. (10.2 cm.)
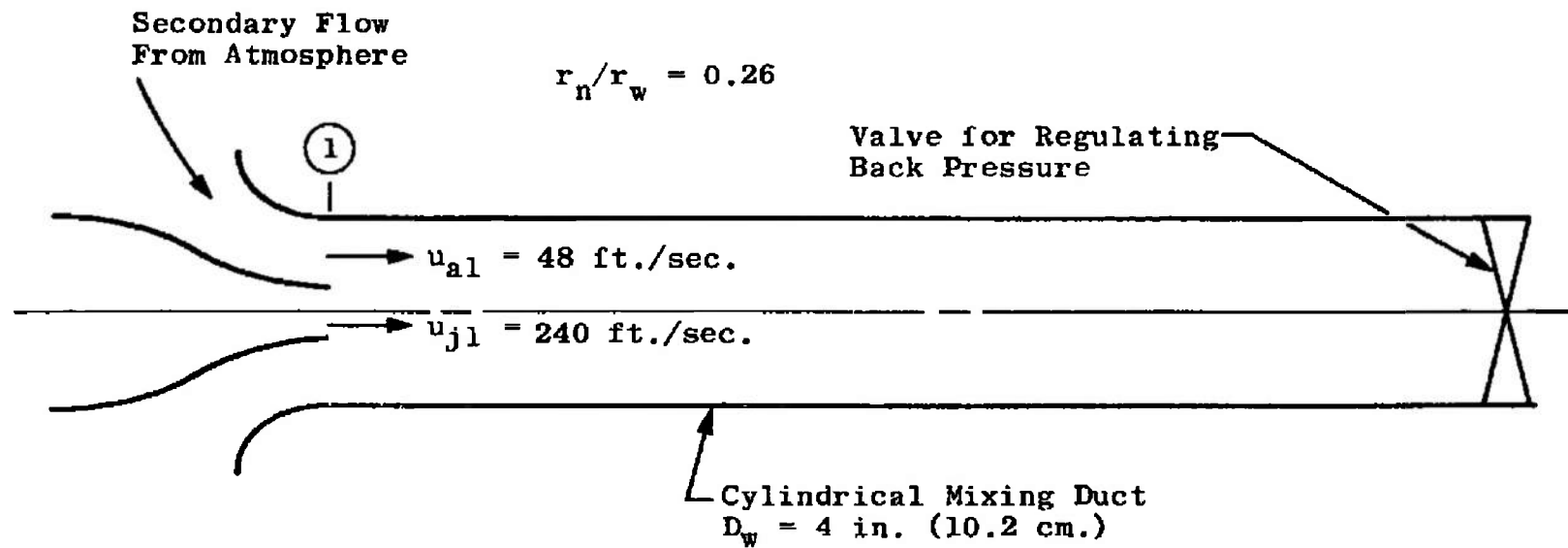
Fig. 8 Apparatus for Low Speed Jet Pump Experiment (Ref. 31)
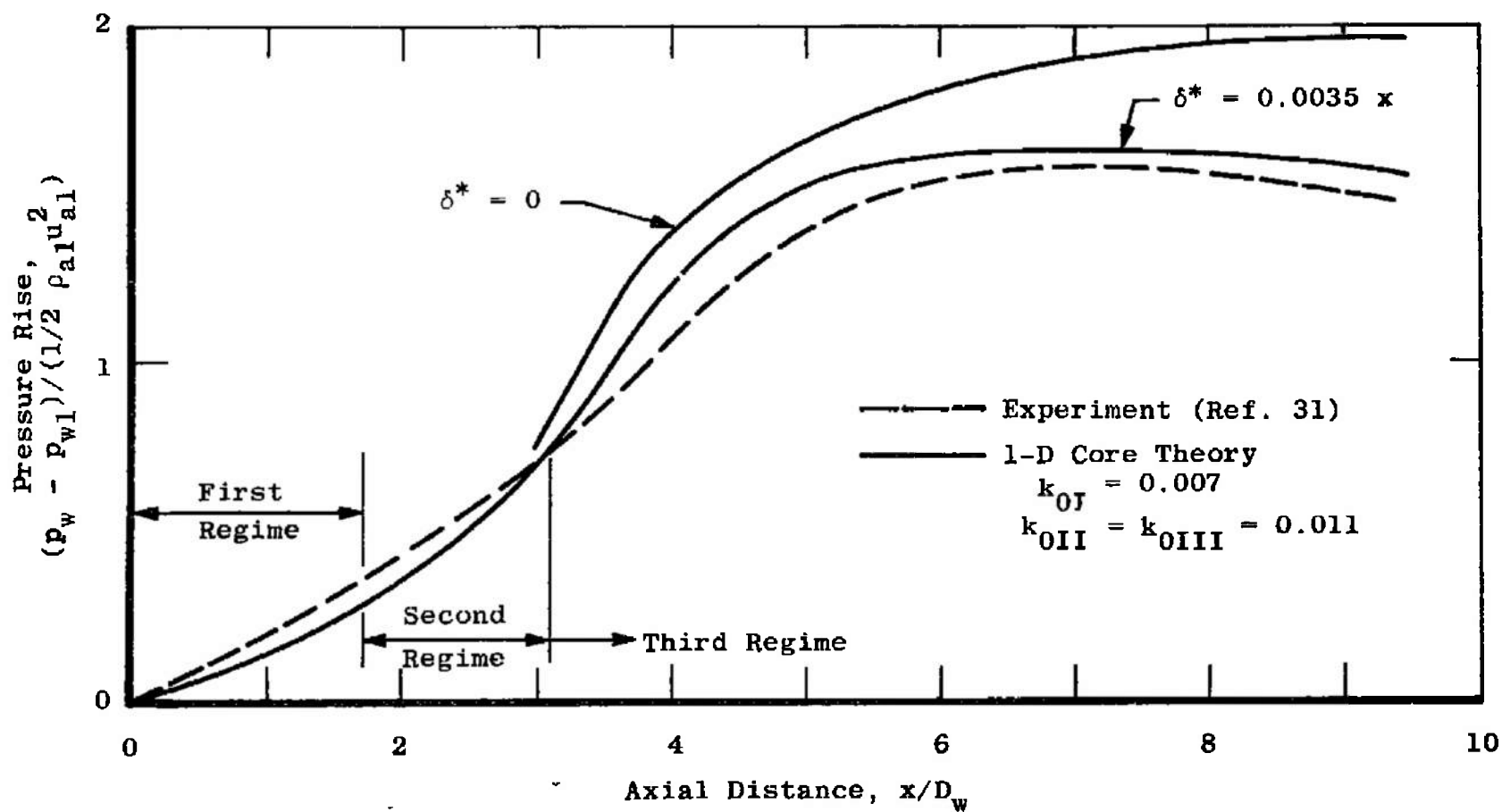
Fig. 9 Wall Pressure Distribution in a Low Speed Jet Pump
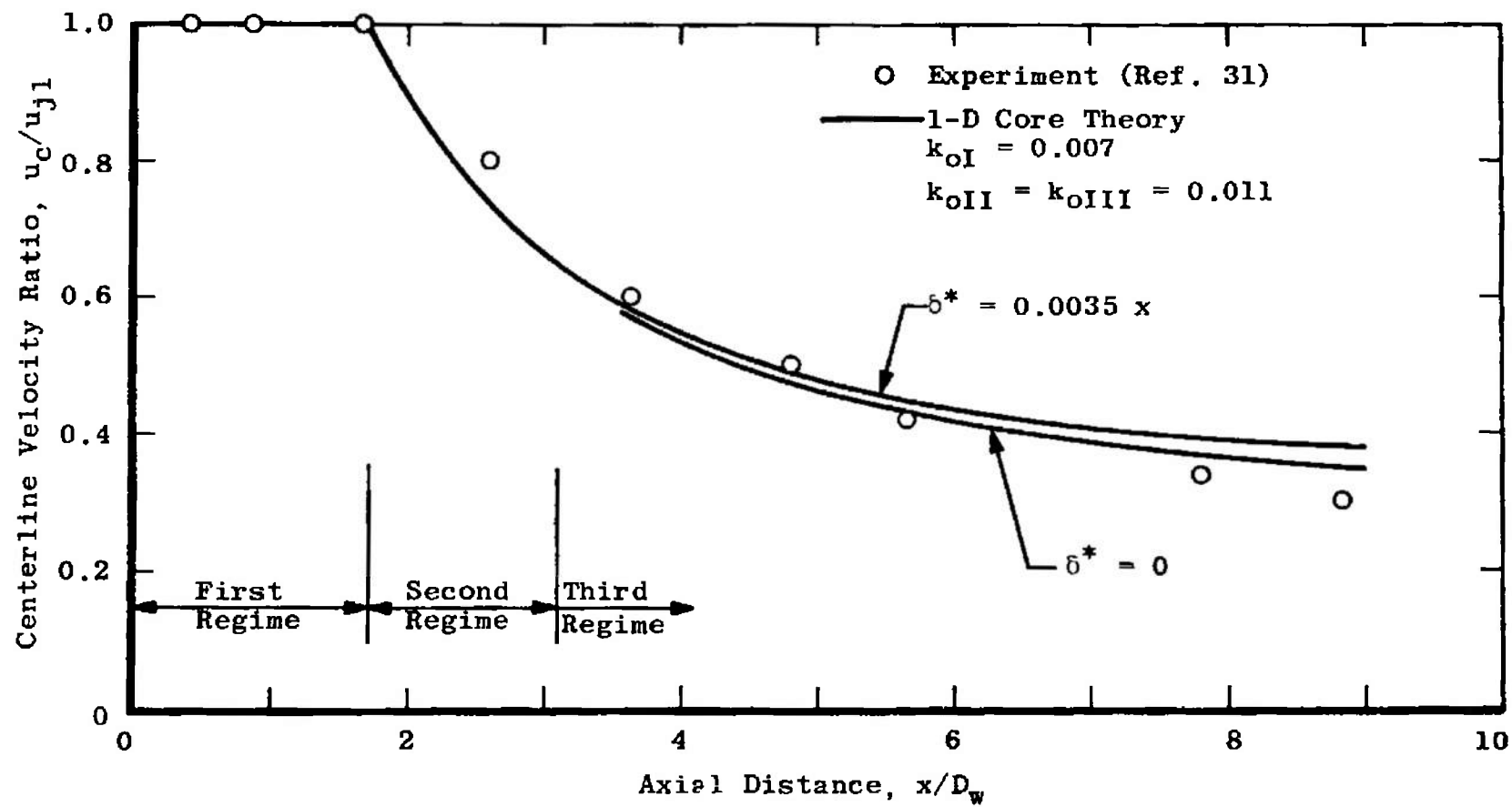
Fig. 10 Centerline Velocity Distribution in a Low Speed Jet Pump

line velocity distribution. In these correlations the third
regime eddy viscosity constant was assumed to be the same
as the second regime constant. The agreement between theory
and experiment indicates that the theoretical model for the
third regime is reasonably valid for an axial distance into
that regime of at least three duct diameters.

Based on these correlations of low speed mixing
experiments, it appears that the theory as formulated
provides a reasonably accurate representation of the con-
stant density mixing process. It should be noted, however,
that the range of applicability of the Prandtl eddy viscosity
model is limited to flows with low secondary velocities
relative to the primary velocity.

PART II
DUCTED MIXING THEORY WITH TWO-DIMENSIONAL INVISCID CORE FLOW
(2-D CORE THEORY)

SECTION X
DEVELOPMENT OF BASIC DIFFERENTIAL-INTEGRAL EQUATIONS

In Part I of this report the first regime flow was solved by assuming that the inviscid core flow is one-dimensional. As pointed out in Section I, the one-dimensional core flow assumption is seriously in error for many practical ducted mixing problems.

In this section, the 2-D Core Theory differential-integral equations are derived for the first mixing regime (Fig. 11). The mixing zone and secondary flow are treated in essentially the same way as in Part I, the major difference being in the method of computing the inviscid core flow. The basic differential-integral equations are derived with the inner mixing zone radius, r_i, as the lower limit on the integrals. (It will be recalled that the corresponding lower limit is zero in the 1-D Core Theory integral equations.) A method of characteristics solution of the inviscid core flow then provides the boundary conditions (at r_i) for the solution of the differential-integral equations.

1. Integration of Boundary Layer Equations

The fundamental equations used in this analysis are the axial momentum equation and the continuity equation (Section IV):

Momentum equation

$$\rho u r \frac{\partial u}{\partial x} + \rho v r \frac{\partial u}{\partial r} = \frac{\partial}{\partial r}(\tau r) - r \frac{\partial p}{\partial x} \tag{1}$$

Continuity equation

$$\frac{\partial}{\partial x}(\rho u r) + \frac{\partial}{\partial r}(\rho v r) = 0 \tag{2}$$
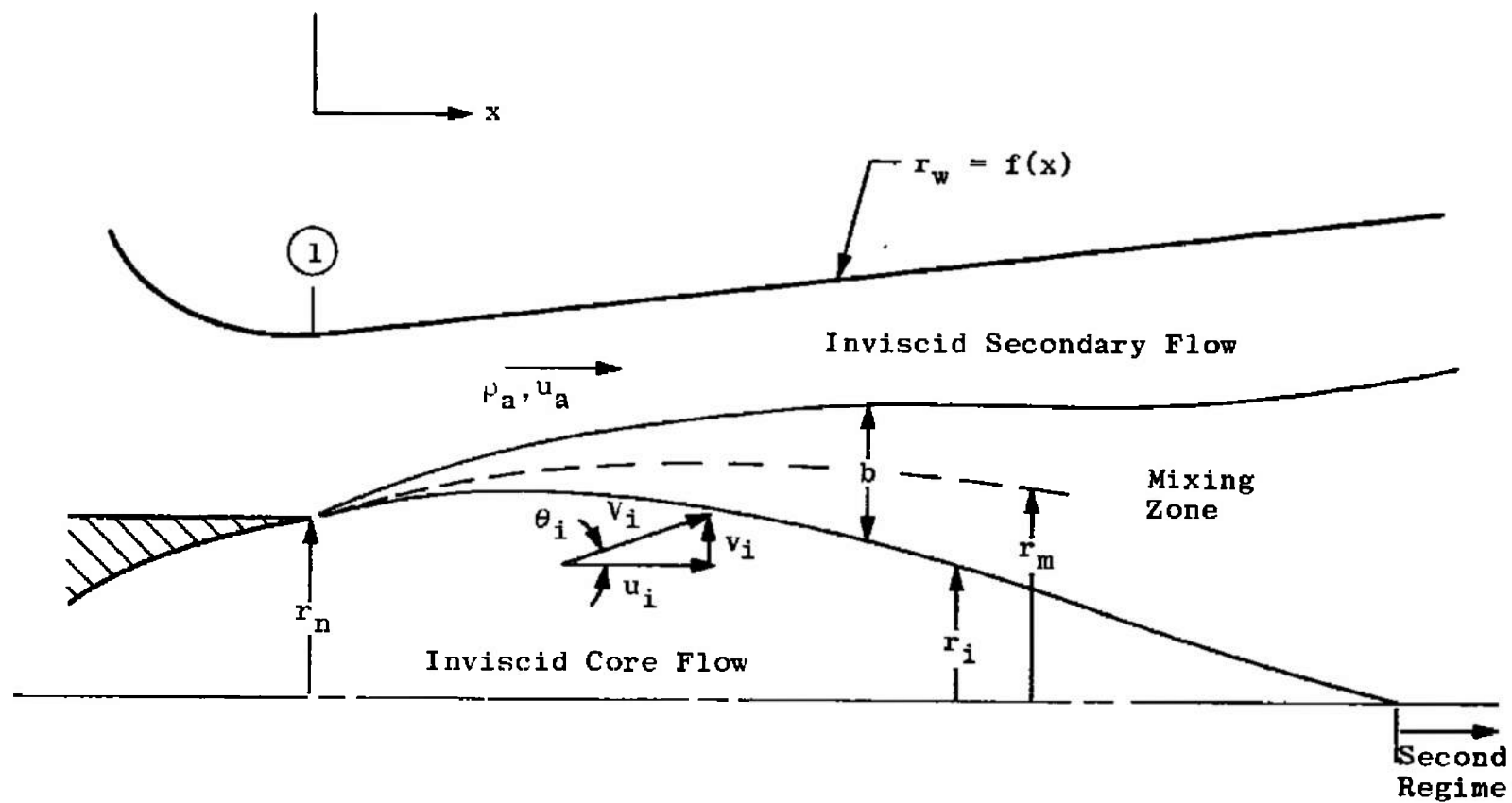
Fig. 11 Nomenclature for 2-D Core Theory

If eq. (1) is integrated between the arbitrarily selected lower and upper limits of r_1 and r_2, the following equation is obtained (Section IV):

$$\int_{r_1}^{r_2} \frac{\partial}{\partial x}(\rho u^2) r \, dr + \rho_2 v_2 u_2 r_2 - \rho_1 v_1 u_1 r_1 = \tau_2 r_2$$
$$-\tau_1 r_1 - \frac{dp_w}{dx} \int_{r_1}^{r_2} r \, dr \qquad (5)$$

Note that the pressure, p_w, is a function of only the axial coordinate.

Integrating the continuity equation between the limits r_1 and r_2 yields

$$\rho_2 v_2 r_2 - \rho_1 v_1 r_1 = -\int_{r_1}^{r_2} \frac{\partial}{\partial x}(\rho u r) \, dr \qquad (73)$$

Substituting eq. (73) into eq. (5) to eliminate the $\rho_2 v_2 u_2 r_2$ term:

$$\int_{r_1}^{r_2} \frac{\partial}{\partial x}(\rho u^2) r \, dr + (u_2 - u_1)\rho_1 v_1 r_1 - u_2 \int_{r_1}^{r_2} \frac{\partial}{\partial x}(\rho u r) \, dr$$
$$= \tau_2 r_2 - \tau_1 r_1 - \frac{dp_w}{dx} \int_{r_1}^{r_2} r \, dr \qquad (74)$$

Now let $r_1 = r_i$ and $r_2 = r_w$, and note that $\tau_i = \tau_w = 0$. Equation (74) becomes

$$\int_{r_i}^{r_w} \frac{\partial}{\partial x}(\rho u^2) r \, dr + (u_w - u_i)\rho_i v_i r_i - u_w \int_{r_i}^{r_w} \frac{\partial}{\partial x}(\rho u r) \, dr$$
$$= -\frac{dp_w}{dx}\left(\frac{r_w^2 - r_i^2}{2}\right) \qquad (75)$$

85

Applying Leibnitz' rule to eq. (75), one obtains

$$\frac{d}{dx}\int_{r_i}^{r_w}\rho u^2 r\, dr + \rho_i u_i^2 r_i \frac{dr_i}{dx} - \rho_w u_w^2 r_w \frac{dr_w}{dx}$$

$$+ (u_w - u_i)\rho_i v_i r_i - u_w \frac{d}{dx}\int_{r_i}^{r_w}\rho u r\, dr - u_w \rho_i u_i r_i \frac{dr_i}{dx}$$

$$+ \rho_w u_w^2 r_w \frac{dr_w}{dx} = -\frac{dp_w}{dx}\left(\frac{r_w^2 - r_i^2}{2}\right)$$

or

$$\frac{d}{dx}\int_{r_i}^{r_w}\rho u^2 r\, dr + \rho_i u_i^2 r_i \frac{dr_i}{dx} + (u_w - u_i)\rho_i v_i r_i - u_w \frac{d}{dx}\int_{r_i}^{r_w}\rho u r\, dr$$

$$- u_w \rho_i u_i r_i \frac{dr_i}{dx} = -\frac{dp_w}{dx}\left(\frac{r_w^2 - r_i^2}{2}\right) \tag{76}$$

Now consider the continuity equation (eq. 73). Letting $r_1 = r_i$ and $r_2 = r_w$, one obtains after applying Leibnitz' rule:

$$\rho_w v_w r_w - \rho_i v_i r_i = -\frac{d}{dx}\int_{r_i}^{r_w}\rho u r\, dr - \rho_i u_i r_i \frac{dr_i}{dx}$$

$$+ \rho_w u_w r_w \frac{dr_w}{dx}$$

but

$$v_w = u_w \frac{dr_w}{dx}$$

thus

$$\frac{d}{dx}\int_{r_i}^{r_w}\rho u r\, dr = \rho_i v_i r_i - \rho_i u_i r_i \frac{dr_i}{dx} \tag{77}$$

Equation (77) is the desired form for the continuity equation.

Substituting eq. (77) into eq. (76), one obtains

$$\frac{d}{dx}\int_{r_i}^{r_w} \rho u^2 r\, dr = \rho_i u_i v_i r_i - \rho_i u_i^2 r_i \frac{dr_i}{dx} - \frac{dP_w}{dx}\left(\frac{r_w^2 - r_i^2}{2}\right) \quad (78)$$

which is the desired form for the "total" momentum equation.

To derive the second momentum equation, again consider eq. (74). Letting $r_1 = r_i$ and $r_2 = r_m$, one obtains

$$\int_{r_i}^{r_m}\frac{\partial}{\partial x}(\rho u^2)r\, dr + (u_m - u_i)\rho_i v_i r_i - u_m\int_{r_i}^{r_m}\frac{\partial}{\partial x}(\rho u r)\, dr$$

$$= \tau_m r_m - \frac{dP_w}{dx}\left(\frac{r_m^2 - r_i^2}{2}\right) \quad (79)$$

Applying Leibnitz' rule to eq. (79) one obtains

$$\frac{d}{dx}\int_{r_i}^{r_m}\rho u^2 r\, dr + \rho_i u_i^2 r_i \frac{dr_i}{dx} - \rho_m u_m^2 r_m \frac{dr_m}{dx}$$

$$+ (u_m - u_i)\rho_i v_i r_i - u_m\frac{d}{dx}\int_{r_i}^{r_m}\rho u r\, dr - u_m \rho_i u_i r_i \frac{dr_i}{dx}$$

$$+ \rho_m u_m^2 r_m \frac{dr_m}{dx} = \tau_m r_m - \frac{dP_w}{dx}\left(\frac{r_m^2 - r_i^2}{2}\right)$$

or

$$\frac{d}{dx}\int_{r_i}^{r_m}\rho u^2 r\, dr - u_m\frac{d}{dx}\int_{r_i}^{r_m}\rho u r\, dr = \tau_m r_m$$

$$+ (u_m - u_i)\left(\rho_i u_i r_i \frac{dr_i}{dx} - \rho_i v_i r_i\right) - \frac{dP_w}{dx}\left(\frac{r_m^2 - r_i^2}{2}\right) \quad (80)$$

which is the desired form of the half-radius momentum equation.

2. Working Form of the Differential-Integral Equations

By expanding the integral terms and noting that $r_m = r_i + b/2$, one obtains the following set of differential-integral equations.

Continuity equation

$$\frac{d}{dx}\int_{r_i}^{r_i+b}\rho u r\,dr + \frac{d}{dx}\left[\rho_a u_a \frac{r_w^2-(r_i+b)^2}{2}\right] = \rho_i v_i r_i - \rho_i u_i r_i \frac{dr_i}{dx} \tag{81}$$

Total momentum equation

$$\frac{d}{dx}\int_{r_i}^{r_i+b}\rho u^2 r\,dr + \frac{d}{dx}\left[\rho_a u_a^2 \frac{r_w^2-(r_i+b)^2}{2}\right] = \rho_i u_i r_i\left(v_i - u_i\frac{dr_i}{dx}\right)$$
$$-\frac{dp_w}{dx}\left(\frac{r_w^2-r_i^2}{2}\right) \tag{82}$$

Half-radius momentum equation

$$\frac{d}{dx}\int_{r_i}^{r_i+b/2}\rho u^2 r\,dr - u_m\frac{d}{dx}\int_{r_i}^{r_i+b/2}\rho u r\,dr = (u_m-u_i)\left(\rho_i u_i r_i \frac{dr_i}{dx} - \rho_i v_i r_i\right)$$
$$+\tau_m(r_i+b/2) - \frac{dp_w}{dx}\left[\frac{(r_i+b/2)^2-r_i^2}{2}\right] \tag{83}$$

One aspect of these differential-integral equations should be noted. In the derivation, the boundary layer assumptions were assumed to apply in the (x, r) coordinate system ($\partial p/\partial r = 0$, etc.). For systems in which the mixing layer is steeply inclined relative to the centerline, i.e., a highly underexpanded primary nozzle, it would

be more realistic to apply the boundary layer equations to a coordinate system aligned with a local characteristic flow direction. Attempts were made to derive the differential-integral equations in such a shifting coordinate system, but the resulting system of equations is prohibitively complicated. The complexity is caused by the necessity for matching the mixing layer region with the adjacent regions of inviscid flow. It was decided, therefore, to use the differential-integral equations as formulated here, even though the results will be strictly consistent with the boundary layer assumptions only for small inclinations of the mixing layer, i.e., $\cos \theta_i \approx 1$. This restriction is not serious for the ducted mixing systems considered in this report; θ_i rarely exceeded $15° - 20°$. Nevertheless, it is important that this restriction be clearly noted so that the equations will not be applied indiscriminately to mixing systems with large inclinations of the mixing layer.

SECTION XI
MIXING ZONE PROFILES

The velocity and density profiles in the mixing zone are computed with the same equations which were developed in Section V for the 1-D Core Theory. In the velocity profile equation (eq. 28a), however, the velocity u_j is replaced by u_i, defined as

$$u_i = V_i \cos \theta_i$$

where V_i is the total velocity vector at r_i (an isentropic function of p_w) and θ_i is the flow angle at r_i. The method of characteristics solution of the inviscid core flow provides the inner boundary angle, θ_i.

The velocity at the control surface, r_m, is

$$u_m = \tfrac{1}{2} (u_i + u_a)$$

Because one does not integrate across the inviscid core flow in the 2-D Core Theory, the species conservation parameter, Q, (eq. 27, Section V) is evaluated in the following manner. All of the species which <u>do</u> <u>not</u> originate from the central jet are evaluated, then this quantity is subtracted from the total mass flow in the system:

$$Q = \frac{1}{W_j} \left\{ W_a + W_j - 2\pi \int_{r_i}^{r_i+b} \rho u (1-\bar{C}) r \, dr \right.$$

$$\left. - \pi \rho_a u_a \left[r_w^2 - (r_i+b)^2 \right] \right\} \tag{27a}$$

SECTION XII
TRANSFORMATION OF DIFFERENTIAL–INTEGRAL EQUATIONS

A system of three differential–integral equations was derived in Section X for the 2–D Core Theory. These equations are similar to the corresponding equations for the 1–D Core Theory, and are transformed by the same method as used in Section VII.

The three basic equations are (Section X):

Continuity equation

$$\frac{d}{dx}\int_{r_i}^{r_i+b}\rho u r\, dr + \frac{d}{dx}\left[\rho_a u_a \frac{r_w^2-(r_i+b)^2}{2}\right] = \rho_i v_i r_i - \rho_i u_i r_i \frac{dr_i}{dx} \qquad (81)$$

Total momentum equation

$$\frac{d}{dx}\int_{r_i}^{r_i+b}\rho u^2 r\, dr + \frac{d}{dx}\left[\rho_a u_a^2 \frac{r_w^2-(r_i+b)^2}{2}\right] = \rho_i u_i r_i \left(v_i - u_i \frac{dr_i}{dx}\right)$$

$$- \frac{dp_w}{dx}\left(\frac{r_w^2 - r_i^2}{2}\right) \qquad (82)$$

Half–radius momentum equation

$$\frac{d}{dx}\int_{r_i}^{r_i+b/2}\rho u^2 r\, dr - u_m\frac{d}{dx}\int_{r_i}^{r_i+b/2}\rho u r\, dr = \tau_m\left(r_i + b/2\right)$$

$$+ \left(u_m - u_i\right)\left(\rho_i u_i r_i \frac{dr_i}{dx} - \rho_i v_i r_i\right) - \frac{dp_w}{dx}\left[\frac{(r_i+b/2)^2-r_i^2}{2}\right] \qquad (83)$$

The details of the transformation are identical to those of Section VII and will not be repeated here. Again, the variables (x, p_w, r_1, b) are considered indepen-

dent. After the transformation, the equations have the same form as in the 1-D Core Theory:

Continuity equation

$$F_1 \frac{dP_w}{dx} + F_2 \frac{dr_i}{dx} + F_3 \frac{db}{dx} = F_4 \tag{55}$$

Total momentum equation

$$G_1 \frac{dP_w}{dx} + G_2 \frac{dr_i}{dx} + G_3 \frac{db}{dx} = G_4 \tag{56}$$

Half-radius momentum equation

$$H_1 \frac{dP_w}{dx} + H_2 \frac{dr_i}{dx} + H_3 \frac{db}{dx} = H_4 \tag{57}$$

The coefficients .F, G and H, however, are different from the corresponding 1-D Core Theory coefficients and are given by the following equations.

$$F_1 = b^2 \int_0^1 \left(\rho \frac{\partial \bar{u}}{\partial P_w} + u \frac{\partial \bar{\rho}}{\partial P_w} \right) y \, dy + b r_i \int_0^1 \left(\rho \frac{\partial \bar{u}}{\partial P_w} + u \frac{\partial \bar{\rho}}{\partial P_w} \right) dy$$

$$+ \left[\frac{r_w^2 - (r_i + b)^2}{2} \right] \left[\rho_a \frac{du_a}{dP_w} + u_a \frac{d\rho_a}{dP_w} \right] \tag{84}$$

$$F_2 = b^2 \int_0^1 \left(\rho \frac{\partial \bar{u}}{\partial r_i} + u \frac{\partial \bar{\rho}}{\partial r_i} \right) y \, dy$$

$$+ b r_i \int_0^1 \left(\rho \frac{\partial \bar{u}}{\partial r_i} + u \frac{\partial \bar{\rho}}{\partial r_i} \right) dy \tag{85}$$

$$F_3 = b^2 \int_0^1 \left(\rho \frac{\partial \bar{u}}{\partial b} + u \frac{\partial \bar{\rho}}{\partial b} \right) y \, dy$$

$$+ b r_i \int_0^1 \left(\rho \frac{\partial \bar{u}}{\partial b} + u \frac{\partial \bar{\rho}}{\partial b} \right) dy \qquad (86)$$

$$F_4 = -b^2 \int_0^1 \left(\rho \frac{\partial \bar{u}}{\partial x} + u \frac{\partial \bar{\rho}}{\partial x} \right) y \, dy - b r_i \int_0^1 \left(\rho \frac{\partial \bar{u}}{\partial x} + u \frac{\partial \bar{\rho}}{\partial x} \right) dy$$

$$+ \rho_i v_i r_i - \rho_a u_a r_w \frac{d r_w}{d x} \qquad (87)$$

$$G_1 = b^2 \int_0^1 \left(2 \rho u \frac{\partial \bar{u}}{\partial P_w} + u^2 \frac{\partial \bar{\rho}}{\partial P_w} \right) y \, dy + b r_i \int_0^1 \left(2 \rho u \frac{\partial \bar{u}}{\partial P_w} + u^2 \frac{\partial \bar{\rho}}{\partial P_w} \right) dy$$

$$+ \left[\frac{r_w^2 - r_i^2}{2} \right] \left[1 + 2 \rho_a u_a \frac{d u_a}{d P_w} + u_a^2 \frac{d \rho_a}{d P_w} \right] \qquad (88)$$

$$G_2 = b^2 \int_0^1 \left(2 \rho u \frac{\partial \bar{u}}{\partial r_i} + u^2 \frac{\partial \bar{\rho}}{\partial r_i} \right) y \, dy$$

$$+ b r_i \int_0^1 \left(2 \rho u \frac{\partial \bar{u}}{\partial r_i} + u^2 \frac{\partial \bar{\rho}}{\partial r_i} \right) dy \qquad (89)$$

$$G_3 = b^2 \int_0^1 \left(2 \rho u \frac{\partial \bar{u}}{\partial b} + u^2 \frac{\partial \bar{\rho}}{\partial b} \right) y \, dy$$

$$+ b r_i \int_0^1 \left(2 \rho u \frac{\partial \bar{u}}{\partial b} + u^2 \frac{\partial \bar{\rho}}{\partial b} \right) dy \qquad (90)$$

$$G_4 = -b^2 \int_0^1 \left(2\rho u \frac{\partial \bar{u}}{\partial x} + u^2 \frac{\partial \bar{\rho}}{\partial x}\right) y \, dy - b r_i \int_0^1 \left(2\rho u \frac{\partial \bar{u}}{\partial x} + u^2 \frac{\partial \bar{\rho}}{\partial x}\right) dy$$

$$+ \rho_i u_i v_i r_i - \rho_a u_a^2 r_w \frac{dr_w}{dx} \qquad (91)$$

$$H_1 = b^2 \int_0^{1/2} \left(2\rho u \frac{\partial \bar{u}}{\partial \rho_w} + u^2 \frac{\partial \bar{\rho}}{\partial \rho_w}\right) y \, dy + b r_i \int_0^{1/2} \left(2\rho u \frac{\partial \bar{u}}{\partial \rho_w} + u^2 \frac{\partial \bar{\rho}}{\partial \rho_w}\right) dy$$

$$- u_m b^2 \int_0^{1/2} \left(\rho \frac{\partial \bar{u}}{\partial \rho_w} + u \frac{\partial \bar{\rho}}{\partial \rho_w}\right) y \, dy - u_m b r_i \int_0^{1/2} \left(\rho \frac{\partial \bar{u}}{\partial \rho_w} + u \frac{\partial \bar{\rho}}{\partial \rho_w}\right) dy$$

$$+ \left[\frac{(r_i + b/2)^2 - r_i^2}{2}\right] \qquad (92)$$

$$H_2 = b^2 \int_0^{1/2} \left(2\rho u \frac{\partial \bar{u}}{\partial r_i} + u^2 \frac{\partial \bar{\rho}}{\partial r_i}\right) y \, dy + b r_i \int_0^{1/2} \left(2\rho u \frac{\partial \bar{u}}{\partial r_i} + u^2 \frac{\partial \bar{\rho}}{\partial r_i}\right) dy$$

$$- u_m b^2 \int_0^{1/2} \left(\rho \frac{\partial \bar{u}}{\partial r_i} + u \frac{\partial \bar{\rho}}{\partial r_i}\right) y \, dy - u_m b r_i \int_0^{1/2} \left(\rho \frac{\partial \bar{u}}{\partial r_i} + u \frac{\partial \bar{\rho}}{\partial r_i}\right) dy \qquad (93)$$

$$H_3 = b^2 \int_0^{1/2} \left(2\rho u \frac{\partial \bar{u}}{\partial b} + u^2 \frac{\partial \bar{\rho}}{\partial b}\right) y \, dy + b r_i \int_0^{1/2} \left(2\rho u \frac{\partial \bar{u}}{\partial b} + u^2 \frac{\partial \bar{\rho}}{\partial b}\right) dy$$

$$- u_m b^2 \int_0^{1/2} \left(\rho \frac{\partial \bar{u}}{\partial b} + u \frac{\partial \bar{\rho}}{\partial b}\right) y \, dy - u_m b r_i \int_0^{1/2} \left(\rho \frac{\partial \bar{u}}{\partial b} + u \frac{\partial \bar{\rho}}{\partial b}\right) dy \qquad (94)$$

$$H_4 = -b^2 \int_0^{1/2} \left(2\rho u \frac{\partial \bar{u}}{\partial x} + u^2 \frac{\partial \bar{\rho}}{\partial x}\right) y \, dy - b r_i \int_0^{1/2} \left(2\rho u \frac{\partial \bar{u}}{\partial x} + u^2 \frac{\partial \bar{\rho}}{\partial x}\right) dy$$

$$+ u_m b^2 \int_0^{1/2} \left(\rho \frac{\partial \bar{u}}{\partial x} + u \frac{\partial \bar{\rho}}{\partial x}\right) y \, dy + u_m b r_i \int_0^{1/2} \left(\rho \frac{\partial \bar{u}}{\partial x} + u \frac{\partial \bar{\rho}}{\partial x}\right) dy$$

$$+ (u_i - u_m) \rho_i v_i r_i + \tau_m (r_i + b/2) \qquad (95)$$

94

As in Part I, eqs. (55) — (57) are linear in the derivatives dp_w/dx, dr_i/dx and db/dx, and can be solved for the derivatives by use of Cramer's rule (eqs. 58–60, Section VII). Equations (58) — (60) are again numerically integrated by use of the Runge–Kutta method.

Many auxiliary functions are necessary to evaluate the coefficients F, G, and H. Those functions which are not the same as those of the 1-D Core Theory (Appendix I) are presented in Appendix II. It is important to note that the coefficients contain terms which depend on the flow angle, θ_i, at r_i. The local value of θ_i is computed in the method of characteristics solution of the inviscid core flow (Section XIII).

SECTION XIII
METHOD OF CHARACTERISTICS SOLUTION OF INVISCID CORE FLOW

Many terms appearing in the coefficients F, G and H (eqs. 84—95, Section XII) depend on the flow conditions at the inner mixing zone boundary. In order to solve the system of equations, one must be able to evaluate the following parameters at r_i: θ_i, $\partial u/\partial x$, $\partial u/\partial r$, $\partial p/\partial r$, $\partial p/\partial x$ (see Appendix II). To provide these parameters, the inviscid core flow is developed (with the irrotational method of characteristics) simultaneously with the numerical solution of the equations for the mixing layer and inviscid secondary flow.

1. Interior Flow Solution

The method of characteristics is a well established method for computing supersonic inviscid flow fields. Detailed discussions of the method of characteristics are presented in standard references on supersonic aerodynamics (Ref. 43, for example). Briefly, the flow field solutions are obtained by computing along "characteristic" lines in the flow field which correspond to Mach lines. The change of flow conditions along these characteristic curves is computed by solving the following set of ordinary differential equations (for axisymmetric irrotational flow):

$$\frac{1}{V}\left(\frac{dV}{d\theta}\right)_{I,II} = \mp \tan\alpha + \frac{\sin\alpha\,\sin\theta}{\sin(\theta \mp \alpha)}\frac{1}{r}\left(\frac{dr}{d\theta}\right)_{I,II} \quad (96)$$

$$\left(\frac{dr}{dx}\right)_{I,II} = \tan(\theta \mp \alpha) \quad (97)$$

The upper sign refers to right running (Family I) characteristics and the lower sign to left running (Family II) characteristics. The local Mach angle is denoted by α.

Consider a unit process in the physical plane (Fig. 12). If the flow conditions are known at points 1 and 2 (which are not on the same characteristic), then eqs. (96) and (97) can be solved to locate point 3 (x_3, r_3) and to define V_3 and θ_3. For a small unit process the Mach lines are assumed to be straight and eqs. (96) and (97) are written in finite difference form. As a first approximation one evaluates the coefficients in the difference equations at the initial conditions. The unit process is then recalculated using average values for the coefficients until the solution converges.

In the inviscid core solution, the initial conditions are prescribed along a radial line AB at the primary nozzle exit plane (Fig. 13). For an underexpanded primary nozzle, the flow will expand at the nozzle lip through a Prandtl-Meyer expansion until the local pressure is equal to p_{w1}. If AC represents the Family I characteristic which originates as the last Mach line in the Prandtl-Meyer expansion fan, then the flow in the region ABC can be computed, based on only the initial conditions. Note, however, that the extent of region ABC depends on the value of p_{w1}.

2. Boundary Solution

Consider the flow near the inner mixing zone boundary at some downstream location, x (Fig. 14). At x, the upstream solution has defined the values of p_w and r_i. The derivatives dp_w/dx and dr_i/dx are also specified at x. Since the flow is completely defined at x, a new Family I characteristic can be generated from the boundary point D.
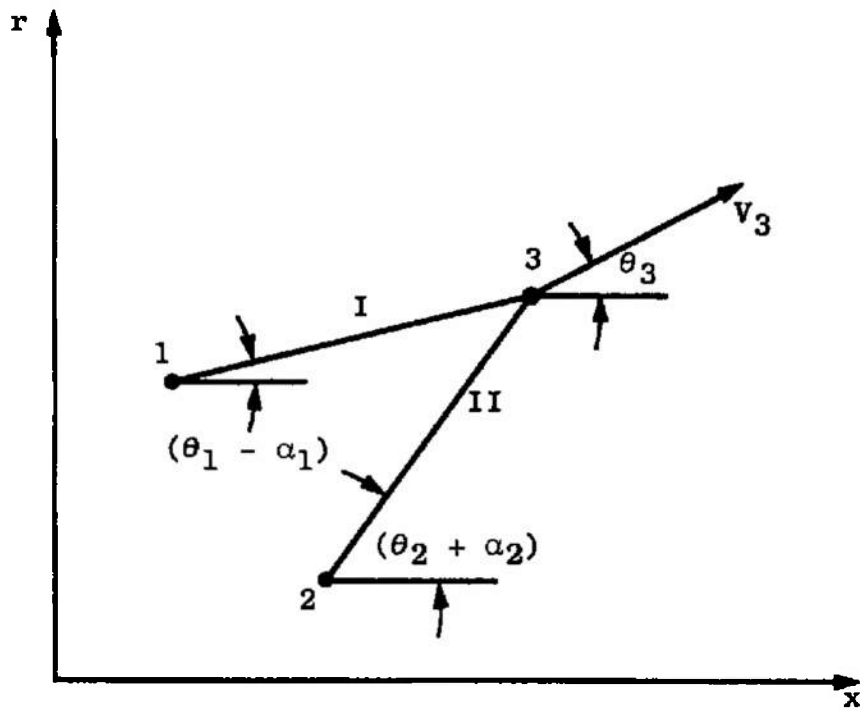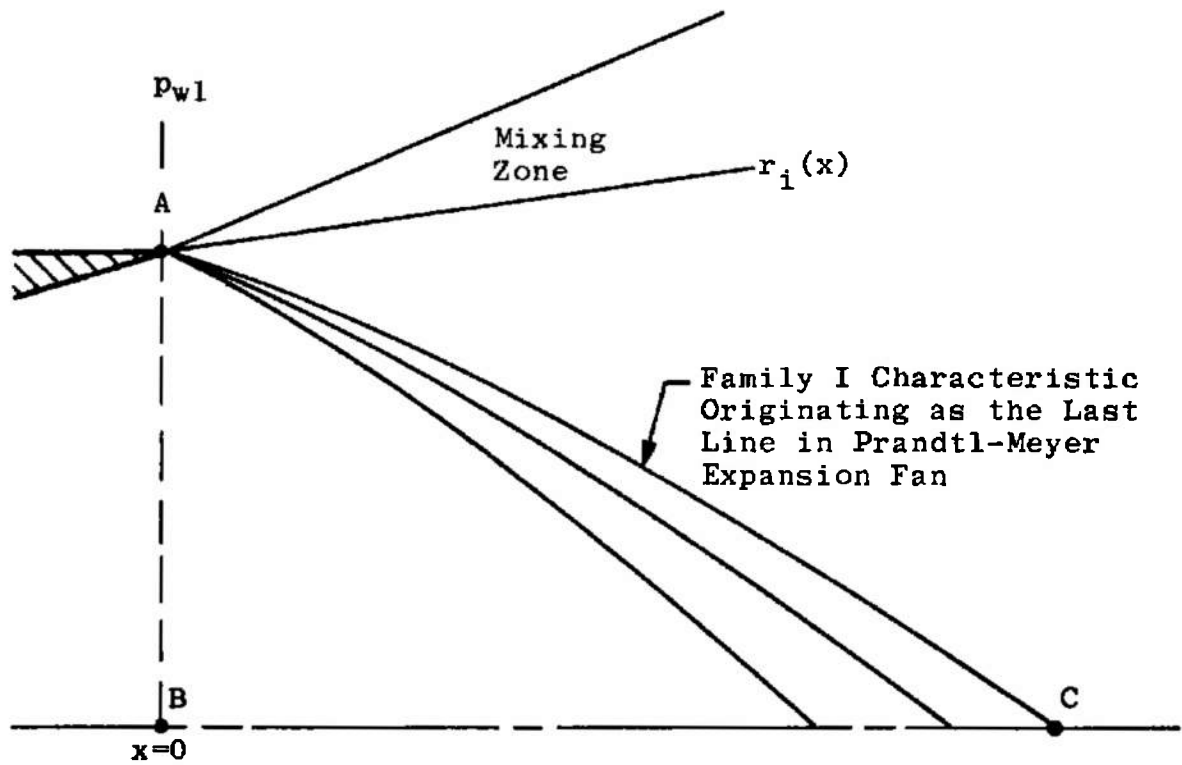
Fig. 12 Unit Process in Method of Characteristics Solution

Fig. 13 Method of Characteristics Solution of Inviscid Core Flow

Fig. 14 Solution at a General Boundary Point

(The "interior" solution is thus extended outward by one Family I characteristic at each computation interval, Δx).

With the conditions at x completely known, the Runge-Kutta method prescribes a series of intermediate points at which dp_w/dx, dr_i/dx and db/dx are to be computed. These specified points (x, p_w, r_i, b) do not necessarily correspond to points on the actual solution, but the solution depends on a weighted combination of the intermediate results. Such a Runge-Kutta point is shown as point E in Fig. 14. With the position of E specified, along with the pressure, the only unknown at E is the angle, θ_i. The angle, θ_i, which is required for the succeeding Runge-Kutta points, is determined by the following procedure. A Family II characteristic EF is constructed, which intersects the last Family I characteristic, along which the flow is completely defined from the interior solution. By an iterative solution of eqs. (96) and (97), the location of F and the value of θ_i at E are determined.

After the system of equations is solved for p_w and r_i at $x + \Delta x$ (point G, Fig. 14), the above procedure is repeated to define the physically correct value of θ_i at $x + \Delta x$.

3. Inner Boundary Derivatives

The value of θ_i at each Runge-Kutta point is computed with the procedure described in the preceding section. In addition to θ_i, the derivatives $\partial u/\partial x$, $\partial u/\partial r$, $\partial p/\partial x$ and $\partial p/\partial r$ at r_i must be computed at each Runge-Kutta point.

Now consider the following system of equations which defines the flow in the inviscid core region:

$$du = \frac{\partial u}{\partial x}dx + \frac{\partial u}{\partial r}dr \tag{98}$$

$$dv = \frac{\partial v}{\partial x}dx + \frac{\partial v}{\partial r}dr \tag{99}$$

$$dp = \frac{\partial P}{\partial x}dx + \frac{\partial P}{\partial r}dr \tag{100}$$

$$\rho u \frac{\partial u}{\partial x} + \rho v \frac{\partial u}{\partial r} = -\frac{\partial P}{\partial x} \tag{101}$$

$$\rho u \frac{\partial v}{\partial x} + \rho v \frac{\partial v}{\partial r} = -\frac{\partial P}{\partial r} \tag{102}$$

$$\frac{\partial}{\partial x}(\rho u r) + \frac{\partial}{\partial r}(\rho v r) = 0 \tag{103}$$

After expansion and introduction of the equation of state, the continuity equation (eq. 103) may be written:

$$\rho r \frac{\partial u}{\partial x} + \rho r \frac{\partial v}{\partial r} + \frac{ur}{RT}\frac{\partial P}{\partial x} + \frac{vr}{RT}\frac{\partial P}{\partial r} = -\rho v \tag{103a}$$

The above system of equations is linear in the derivatives $\partial u/\partial x$, $\partial u/\partial r$, $\partial v/\partial x$, $\partial v/\partial r$, $\partial P/\partial x$ and $\partial P/\partial r$, and is solved for these derivatives at each Runge-Kutta point by means of standard matrix techniques[*].

---

[*] This method of computing the inner mixing zone boundary derivatives was suggested by the work of Loper and Lightsey (Ref. 44).

Referring to Fig. 14, the total differentials are represented by the following differences:

$$dx = x_E - x_D$$

$$dr = r_{iE} - r_{iD}$$

$$du = u_{iE} - u_{iD}$$

$$dv = v_{iE} - v_{iD}$$

$$dp = p_{wE} - p_{wD}$$

Treating these total differentials as differences is admittedly approximate; however, the accuracy of this approximation is consistent with the accuracy of the method of characteristics solution which involves similar approximations.

SECTION XIV
NUMERICAL CONSIDERATIONS-2-D CORE THEORY

The computer program for the 2-D Core Theory is
much more complex than the program for the 1-D Core Theory,
and the details of the program will not be presented here.
The purpose of this section is to give a brief discussion
of the numerical solution from the point of view of the
engineering results.

Axial Step Size — The axial step size, Δx, for the
Runge-Kutta integration of the system of differential equa-
tions must be much smaller than the corresponding step size
in the 1-D Core Theory. The step size is chosen to be about
the same size as a typical grid in the method of charac-
teristics network (typically 0.05-0.10 times r_n). If the
step size were to be larger, the accuracy of the "boundary
solution" (Section XIII) would be poor.

Method of Characteristics — The accuracy of the
method of characteristics is well established as long as
the network is made reasonably small compared to the local
rate of change of the flow conditions. One point of interest
is that the network of points is redistributed along a
radial line (by interpolation) at each axial station in the
solution. By this redistribution procedure, the problem of
network "foldback", indicative of the onset of boundary
shock formation, is avoided. The method of characteristics
portion of the program has been compared with standard "jet
plume" programs and the results are nearly identical.

Computation Time — The numerical solutions were
obtained by use of an IBM-360/50 digital computer. A
typical problem is solved in 100 to 120 axial steps,
requiring a total time of approximately 10 minutes.

__Program Inputs and Printout__ – The input parameters
and parameters which are printed out are given in Appendix
III.

SECTION XV
REGIMES OF SOLUTIONS

The method of computation depends on the mode of operation of the ducted mixing system (Fig. 2, Section I). In all cases, the procedure is to assume a value of the initial static pressure, p_{wl}, make a flow field computation, and then iterate on p_{wl} until some downstream criterion is satisfied. In the "downstream choking" and "back pressure dependent" modes the criterion is either that the flow must choke at the duct exit or that the duct exit pressure must match a prescribed back pressure.

The problem is much more complex in the case of the "upstream choking" mode (Fig. 2a, Section I). In this mode the flow must accelerate to the critical condition, and then the solution must pass smoothly into the supercritical regime. When the flow becomes critical, the determinant $|D|$ for the system of equations (Section VII) is zero. The basic premise which is used to compute the correct solution is that the static pressure is continuous through the critical region; therefore, one iterates on p_{wl} until the determinants $|D|$ and $|P|$ (Section VII) simultaneously become zero. The technique for finding the correct solution is illustrated in Fig. 15. If one chooses a value of p_{wl} which is higher than the correct value, the flow will accelerate and then decelerate, with $|D|$ remaining positive. If the selected p_{wl} is too low, then $|D|$ will go to zero upstream of the position where $|P|$ goes to zero.

Although not required by this solution technique, the determinants $|R|$ and $|B|$ (Section VII) also go to zero at the critical section. Thus the parameters r_1 and b are continuous through the critical region.
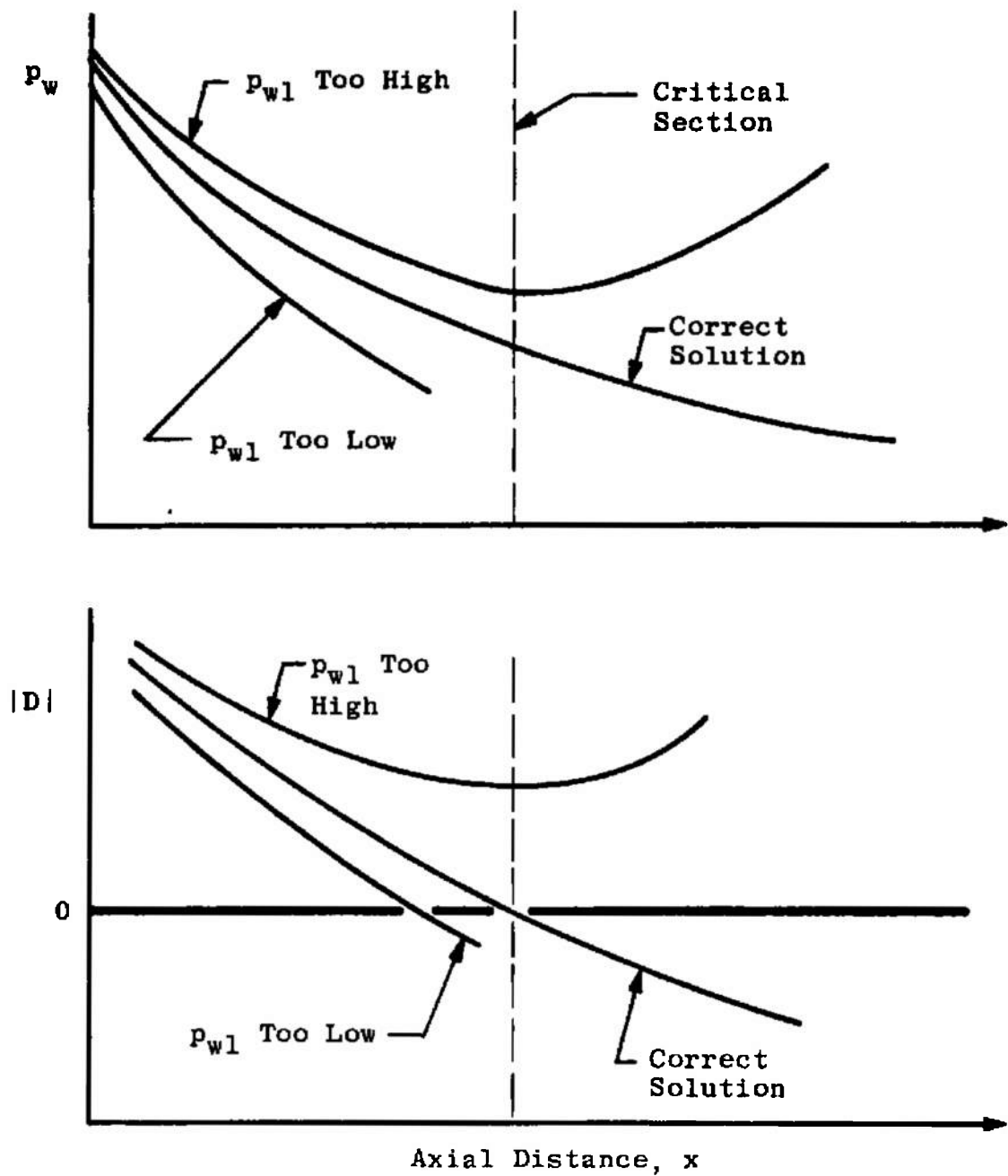
Fig. 15 Solutions for Ducted Mixing System Operating in Upstream Choking Mode

In principle, one needs only to define the correct value of p_{w1} within sufficiently small limits and then the solution will run smoothly through the critical point. By luck, the first solution attempted ran smoothly without a very small tolerance on p_{w1}. It was later found that, in general, the solutions would not run smoothly even with a tolerance on p_{w1} as small as one part in a million. To eliminate the necessity for the extremely large number of iterations required to bracket p_{w1} to the required tolerance, the following procedure was used. After bracketing p_{w1} within a reasonably small range (to one part in 10^4, typically), the solution is rerun for p_{w1} at the average value of the last "low" and "high" solutions (Fig. 15). The secondary stream total pressure is arbitrarily increased by a small amount (typically 1%) at the axial computation station immediately upstream of the position where the flow tends to become critical. The solution then runs smoothly into the super-critical regime. This method of computing the supercritical solutions has been automated in the computer program.

If one does not know beforehand in which mode that a particular ducted system will operate, the procedure is to select a high initial value of p_{w1}. Successive computations are then made at lower and lower values of p_{w1}, until (1) the duct exit pressure matches the prescribed back pressure, (2) the flow chokes at the duct exit (indicated by $|D| = 0$) or (3) the flow becomes critical at some upstream position in the duct.

It should be noted that the above procedures are also applicable to the 1-D Core Theory, although the upstream choking mode would not ordinarily be encountered if the inviscid core flow is assumed to be one-dimensional.

SECTION XVI
CORRELATION OF 2-D CORE THEORY WITH AIR-AIR EJECTOR EXPERIMENTS

The 2-D Core Theory has been correlated with the air-air ejector experiments of Chow and Addy (Ref. 5) and of Chow and Yeh (Ref. 45). All of the experimental cases considered here were operated in the upstream choking mode, i.e., with relatively low back pressure. The experimental configurations are shown in Fig. 16.

1. Constant Area Air-Air Ejectors

Chow and Addy (Ref. 5) presented a series of experiments for the cylindrical air-air ejector shown in Fig. 16a. The primary nozzle was designed to provide a uniform primary flow at $M_{j1} = 2$. Only the nozzle configuration with the thinnest lip will be considered here. Both the primary and secondary streams were unheated air.

The experimental mass flow ratio, w_a/w_j, is shown in Fig. 17, along with the results of the 2-D Core Theory. The agreement between theory and experiment is very satisfactory for the entire range of p_{oa}/p_{oj} over which the theory is applicable. At total pressure ratios below about 0.05, the mixing zone impinges on the wall, and the 2-D Core Theory as presently formulated is not valid. To compute these low secondary mass flows, Chow and Addy used the base pressure analysis of Korst, et al. (Ref. 26), suitably modified to include base bleed effects. Such a base pressure analysis was not incorporated into the 2-D Core Theory because the main interest is in ducted mixing with relatively large secondary flows. The theoretical results of Chow and Addy are not shown in Fig. 17; they are nearly identical to the 2-D Core Theory results.
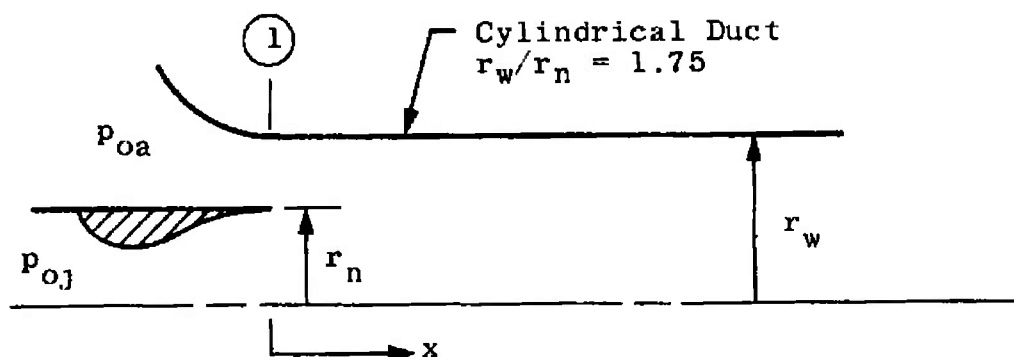
a. Cylindrical Duct of Chow and Addy (Ref. 5)
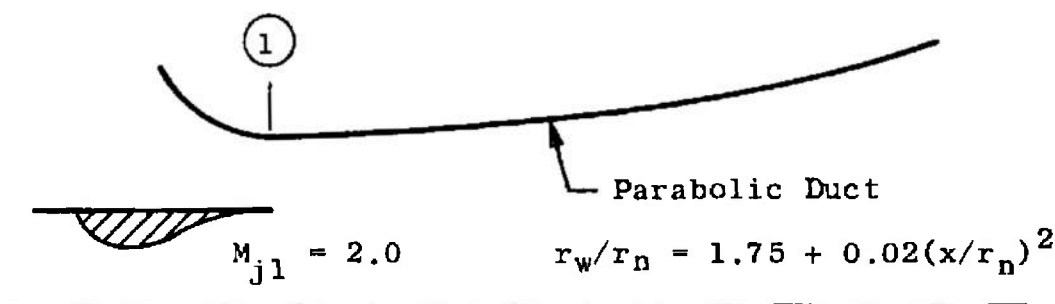
b. Parabolic Duct of Chow and Yeh (Ref. 45)
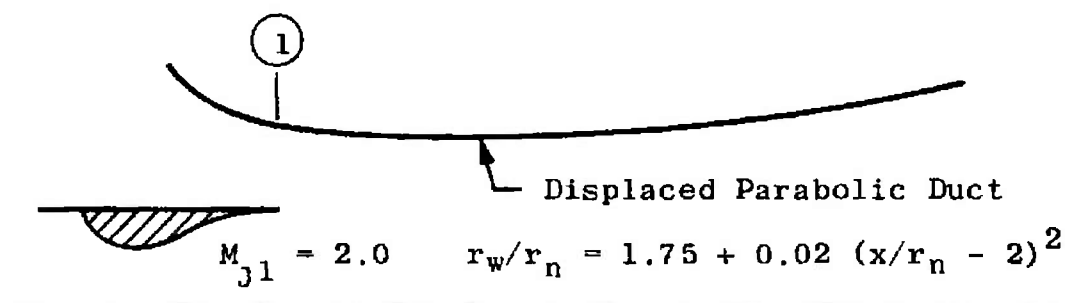
c. Displaced Parabolic Duct of Chow and Yeh (Ref. 45)

Fig. 16 Air—Air Ejector Configurations

Fig. 17 Mass Flow Ratio for a Cylindrical Air–Air Ejector

The initial secondary Mach number, M_{al}, is plotted against the pressure ratio p_{wl}/p_{oj} in Fig. 18. Again, the agreement between the 2-D Core Theory and 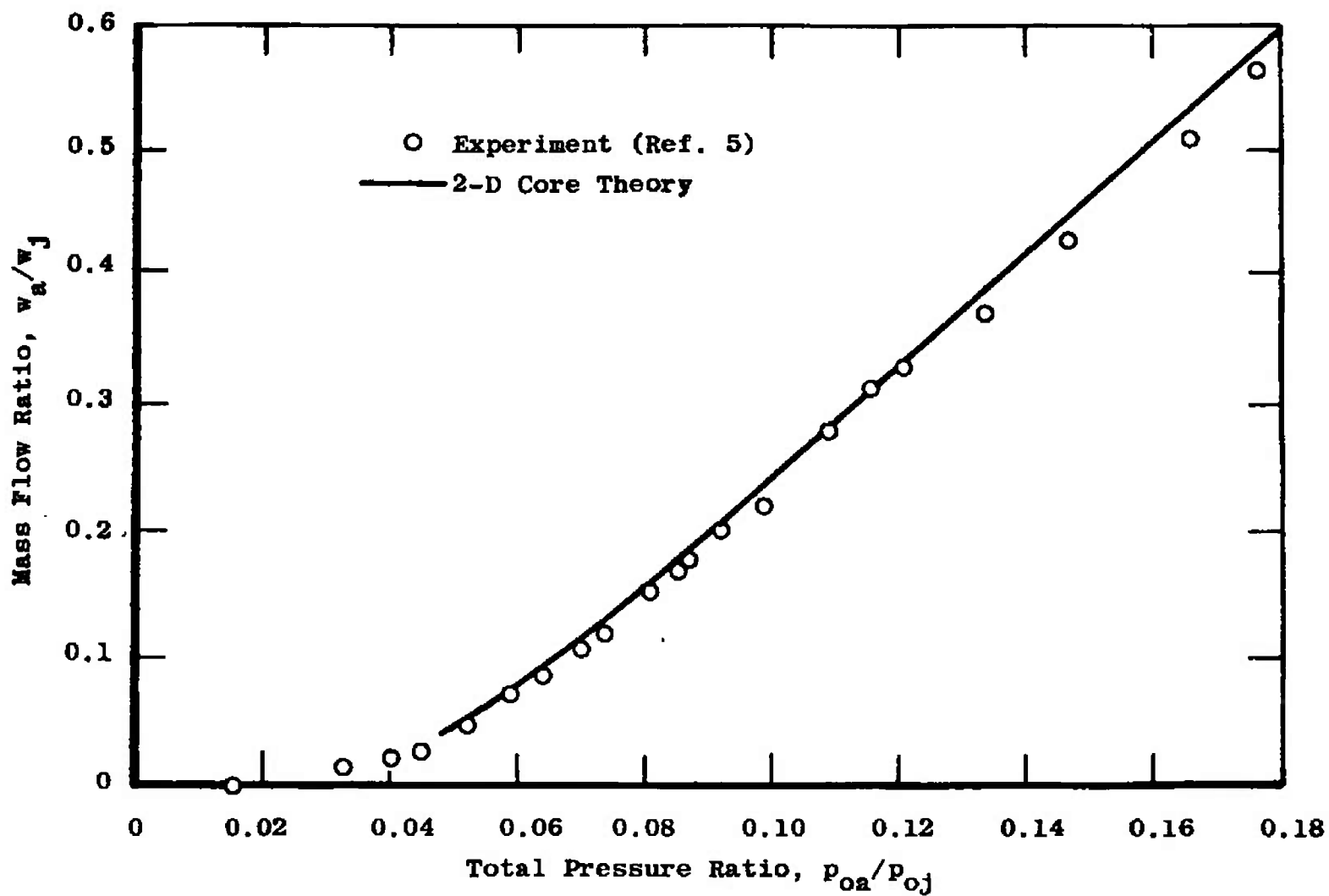experiment is very good over the range of applicability of the theory. For $p_{wl} > p_{jl}$, $M_{al} = 1$ which corresponds to Fabri and Paulon's "saturated supersonic regime."

The wall pressure distributions from Chow and Addy's experiments are shown in Fig. 19. The 2-D Core Theory predicts the experimental distributions fairly well for all three pressure ratios shown. Also shown in Fig. 19 is the locus of positions where the theoretical flow becomes critical. It is noteworthy that the secondary Mach number is subsonic at the critical point, and becomes more subsonic as the secondary flow is decreased. The system of equations is written for the combined supersonic and subsonic portions of the flow, and the results reflect that if part of the flow is supersonic at the critical point, then another part of the flow must be subsonic. This phenomenon is consistent with some of the recent results on the choking of a nonuniform flow (Ref. 46, for example)*.

2. Variable Area Air-Air Ejectors

Chow and Yeh (Ref. 45) presented a series of experiments for an air-air ejector in which the wall shape was parabolic (Fig. 16b). They also made experiments with the parabolic duct displaced downstream, so that the minimum duct area was located $2r_n$ downstream from the primary nozzle exit (Fig. 16c).

The mass flow ratio, w_a/w_j, is shown in Fig. 20 for the parabolic duct (Fig. 16b). As was the case for the cylindrical duct, the 2-D Core Theory predicts the experimental results quite accurately over the entire range of applicability.

---

* The interpretation that $|D| = 0$ corresponds to physical choking is strengthened by the fact that $|D| = 0$ occurs almost exactly at $M_a = 1$ for coaxial flows computed with the assumption of zero mixing zone shear stress (no mixing case).
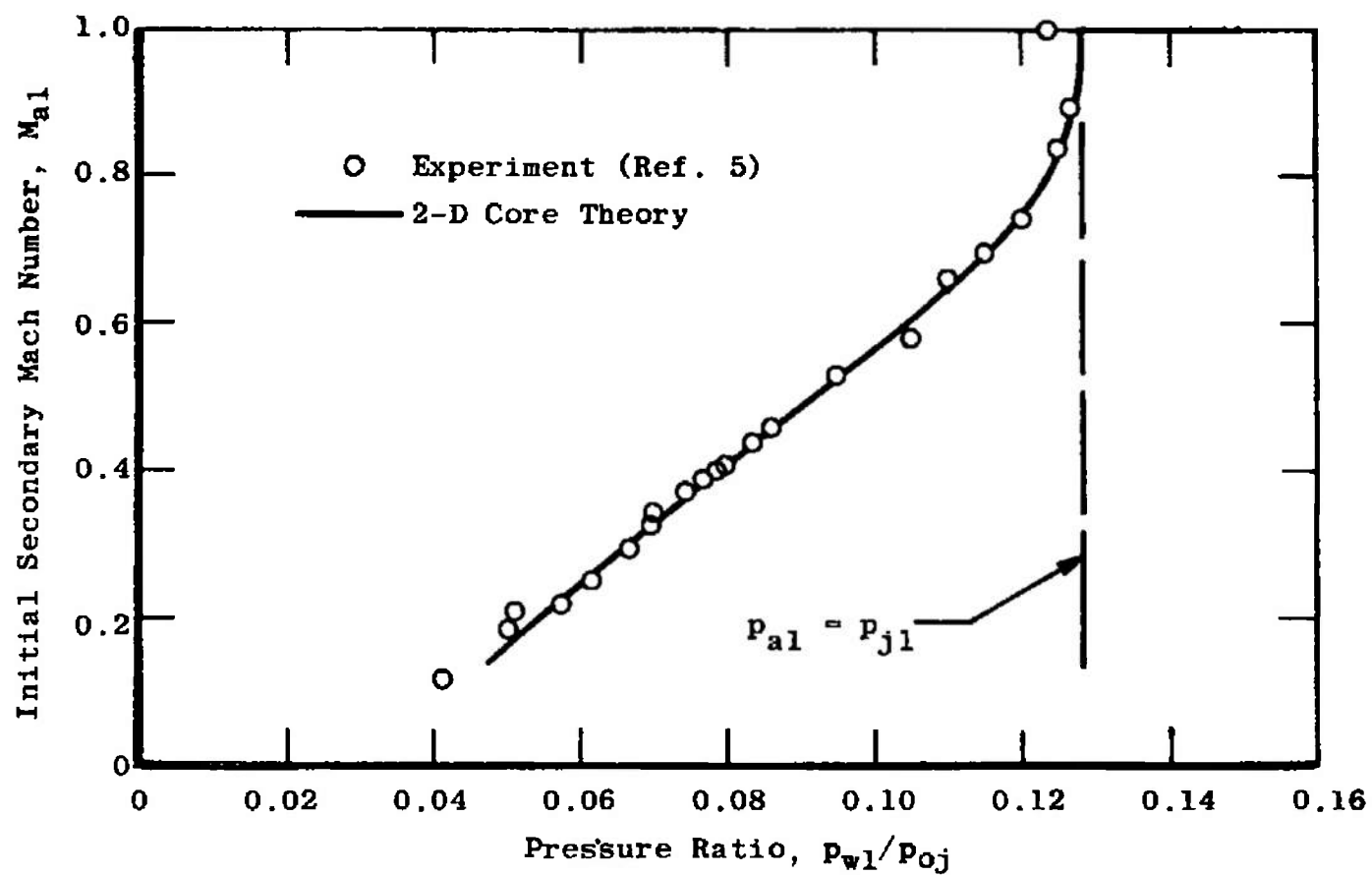
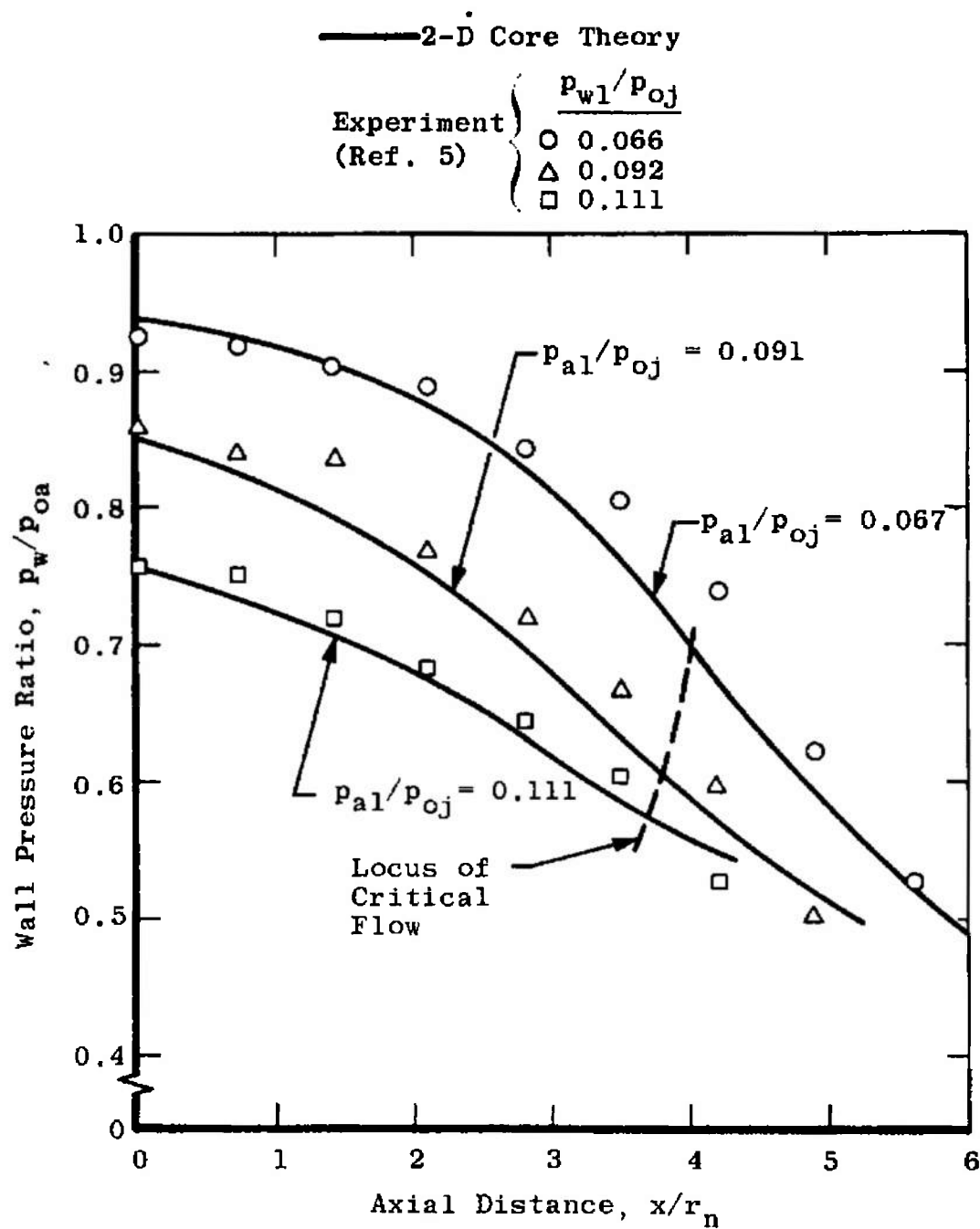Fig. 18 Initial Secondary Mach Number in a Cylindrical Air—Air Ejector

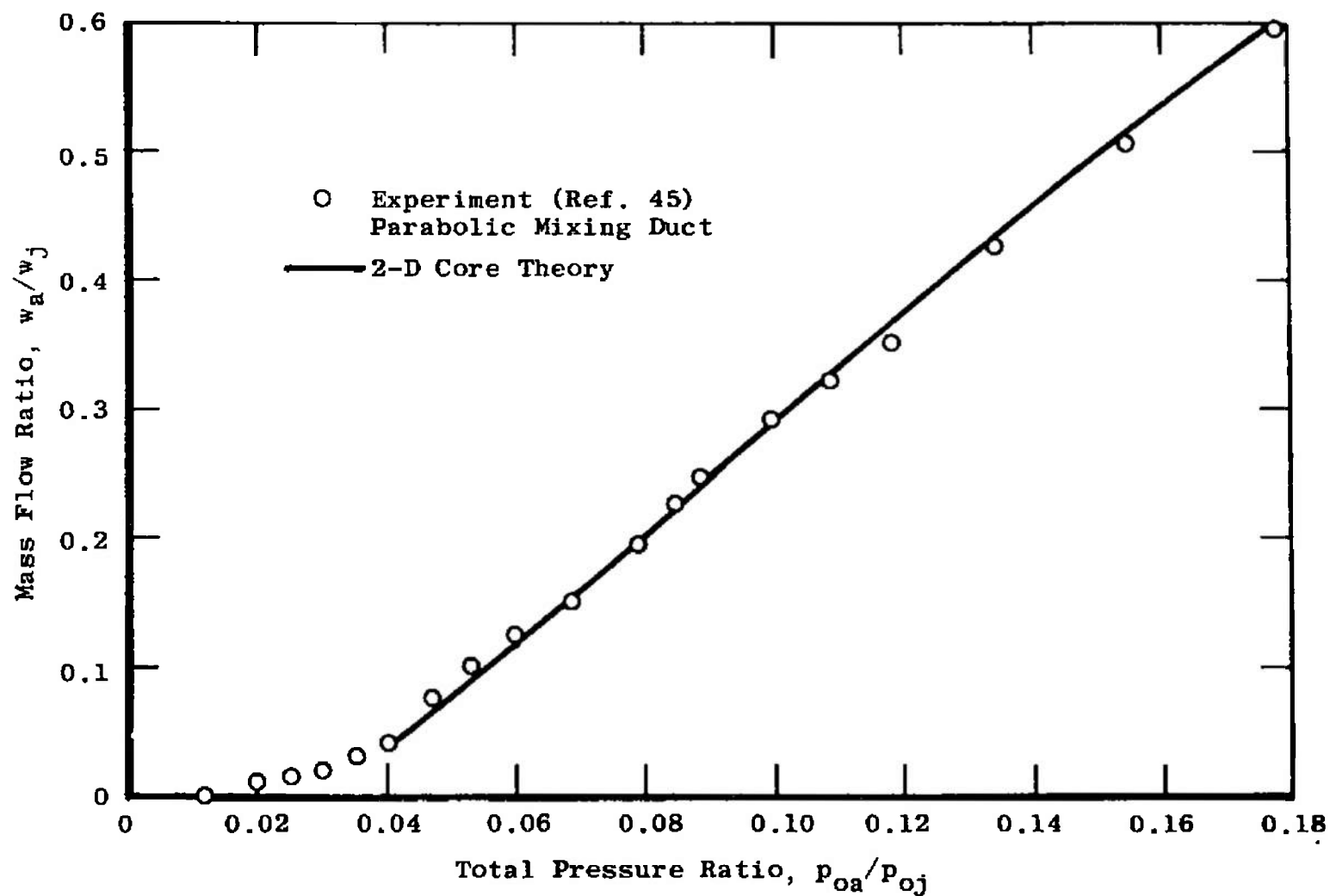Fig. 19 Wall Pressure Distributions in a Cylindrical Air–Air Ejector

Fig. 20 Mass Flow Ratio for a Variable Area Air–Air Ejector

The initial secondary Mach number, M_{a1}, is plotted against the pressure ratio p_{w1}/p_{oa} in Fig. 21 for both the parabolic duct and the displaced parabolic duct. Because of the downstream displacement of the minimum area, the saturated supersonic regime is not encountered with the displaced parabolic duct.

The wall pressure distributions for the displaced parabolic duct are shown in Fig. 22. Some of the experiments were made with fairly high back pressure, and these experimental distributions show that the back pressure has caused the wall boundary layer to separate downstream of the critical point (especially for $p_{w1}/p_{oj} = 0.06$). The 2—D Core Theory predicts the experimental distributions fairly well, especially at the lower values of p_{w1}/p_{oa} (lower values of w_a/w_j).

Based on these correlations of air—air ejector experiments, it appears that the 2—D Core Theory accurately represents the flow processes in such configurations. Even though u_a/u_j exceeded 0.5 in the downstream portions of the flow fields, the deficiency in the Prandtl eddy viscosity model is not apparent from these correlations. As pointed out by Chow and Addy, the flow in such air—air ejectors (with relatively large secondary mass flows) is predominately controlled by the inviscid stream interactions. The effects of mixing are small enough so that errors in the mixing rate are not readily discernible.

Because the viscous effects are small in these supersonic air—air ejector configurations, the accurate prediction of the experimental performance depends primarily on accurately computing the inviscid flow fields. These correlations of the 2—D Core Theory with experiment indicate, therefore, that the present method of computing the inviscid flows is satisfactory, at least in the near field ($x \lesssim 5$—6 r_n).
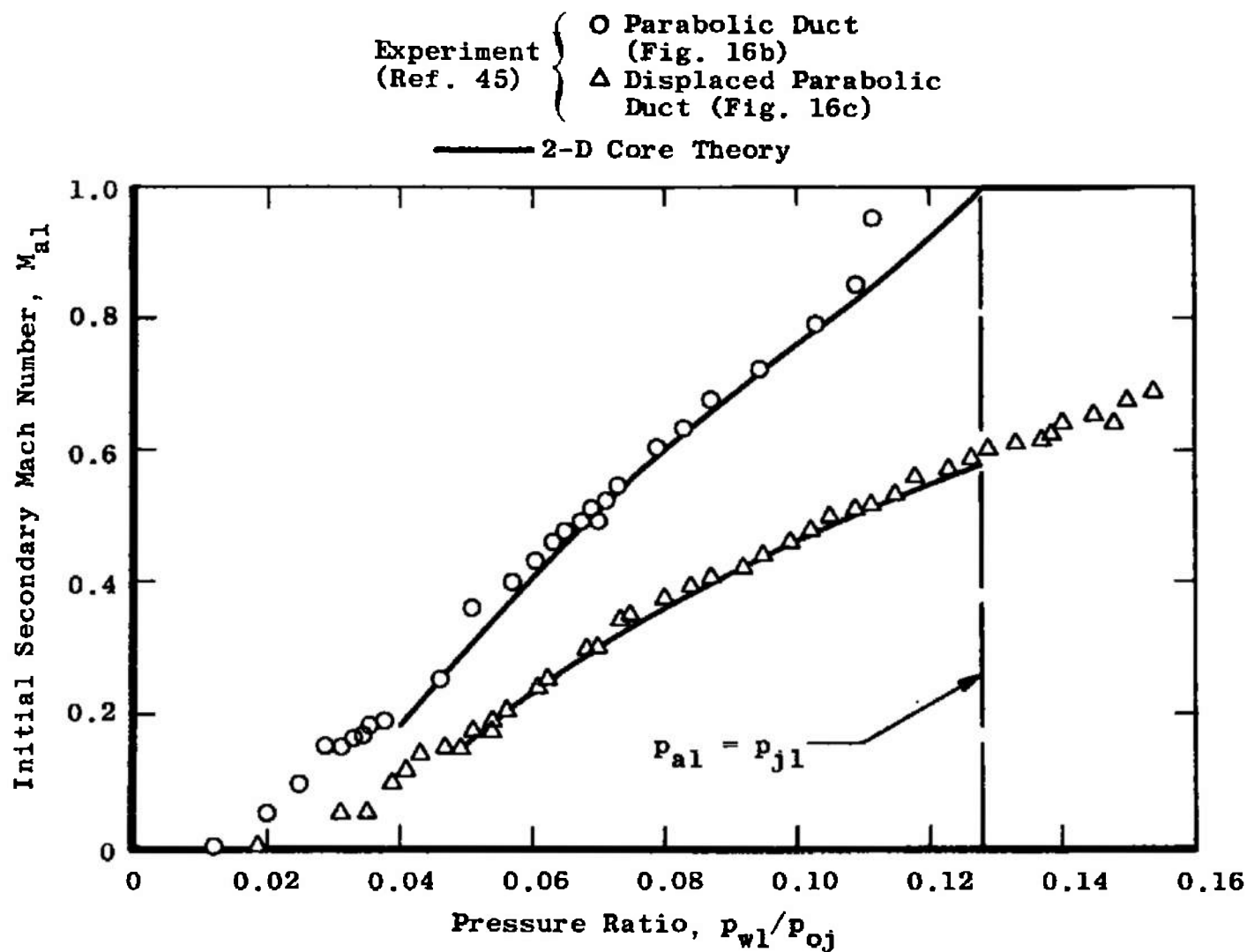
Fig. 21 Initial Secondary Mach Number in a Variable Area Air—Air Ejector

—— 2-D Core Theory

	p_{w1}/p_{oj}	p_b/p_{oj}	
∇ 0.06	0.1315	Displaced
Experiment $\triangle$ 0.08	0.1315	Parabolic
(Ref. 45) O 0.10	--	Duct
□ 0.12	--	(Fig. 16c)

$p_{al}/p_{oa} = 0.0602$

$p_{al}/p_{oa} = 0.0800$

Locus of Critical Flow

$M_a = 1$

$p_{al}/p_{oa} = 0.0995$

$p_{al}/p_{oa} = 0.1204$

Wall Pressure Ratio, p_w/p_{oa}

Axial Distance, x/r_n

Fig. 22 Wall Pressure Distributions in a Variable Area Air—Air Ejector

SECTION XVII
CORRELATION OF 2-D CORE THEORY WITH ROCKET-AIR MIXING EXPERIMENTS

The main objective of this investigation has been to predict the performance of ducted mixing systems in which chemical reactions occur. Peters, et al. (Ref. 6) and Cunningham and Peters (Ref. 7) presented experimental results on ducted mixing systems in which the primary stream was the exhaust from a hydrogen-oxygen rocket and the secondary stream was unheated air. The rocket was operated with approximately 2.5 times stoichiometric fuel (O/F = 3.2), therefore, there was potential for considerable heat release in the mixing process. The rocket nozzle area ratio was approximately 5, and the rocket was operated with a combustion chamber pressure (p_{oj}) of approximately 20 atm. for all tests. The two mixing duct configurations shown in Fig. 23 will be considered here. Experimental results were presented in Ref. 6 for the conical mixing duct of Fig. 23a. The mixing system was operated in the upstream choking mode (Fig. 2, Section I). Results were presented in Ref. 7 for the same basic apparatus, except that a cylindrical extension was added to the conical mixing duct (Fig. 23b) so that th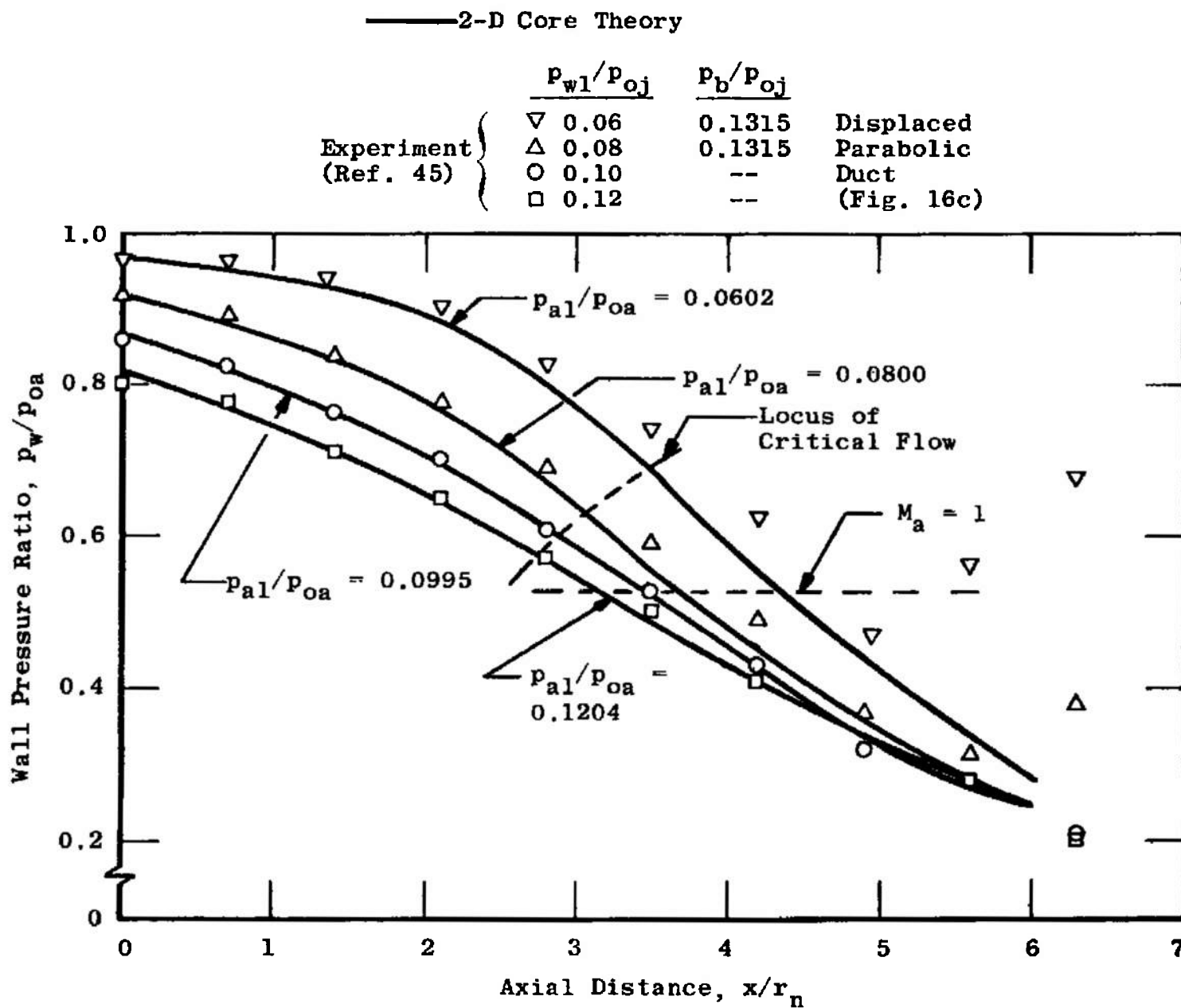e system operated in the downstream choking mode. Results were also presented in Ref. 7 for the configuration of Fig. 23b operated in the back pressure dependent mode.

References 6 and 7 present experimental wall pressure distributions, secondary-primary mass flow ratios, mixing duct thrust ratios, and radial distributions of Pitot pressure and gas composition at the duct exit plane.

The mixing duct thrust, F_d, is defined as the axial pressure force exerted on the mixing duct between the

$r_n/r_{w1} \propto 0.38$, $r_{w1} = 3$ in. (≈ 7.5 cm.)
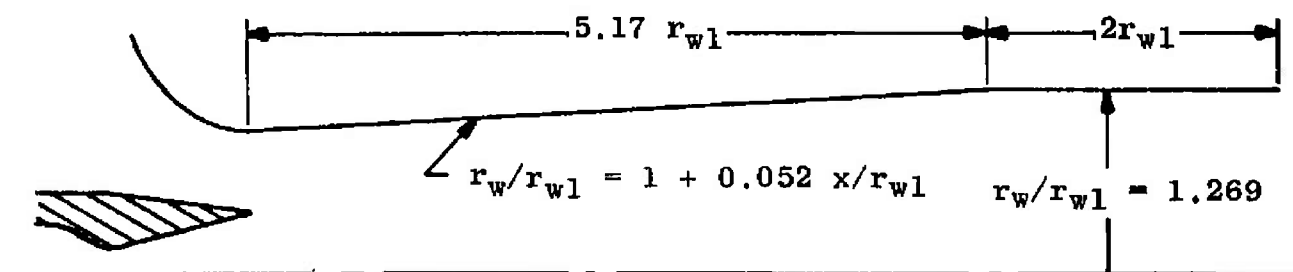Conical Rocket Nozzle (15° Half Angle)
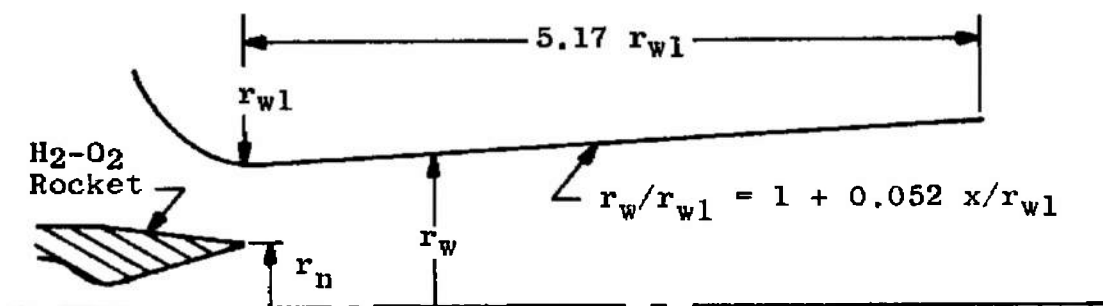
a. Conical Mixing Duct (Ref. 6)

b. Conical Mixing Duct with Cylindrical Extension (Ref. 7)

Fig. 23 Rocket-Air Mixing Configurations

entrance and exit sections, i.e.,

$$F_d = 2\pi \int_0^L p_w r_w \left(\frac{dr_w}{dx}\right) dx \qquad (104)$$

where L is the length of the mixing duct and r_w is a known function of x.

1. Mixing System Operating in the Upstream Choking Mode

This section presents the correlation of the 2–D Core Theory with the experimental results for the configuration of Fig. 23a (Ref. 6).

Axial distribution of theoretical flow parameters — Before discussing the correlations of the 2–D Core Theory with experiments, consider the theoretical distributions of the flow field parameters shown in Fig. 24. The axial distributions of p_w, r_i, b and Q are shown in Fig. 24a for a typical ducted mixing computation. The distributions of θ_i and the coefficient determinant, $|D|$, are shown in Fig. 24b. This flow field solution was obtained by using the procedure described in Section XV, i.e., the initial static pressure, p_{w1}, was iterated until the solution was bracketed to a small tolerance. The secondary stream total pressure, p_{oa}, was then increased slightly (by 0.3% in this case) to allow the solution to proceed smoothly into the supercritical regime.

The pressure distribution, p_w/p_{oa}, shown in Fig. 24a indicates that the secondary Mach number, M_a, is initially 0.71; M_a increases to approximately 0.94 at the critical section. The value of M_a at the duct exit is approximately 1.3.

The axial distribution of r_i (Fig. 24a) shows the usual tendency of a jet from a conical nozzle to have a periodic structure. If the flow were inviscid, the second peak in r_i would be about as large as the first peak. With
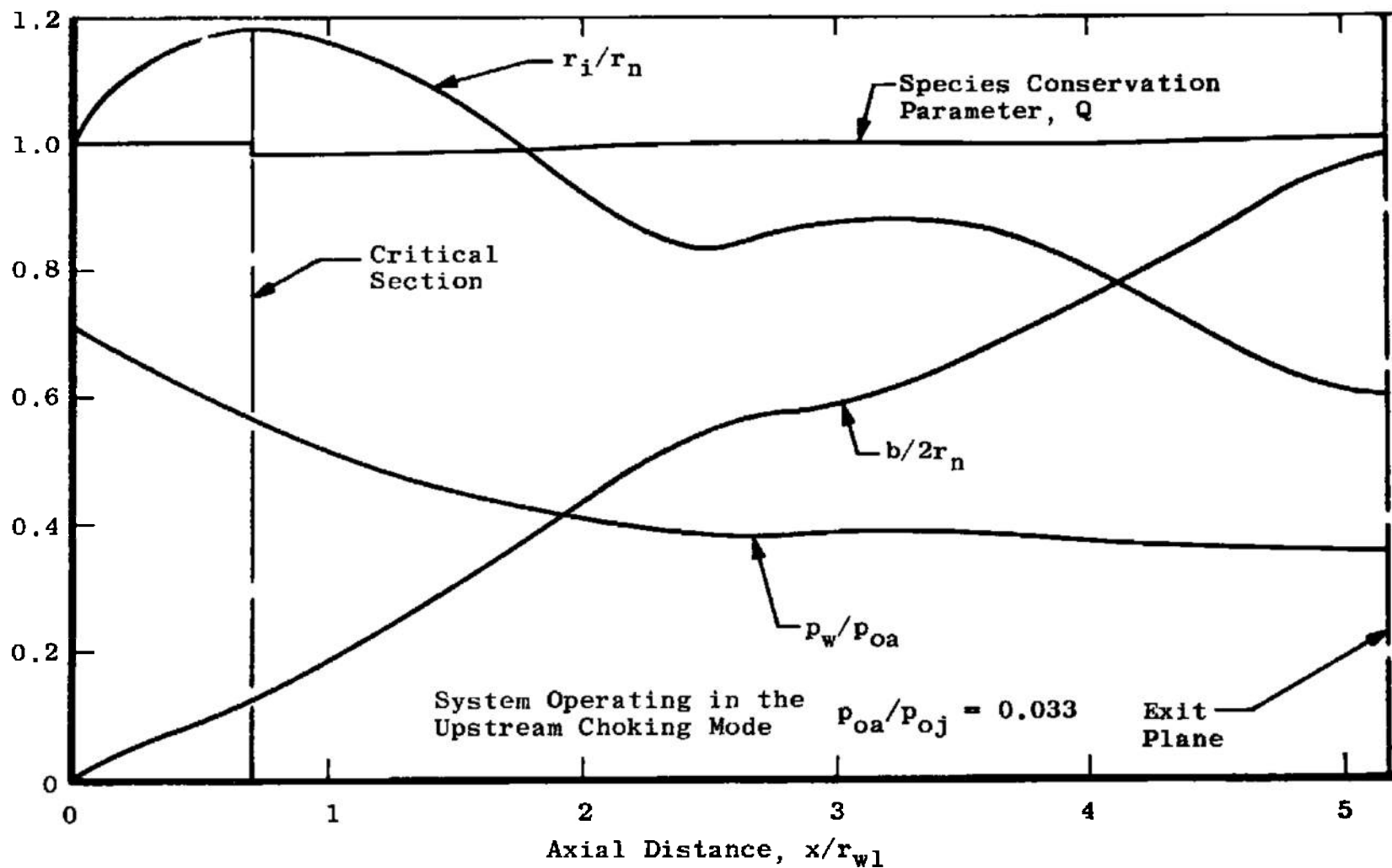
a. (p_w, r_i, b, Q) vs. x

Fig. 24 Variation of Theoretical Flow Parameters for a Typical Rocket-Air Mixing Computation
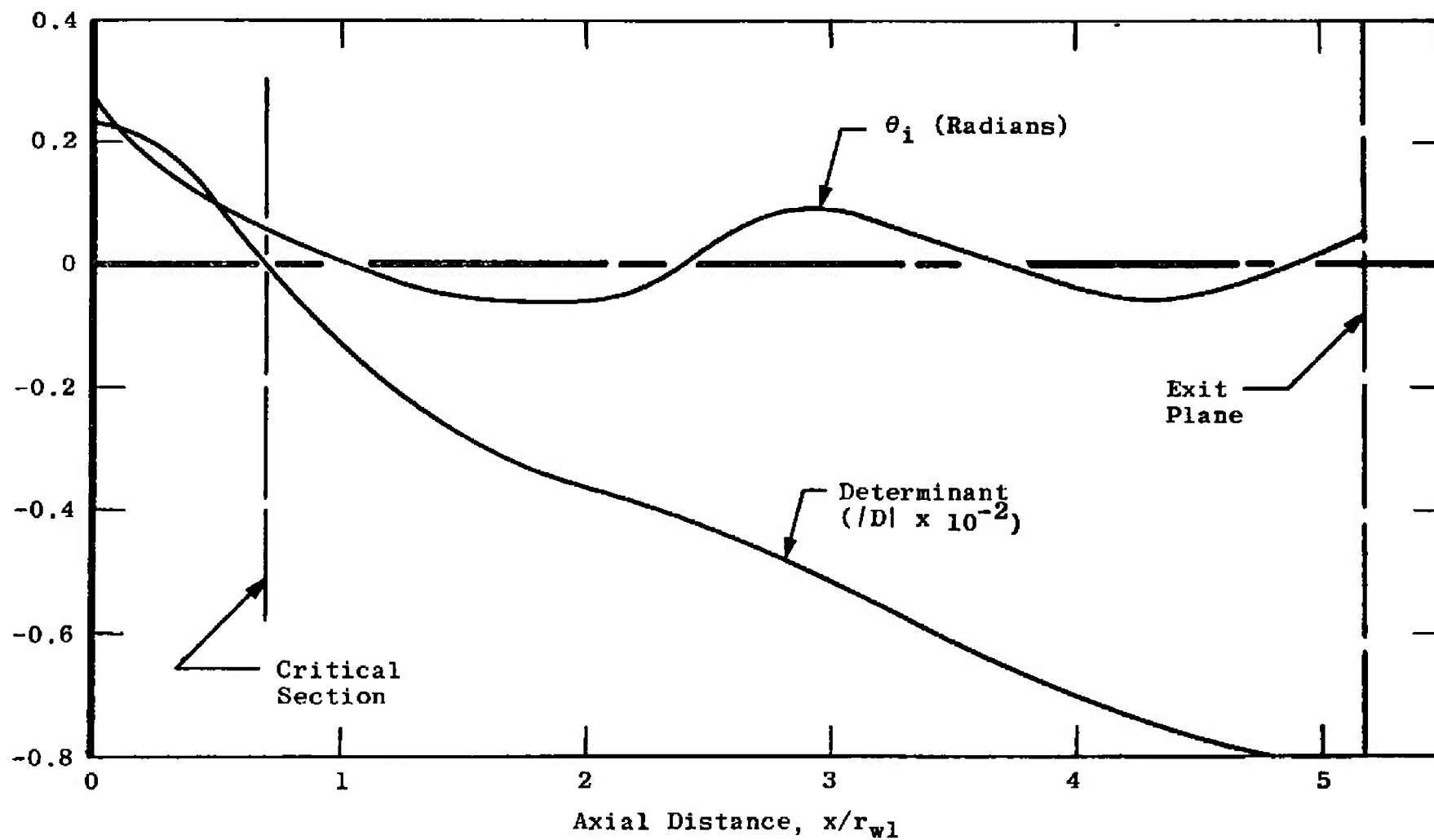
b. $(\theta_i, |D|)$ vs. x

Fig. 24 Concluded

mixing, the core flow tends to expand and contract, but with gradually decreasing r_i. This gradual decrease in r_i is caused by the mixing zone growing into the inviscid core flow. If the duct were sufficiently long the inviscid flow would eventually be completely dissipated. With this configuration, however, only the first mixing regime is encountered.

The axial distribution of b (Fig. 24a) shows that the mixing zone growth rate, db/dx, is not approximately constant, but is significantly influenced by the periodic nature of the inviscid core flow. Computations have been made for similar pressure distributions with the 1-D Core Theory, and no large variation of db/dx was predicted. It is concluded, therefore, that the variations of db/dx indicated by Fig. 24a are primarily caused by the angularity of the flow at r_i. There is a definite qualitative relation between the distribution of θ_i (Fig. 24b) and b, with negative values of θ_i tending to increase the mixing zone growth rate.

The axial distribution of the coefficient determinant, $|D|$, for the system of equations (Fig. 24b) shows that $|D|$ is positive for subcritical flow and passes smoothly through zero at the critical point.

The species conservation parameter, Q, (defined by eq. 2'., Section XI) is shown in Fig. 24a. It will be recalled that if Q does not deviate from unity, then the use of eq. (25a) (Section V) to relate the velocity, composition and enthalpy profiles is justified. It is seen that Q is initially unity, then undergoes a step decrease to about 0.98 at the critical section where p_{oa} was arbitrarily increased. Downstream of the critical section, Q gradually increases and has a value of 1.01 at the duct exit. This behavior of Q is typical for all of the rocket-air mixing cases considered. In no case does Q deviate from unity by more than about 2%.

It can be concluded, therefore, that eq. (25a) satisfactorily relates the species and enthalpy profiles to the mixing zone velocity profiles, at least for use in an integral method.

Wall pressure distributions – Experimental wall pressure distributions are shown in Figs. 25a and 25b for two values of the total pressure ratio, p_{oa}/p_{oj}. Also shown are the pressure distributions predicted by the 2-D Core Theory with the assumption of equilibrium mixing zone chemistry. The theoretical pressure distribution agrees fairly well with the experiment in the upstream half of the duct, but falls somewhat below the experiment in the downstream part of the flow. One should note the tendency of the inviscid core flow to alternately expand and contract (Fig. 24a) which has a corresponding effect on the wall pressure distribution. The theoretical second peak in r_1 is apparently too small. This deviation from experiment may be explained, at least qualitatively, by the presence of shock waves in the experimental core flow. If the total pressure of the core flow were reduced, on the average, by a system of shock waves, then the core flow would occupy a larger area in order to satisfy continuity relations. The greater area occupied by the core flow would decrease the area available for the supersonic secondary flow, therefore, the theoretical wall static pressure would be increased in the downstream part of the flow.

A theoretical pressure distribution is also shown in Fig. 25a for the case of no mixing. Upstream of the critical section, the wall pressure is slightly lower than in the case with mixing. Because of the higher M_{a1}, the secondary mass flow is approximately 3% higher for the zero mixing case. The theoretical pressure distribution for zero mixing is considerably lower than the theoretical distribution with mixing in the downstream part of the flow. Consequently, the mixing duct thrust, F_d, is about 25% lower than the value obtained with mixing.
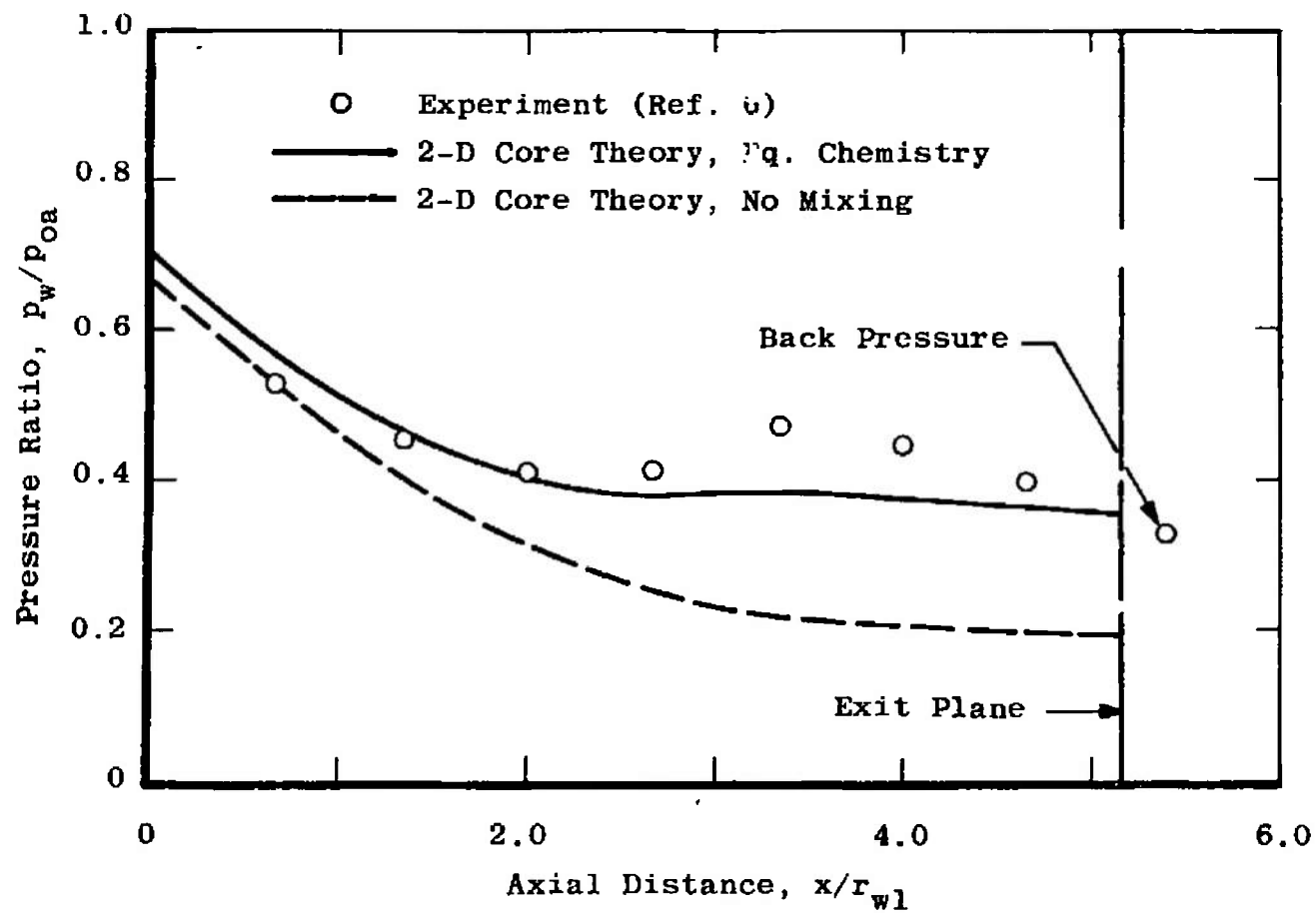
a. $p_{oa}/p_{oj} = 0.033$

Fig. 25 Wall Pressure Distribution for Ducted Rocket-Air Mixing (Upstream Choking Mode)
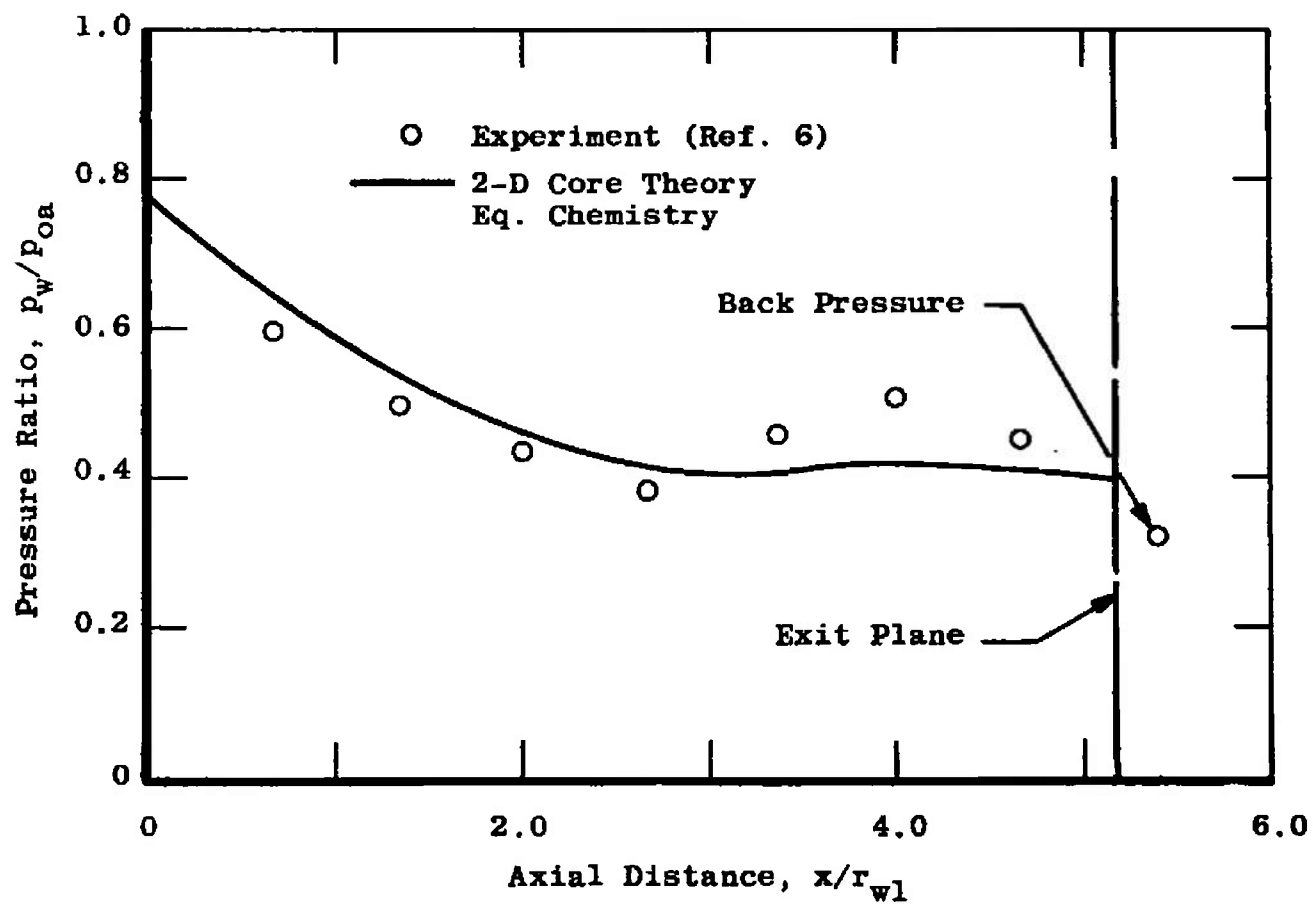
b. $p_{od}/p_{oj} = 0.025$

Fig. 25 Concluded

Comparing the two theoretical pressure distributions in Fig. 25a, one sees that the mixing acts as blockage to the flow. An effective displacement thickness, δ^*, for the mixing layer is then positive. It is noteworthy that for mixing in air-air ejectors, such as considered in Section XVI, the effective displacement thickness is negative, i.e., the secondary flow is larger with mixing than without mixing (Ref. 35). The positive δ^* in the rocket-air mixing system can be attributed in part to the large heat release in the mixing layer.

Second-primary mass flow ratio - The experimental mass flow ratio, w_a/w_j, is shown in Fig. 26 as a function of p_{oa}/p_{oj}. The 2-D Core Theory predicts the correct form for the mass flow function, but the theoretical mass flows are 4-5% higher than the experiment. The quantitative deviation between theory and experiment can perhaps be attributed to deviations from conical flow in the primary nozzle. The theoretical computations were based on a source-type flow in the primary nozzle, but it is well known that the source flow assumption can be considerably in error for such short conical nozzles.

Mixing duct thrust - The mixing duct thrust is shown in Fig. 27 as the ratio F_d/F_n where F_n is the vacuum thrust of the primary nozzle. The 2-D Core Theory predicts the thrust ratio fairly well at $p_{oa}/p_{oj} = 0.025$, but the theoretical value is about 8% below the experiment at $p_{oa}/p_{oj} = 0.034$.

Radial Pitot pressure profiles - The radial distribution of Pitot pressure at the duct exit is shown in Figs. 28a and 28b for two values of p_{oa}/p_{oj}. It should be noted that the exit plane distributions are composite plots of several short duration tests. Because of the difficulty in exactly reproducing all of the experimental conditions from test to test,

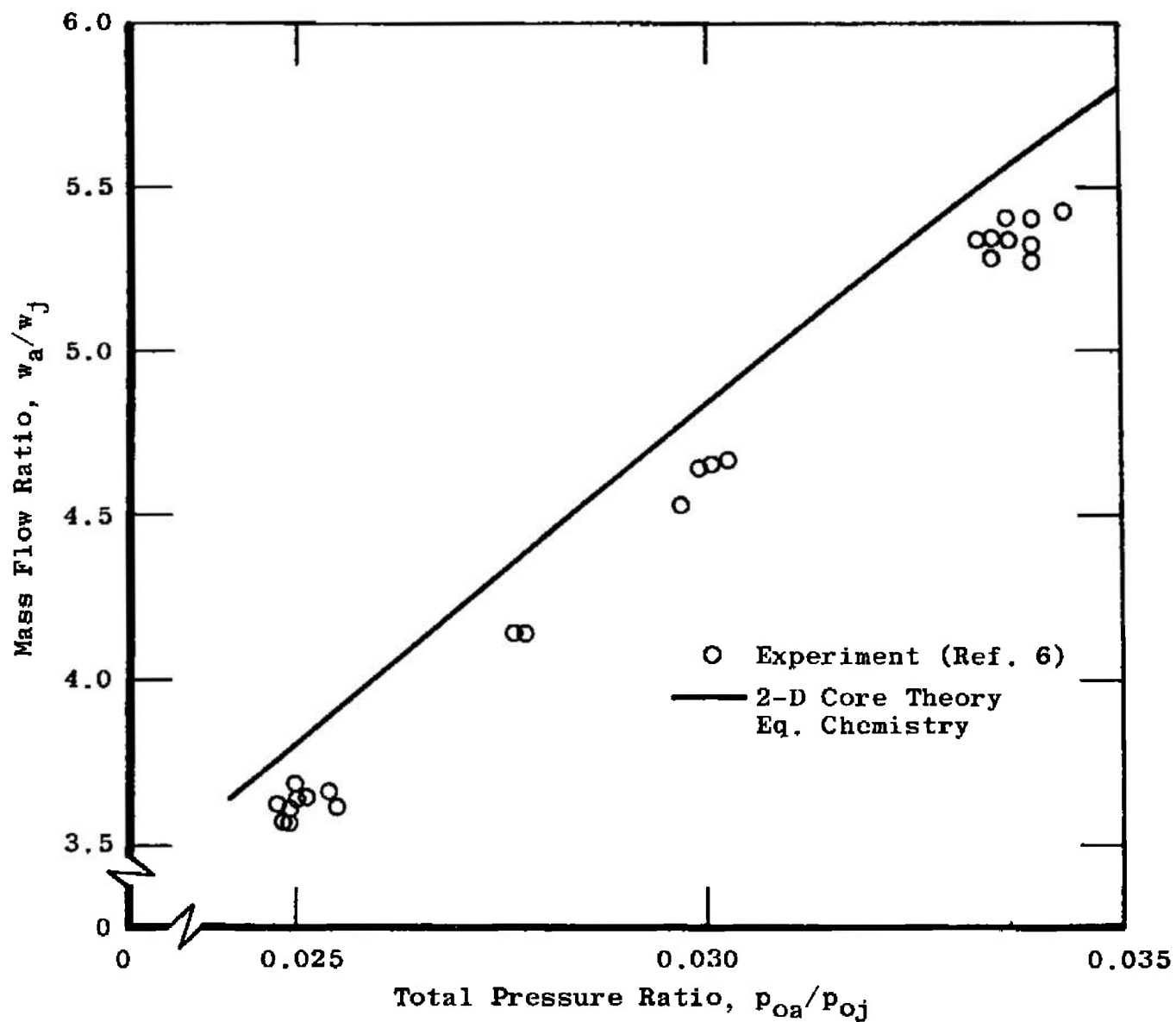Fig. 26 Mass Flow Ratio for Ducted Rocket-Air Mixing (Upstream Choking Mode)

Fig. 27 Mixing Duct Thrust for Ducted Rocket-Air Mixing (Upstream Choking Mode)
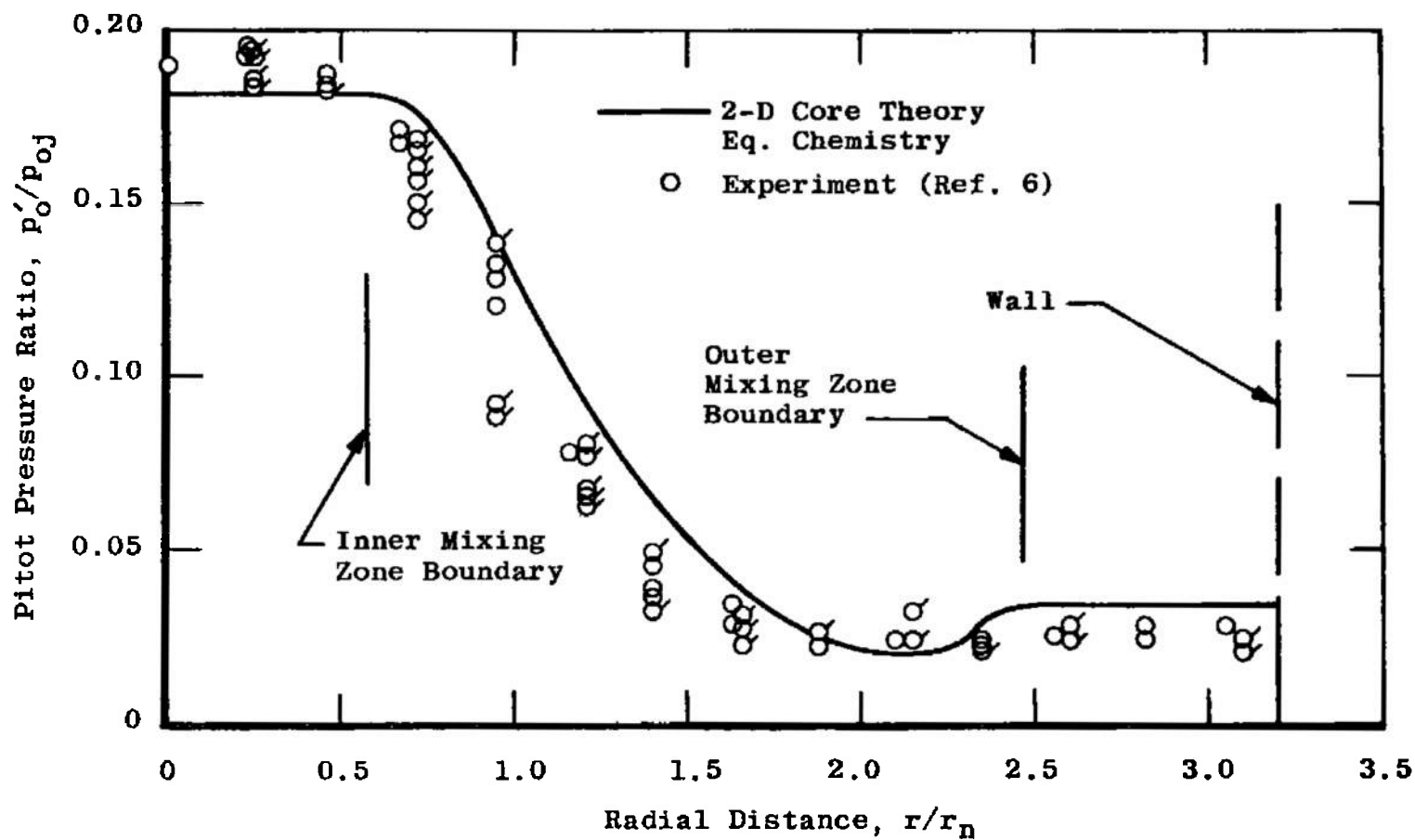
a. $p_{oa}/p_{oj} = 0.033$

Fig. 28 Exit Plane Pitot Pressure Profiles for Ducted Rocket-Air Mixing (Upstream Choking Mode)
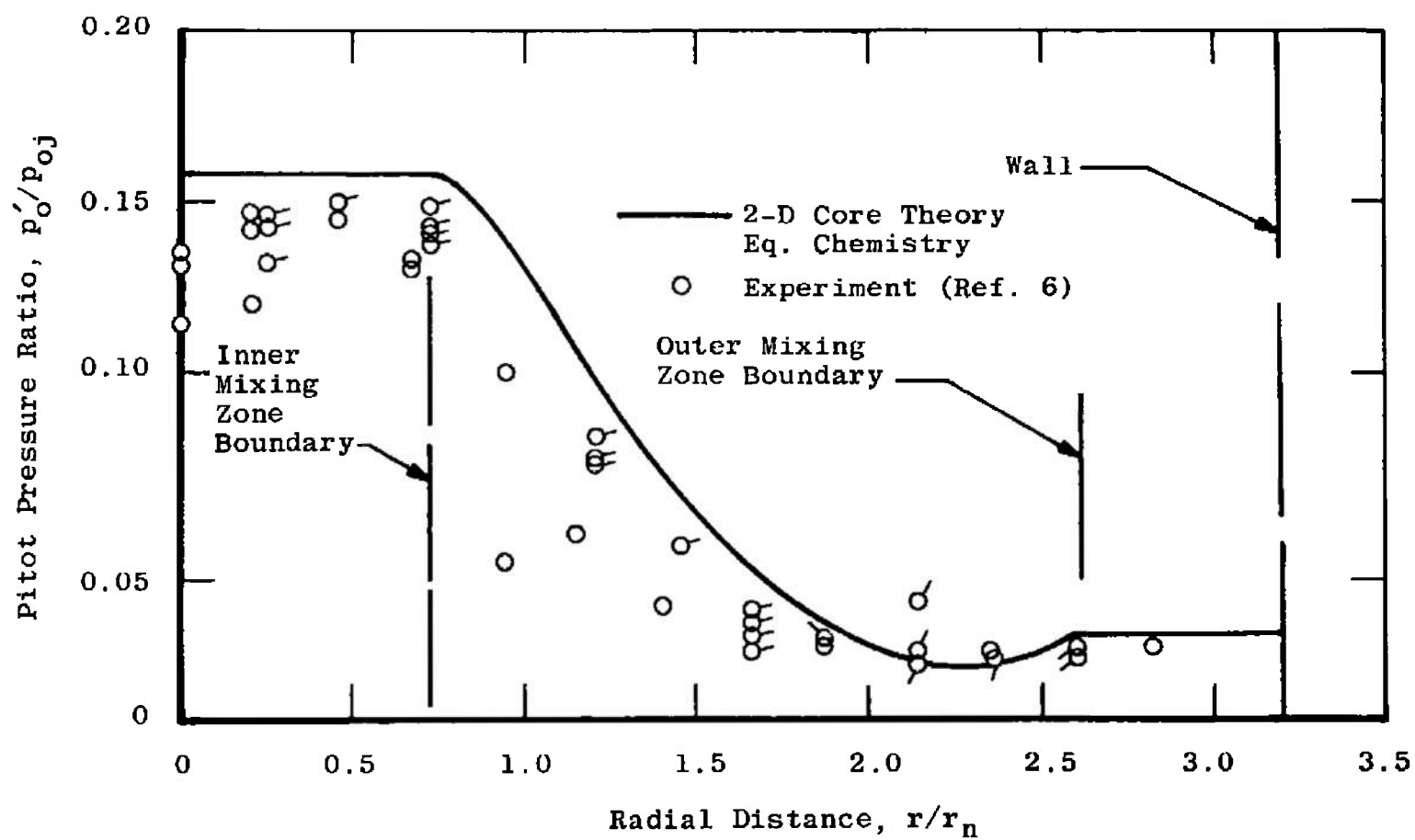
b. $P_{oa}/P_{aj} = 0.025$

Fig. 28 Concluded

considerable data scatter is inevitable[*]. The theory adequately predicts the shape of the Pitot pressure profile for the higher pressure ratio case (Fig. 28a), but the theoretical profile is displaced radially outward compared to the experiment. The same is true of the p_{oa}/p_{oj} = 0.025 case (Fig. 28b), and in addition, the experiment shows a decrease in p_o' near the centerline of the duct. This decrease in p_o' is undoubtedly caused by the presence of strong shock waves in the inviscid core flow. The shock system would tend to be somewhat stronger for lower values of p_{oa}/p_{oj} compared to higher pressure ratios because the primary flow is initially underexpanded to a greater extent.

Radial composition profiles – Before considering the experimental composition profiles at the duct exit, the differences between the frozen and equilibrium profiles will be discussed. The experimental technique reported in Refs. 6 and 7 was to take a sample of gas, then analyze it after removing the water vapor. The composition profiles were then presented as "dry mole fractions" of O_2, H_2 and N_2. The theoretical dry mole fraction profiles across the mixing zone are shown in Fig. 29. The major characteristic of the equilibrium profiles is that the N_2 tends to peak, and the H_2 goes to zero, near the stoichiometric point in the mixing layer. The frozen distributions, on the other hand, are monotonic and continuous across the mixing zone.

---

[*] Measurements of Pitot pressure and gas composition were made across the entire duct exit plane during the AEDC experiments. The flagged symbols represent measurements made on the opposite side of the centerline from the measurements represented by the unflagged symbols (Figs. 28, 30, 34 and 35).
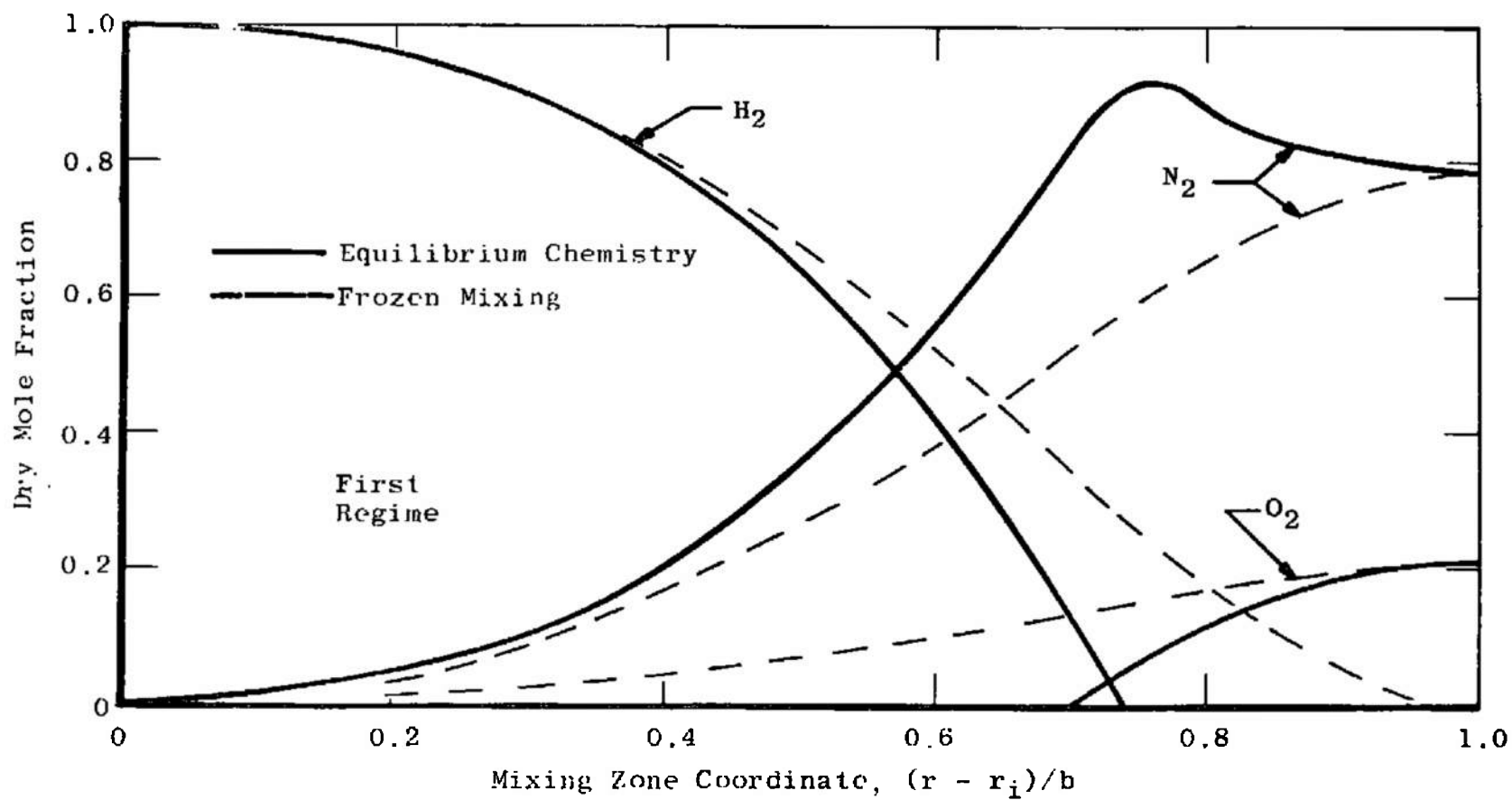
Fig. 29 Theoretical Composition Profiles in Mixing Zone (Without Water)

Experimental radial profiles of H_2, O_2 and N_2 are shown in Figs. 30a and 30b for $p_{oa}/p_{oj} = 0.033$ and 0.025, respectively. Although there is considerable scatter in the data, the 2-D Core Theory with equilibrium chemistry predicts the shape of the experimental profiles reasonably well, especially the tendency of the H_2 to go to zero within the mixing zone. As was the case with the Pitot pressure profiles, the theoretical profiles are displaced outward from the duct centerline compared to the experimental profiles. This outward displacement of the mixing zone can be explained by the neglect of shock waves in the inviscid core flow. If the shock waves were included in the theory, then the momentum of the core flow would be less than the isentropic momentum, and the mixing zone would tend to be oriented more toward the duct centerline. In general, alteration of the momentum ratio in a two stream mixing process causes the mixing zone to shift toward the stream which is decreased in relative momentum.

Comparison of 1-D Core Theory with 2-D Core Theory — Although not well adapted for analyzing mixing systems operating in the upstream choking mode, the 1-D Core Theory can be applied to such flows. The central stream is assumed to be initially uniform. Immediately downstream from the primary nozzle the primary and secondary streams are assumed to undergo isentropic area changes such that the pressures are equilibrated; the combined primary and secondary stream areas must equal the initial duct area. This initial readjustment process between the two streams is the same as the "quasi-one-dimensional" approaches discussed in Section I, with the additional requirement that the readjustment process occurs instantaneously.

Applying the preceding procedure to the ducted mixing system, the secondary stream choking section occurs at the duct entrance. For the range of p_{oa}/p_{oj} reported
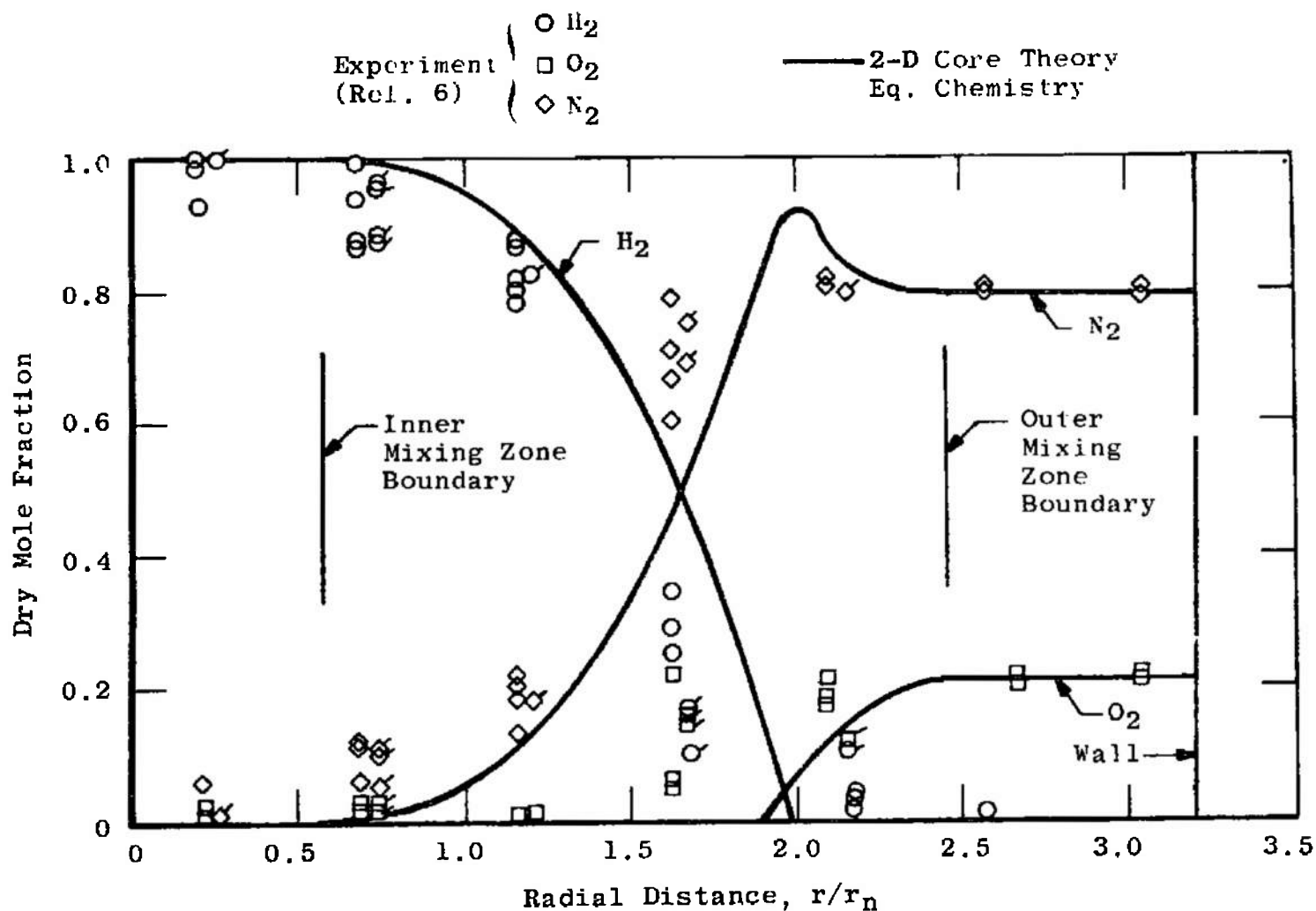
a. $P_{a\alpha}/P_{oj} = 0.033$

Fig. 30 Exit Plane Composition Profiles for Ducted Rocket-Air Mixing (Upstream Choking Mode)
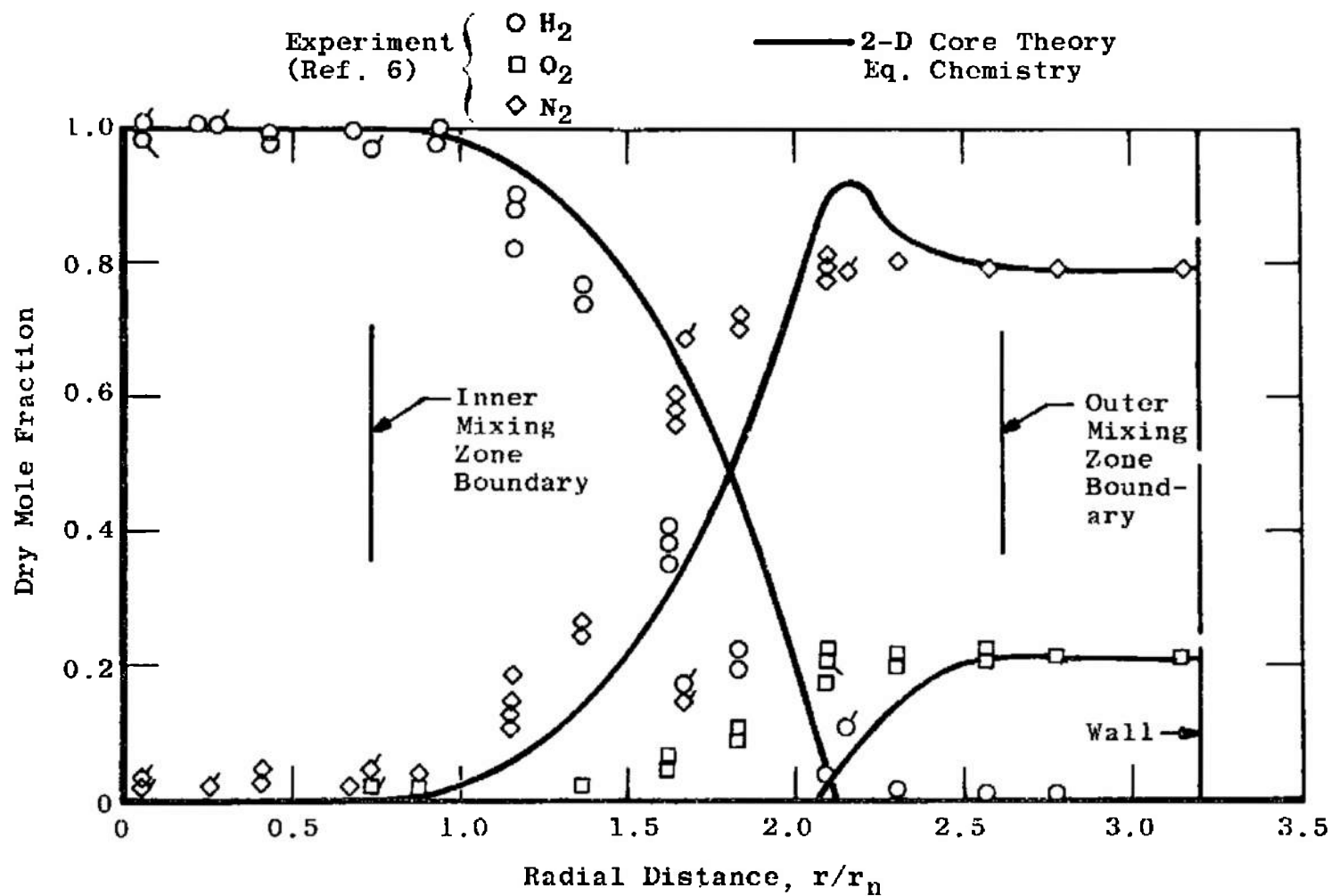
b. $p_{oa}/p_{oj} = 0.025$

Fig. 30 Concluded

in Ref. 6, the secondary mass flow, w_a, is 5 to 7% higher than predicted by the 2-D Core Theory (Fig. 26). Because the secondary flow is initially sonic, $p_{w1}/p_{oa} = 0.528$, considerably lower than predicted by the 2-D Core Theory (Fig. 25). The wall pressure monotonically decreases with downstream distance, and the mixing duct thrust is substantially lower than predicted by the 2-D Core Theory. These results clearly show the need for the 2-D Core Theory for mixing systems operating in the upstream choking mode.

It should be noted that a less refined version of the 1-D Core Theory was used in Ref. 6 to compute the theoretical performance of the rocket-air mixing system operated in the upstream choking mode. The flow upstream of the secondary stream choking section was computed by an approximate inviscid technique. The plume from the primary nozzle was approximated by a constant pressure plume at the secondary stream sonic pressure (plume computed by a standard method of characteristics program). Downstream from the choking section the duct wall was assumed to be shifted inward to account for the difference between the plume area and the one-dimensional primary stream area. The mixing theory computation was then initiated at the secondary stream choking section.

Although the preceding procedure gives results comparable to the 2-D Core Theory for the experiments considered here, it was pointed out in Ref. 6 that the procedure is questionable for many mixing configurations. For example, if the axial distance to the secondary stream choking section is large compared to the duct length, then most of the influence of the mixing process is neglected.

2. Mixing System Operated in the Downstream Choking Mode

This section presents the correlations of the 2-D Core Theory with experimental results for the configuration

of Fig. 23b operated in the downstream choking mode (Ref. 7). The theoretical computations for these cases were made by iterating on p_{w1} until the coefficient determinant, $|D|$, was equal to zero at the duct exit plane.

Wall pressure distributions - Experimental wall pressure distributions are shown in Figs. 31a-c for p_{oa}/p_{oj} of 0.036, 0.0304, and 0.027, respectively. The 2-D Core Theory predicts the correct shape for the pressure distributions, but the theoretical pressure is generally too high. This disagreement between theory and experiment is more pronounced at p_{oa}/p_{oj} = 0.036 than at the lower pressure ratios. As was the case for the upstream choking mode, the deviation of theory from experiment in the downstream part of the flow can be attributed to the neglect of shock waves in the theory. The inclusion of shocks in the theory would cause the area occupied by the inviscid core flow to increase, and the area for the subsonic secondary flow would decrease. Consequently, the wall pressures would be decreased.

Note that the inviscid core flow is completely dissipated in this configuration, and the flow at the duct exit is in the second mixing regime. It should also be noted that the flow is strongly influenced by viscous effects. Without mixing, this configuration would operate in the upstream choking mode. Comparing the pressure distributions of Figs. 25 and 31, one sees that the addition of the constant area extension to the conical mixing duct causes the wall pressure to be maintained at a high value for the entire duct length. This high wall pressure is desirable for a propulsion system because the wall pressures are directly equivalent to axial thrust.

Secondary-primary mass flow ratio - The experimental mass flow ratio, w_a/w_j, is shown in Fig. 32 as a function of the
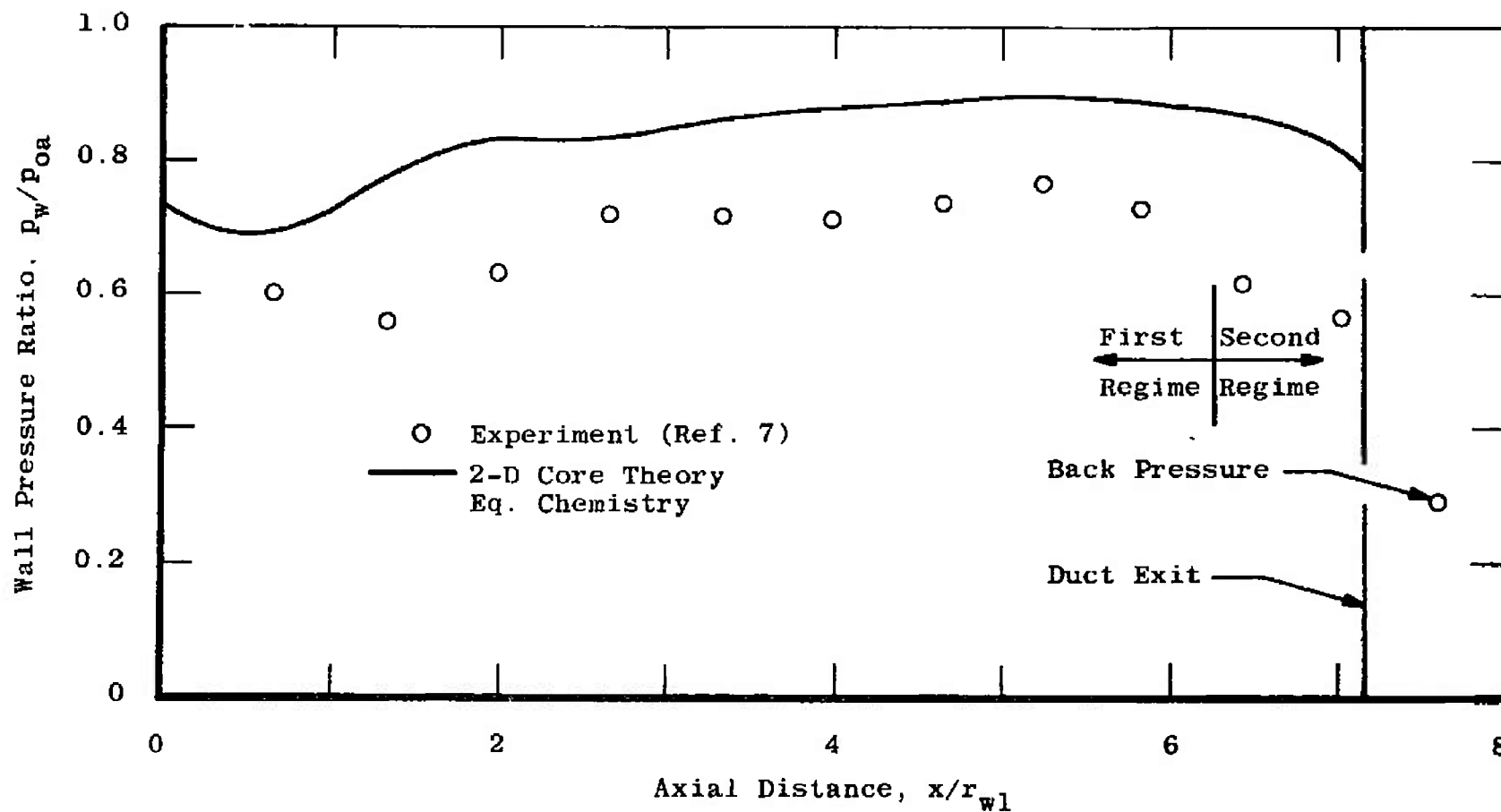
a. $p_{oa}/p_{oi} = 0.036$

Fig. 31 Wall Pressure Distribution for Ducted Rocket-Air Mixing (Downstream Choking Mode)
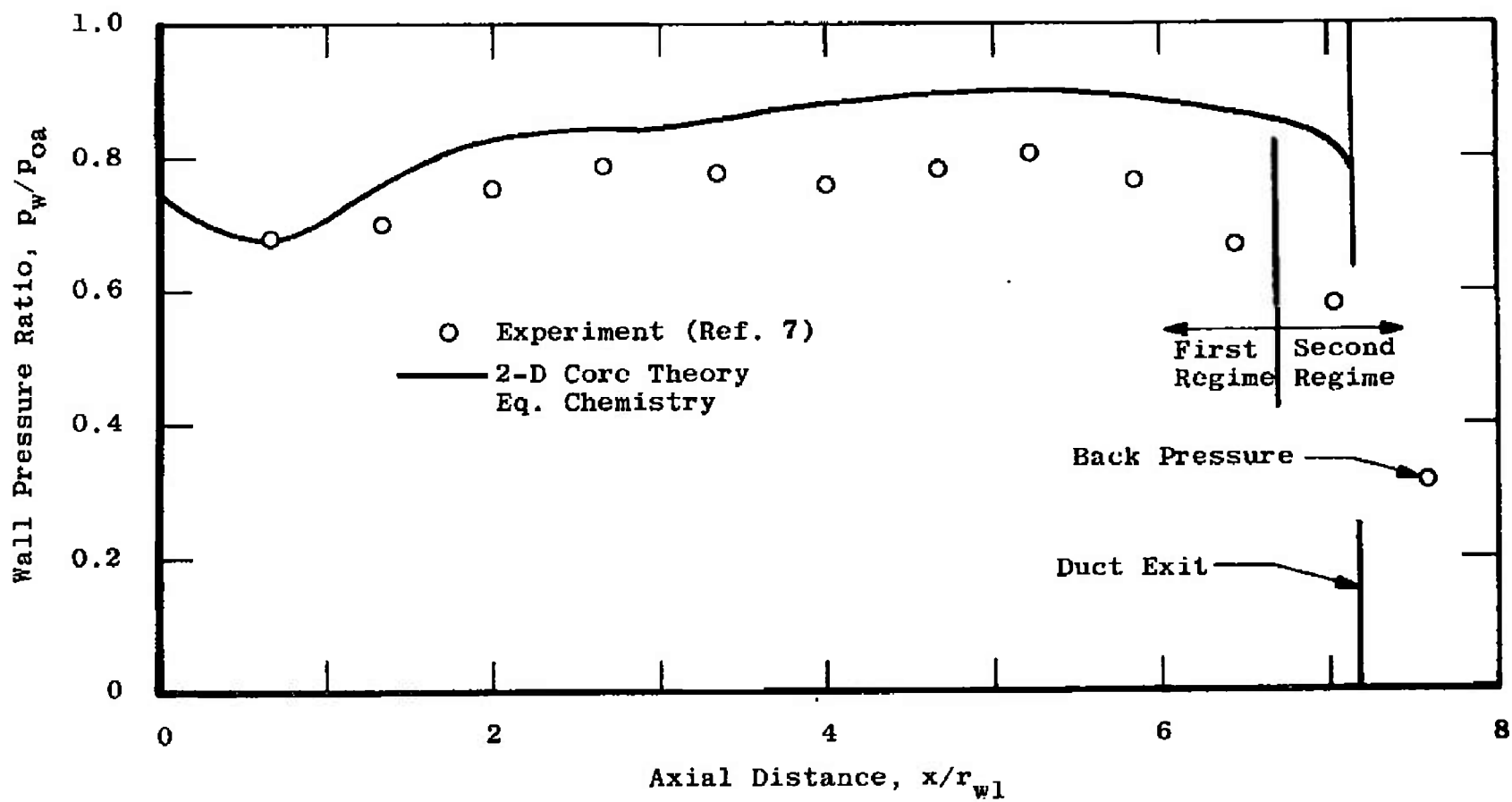
b. $p_{oa}/p_{oi} = 0.0304$

Fig. 31 Continued
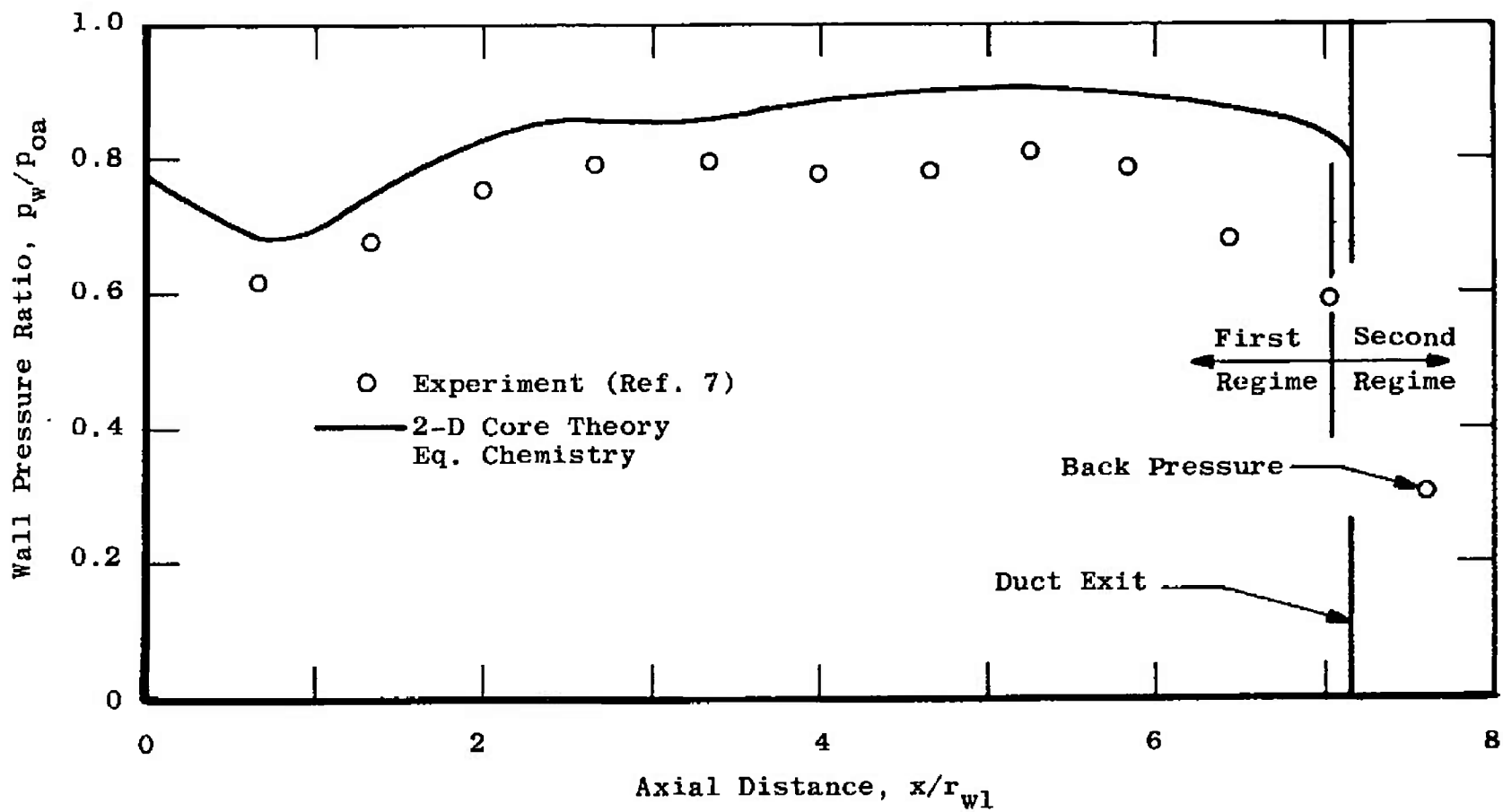
c. $p_{oa}/p_{oi} = 0.027$

Fig. 31 Concluded
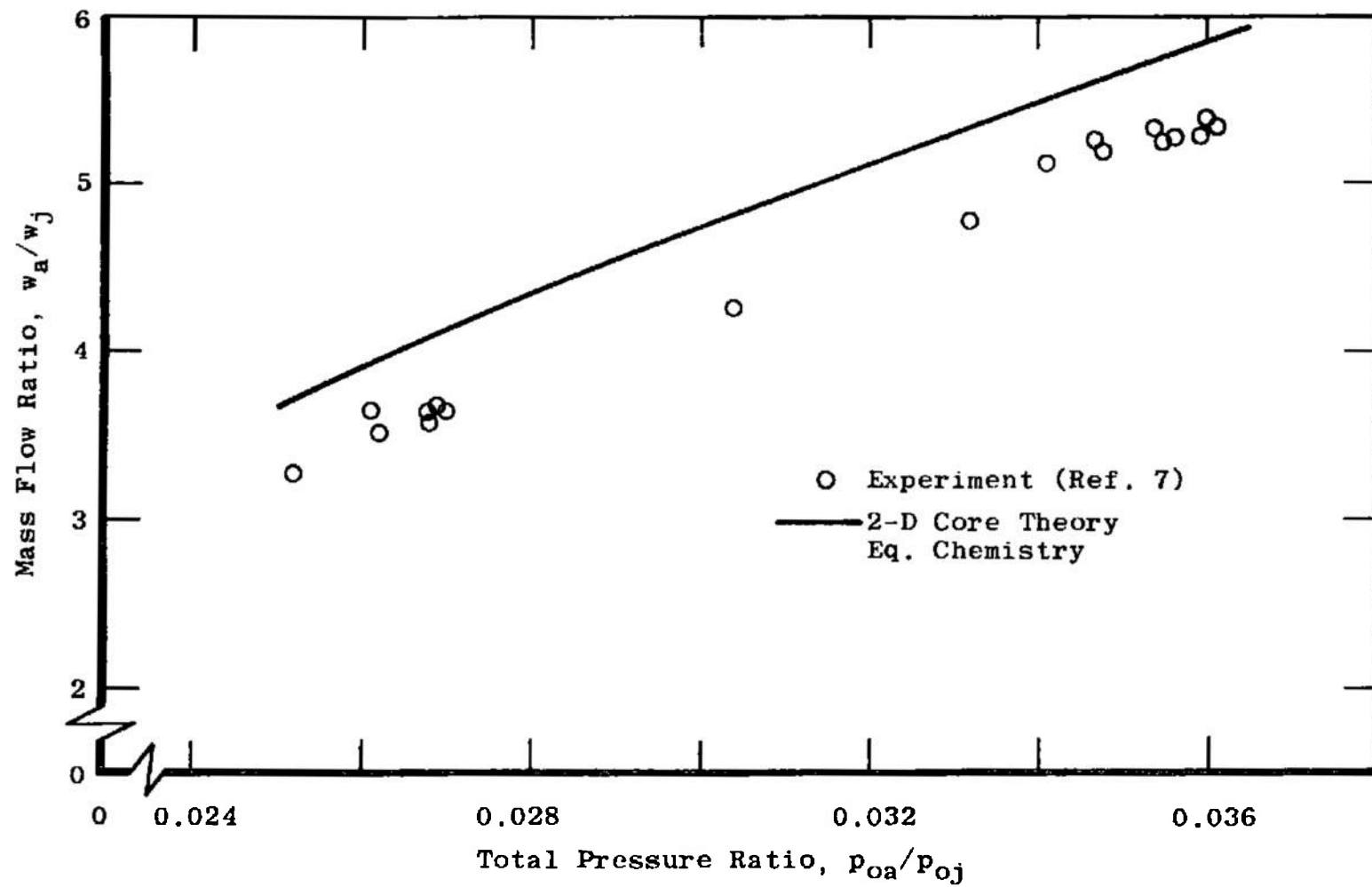
Fig. 32 Mass Flow Ratio for Ducted Rocket-Air Mixing (Downstream Choking Mode)

total pressure ratio. The 2-D Core Theory predicts the correct form for the mass flow function, but the theoretical mass flows are 10-15% higher than experiment. The rocket engine used for these experiments had a lower combustion efficiency than the rocket in Ref. 6. Consequently, the theoretical mass flow, w_j, is about 4% below the experimental w_j for a given p_{oj}. The theoretical and experimental values of w_a/w_j shown in Fig. 32 are nondimensionalized with the corresponding value of w_j. Because the theoretical w_j is lower than the experimental w_j, the theoretical mass flow ratio tends to be too high. The agreement between the theoretical and experimental values of w_a is, therefore, better by about 4% than indicated by Fig. 32.

Mixing duct thrust — The mixing duct thrust ratio, F_d/F_n is shown in Fig. 33. Because the theoretical wall pressures are generally higher than experiment, the theoretical thrust ratio is also too large. The theoretical thrust ratio is about 6% larger than experiment at the lower values of p_{oa}/p_{oj}, and about 16% too large at the higher values of the total pressure ratio.

Radial Pitot pressure profiles — The exit plane distributions of the Pitot pressure are shown in Figs. 34a and 34b for p_{oa}/p_{oj} of 0.036 and 0.027, respectively. Considering the data scatter, the agreement of theory and experiment is fair for p_{oa}/p_{oj} = 0.036. The experiment for p_{oa}/p_{oj} = 0.027, however, shows very low Pitot pressures compared with the theory near the duct centerline. A strong shock system has undoubtedly occurred in the inviscid core flow upstream of the duct exit. As was the case for the upstream choking mode, a stronger shock system would be expected as the total pressure ratio is decreased (greater underexpansion of the primary nozzle).

Fig. 33 Mixing Duct Thrust for Ducted Rocket-Air Mixing (Downstream Choking Mode)
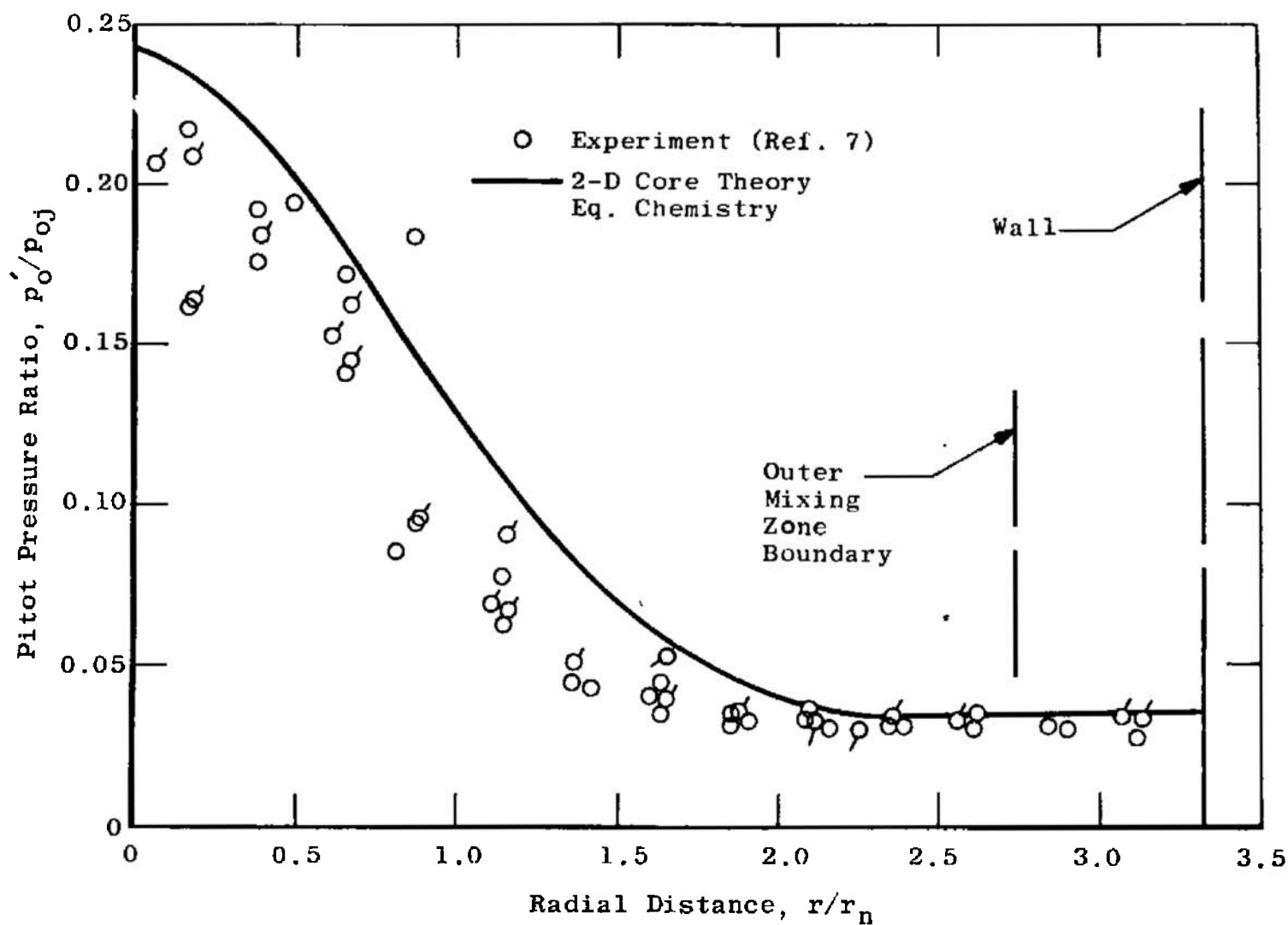
a. $p_{oa}/p_{oj} = 0.036$

Fig. 34 Exit Plane Pitot Pressure Profiles for Ducted Rocket-Air Mixing (Downstream Choking Mode)
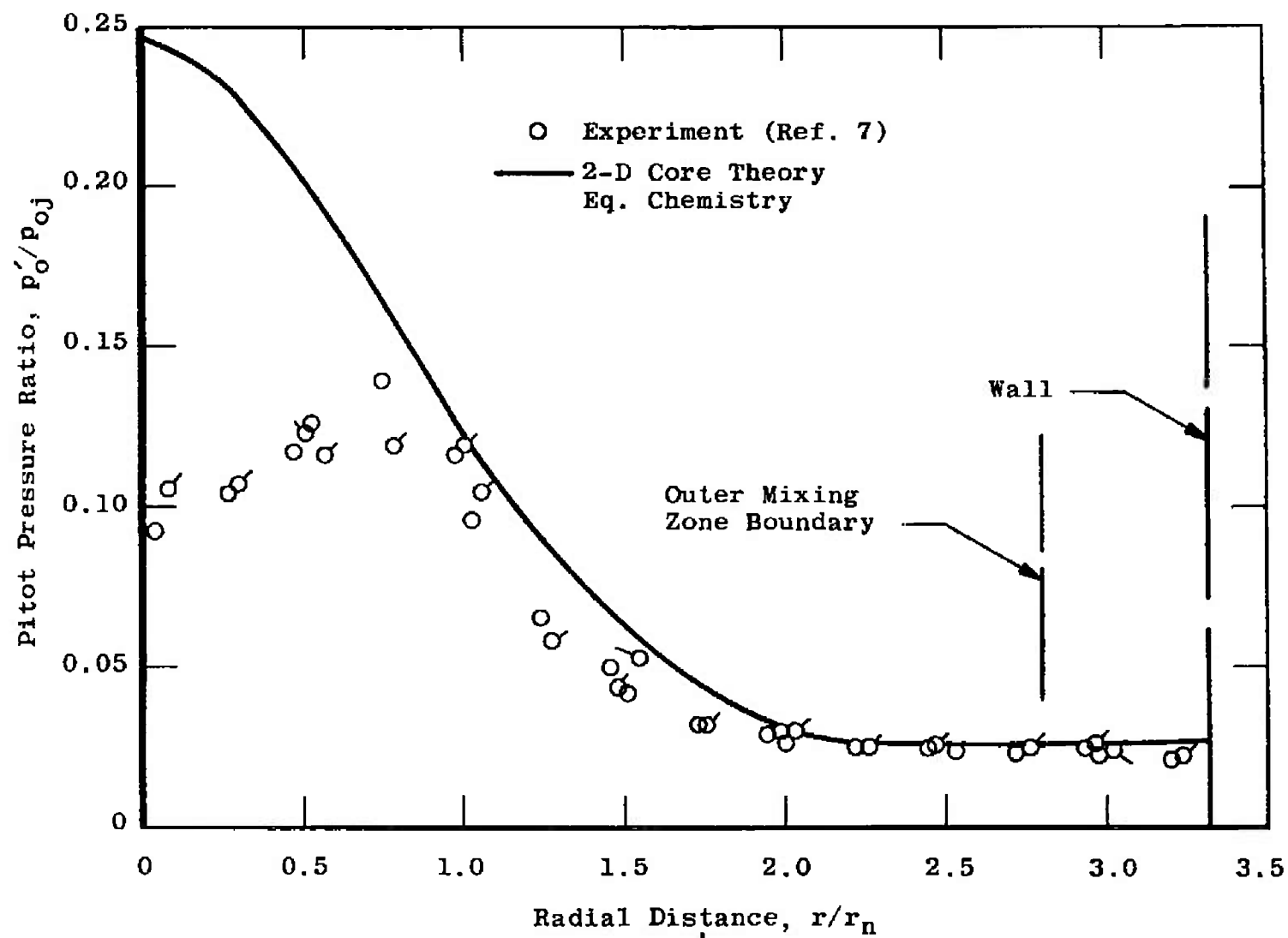
b. $p_{nn}/p_{oj} = 0.027$

Fig. 34 Concluded

Radial composition profiles — Exit plane profiles of H_2, O_2 and N_2 are shown in Fig. 35 for $p_{oa}/p_{oj} = 0.036$. The agreement between theory and experiment is quite good for this case. The experimental N_2 distribution clearly shows the peak predicted by the theory with the assumption of equilibrium chemistry. These results leave little doubt that the assumption of equilibrium mixing zone chemistry is good for these experimental conditions.

Exit plane choking parameter — These computations for a ducted mixing system operating in the downstream choking mode were made by assuming that choking occurs at the duct exit, and that choking corresponds to the system of equations becoming critical ($|D| = 0$). It is of interest to compare these results with an exterior hypothesis about the choking of a nonuniform flow. Herpfer (Ref. 46) derived a choking criterion for nonuniform flow based on the principle that choking corresponds to a condition of maximum mass flux. He assumed that there are no radial pressure gradients in the flow and that the local speed of propagation is the isentropic value. Choking then occurs when the parameter Ch,

$$Ch = \frac{2\pi}{P} \int_{0}^{r_w} \frac{(1 - M^2)}{\gamma M^2} \, r \, dr \qquad (105)$$

is equal to zero. This choking criterion states that if a portion of a choked flow is supersonic, then another portion of the flow must be subsonic.

The parameter Ch was computed in the second regime for the ducted mixing conditions presented in this section. If one defines an effective uniform stream Mach number, M_u, such that
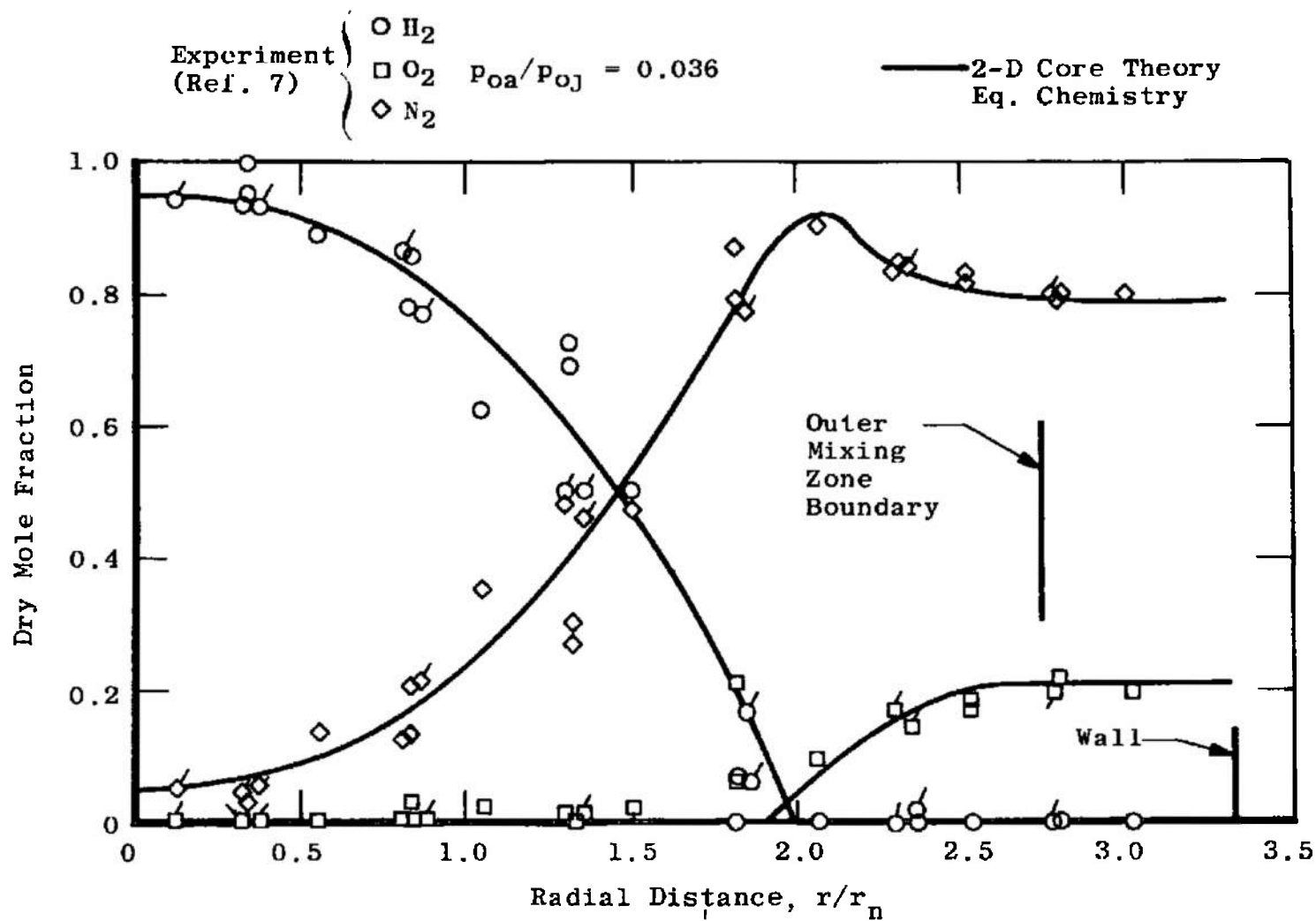
Fig. 35 Exit Plane Composition Profiles for Ducted Rocket-Air Mixing (Downstream Choking Mode)

$$Ch = \pi \; \frac{\left(1 - M_u^{\,2}\right)}{\gamma \, P \, M_u^{\,2}} \; r_w^{\,2} \tag{106}$$

then M_u should be unity when $|D| = 0$ if $Ch = 0$ is the correct choking criterion. From the ducted mixing theory, M_u was found to be 0.94 – 0.95 when $|D| = 0^*$. Thus the system of equations for the ducted mixing problem shows that part of the nonuniform flow is indeed subsonic when the flow becomes critical. The value of the secondary Mach number, M_a, is even lower than would be predicted by $Ch = 0$. Inspection of Fig. 31 shows that the theoretical value of p_w/p_{oa} is approximately 0.8 at the duct exit, therefore, M_a is approximately 0.57.

3. Mixing System Operated in the Back Pressure Dependent Mode

This section presents correlation of the 2–D Core Theory with experimental results for the configuration of Fig. 23b operated in the back pressure dependent mode. The theoretical solutions were obtained by iterating on p_{w1} until the theoretical wall pressure matched the experimental pressure at the last station in the mixing duct where the static pressure was measured.[**]

---

* To evaluate eq. (106) an effective value of γ must be chosen: however, the results for M_u are insensitive to the value chosen for γ.

** For these experimental conditions, p_{w1} is higher than the primary nozzle exit pressure. The 2–D Core Theory is not applicable to an overexpanded primary nozzle, therefore, the computations were made with the following approximation. The conical primary nozzle was assumed to be shorter than the experimental nozzle (with a smaller area ratio) such that the nozzle exit pressure was slightly higher than p_{w1}.

Wall pressure distributions — Axial distributions of wall static pressure are shown in Figs. 36a and 36b for two values of p_{oa}/p_{oj}. In these cases the theoretical pressure naturally agrees well with experiment in the downstream part of the duct, but the theory is too low near the duct entrance. As a result of the low theoretical values for p_{w1}, the theoretical values of the secondary-primary mass flow ratio are too high (by 32% and 28%, respectively). The theoretical thrust ratios are much less in error, being low by 6–7%.
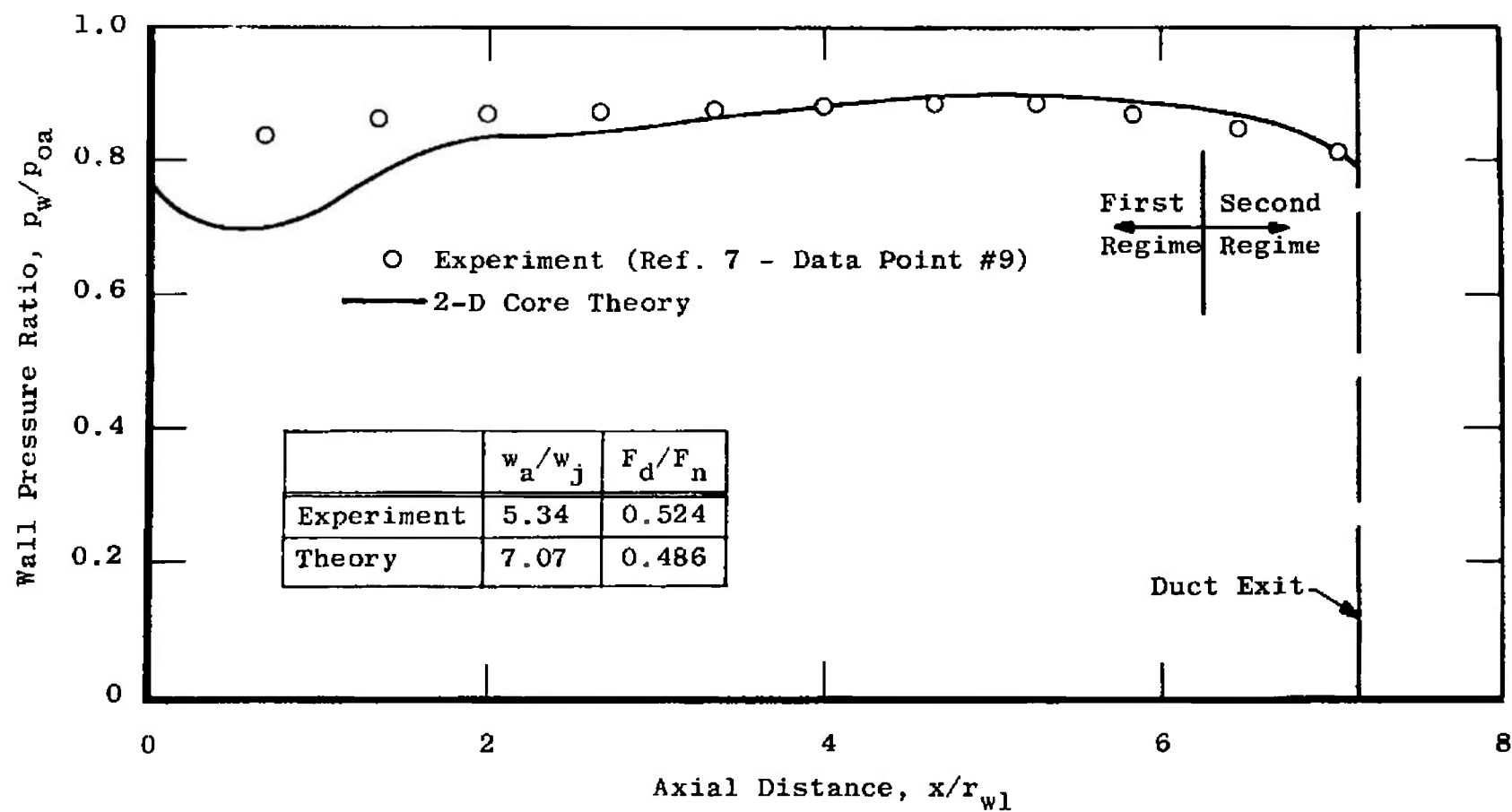
a. $p_{oa}/p_{oi} = 0.0435$

Fig. 36 Wall Pressure Distribution for Ducted Rocket-Air Mixing (Back Pressure Dependent Mode)
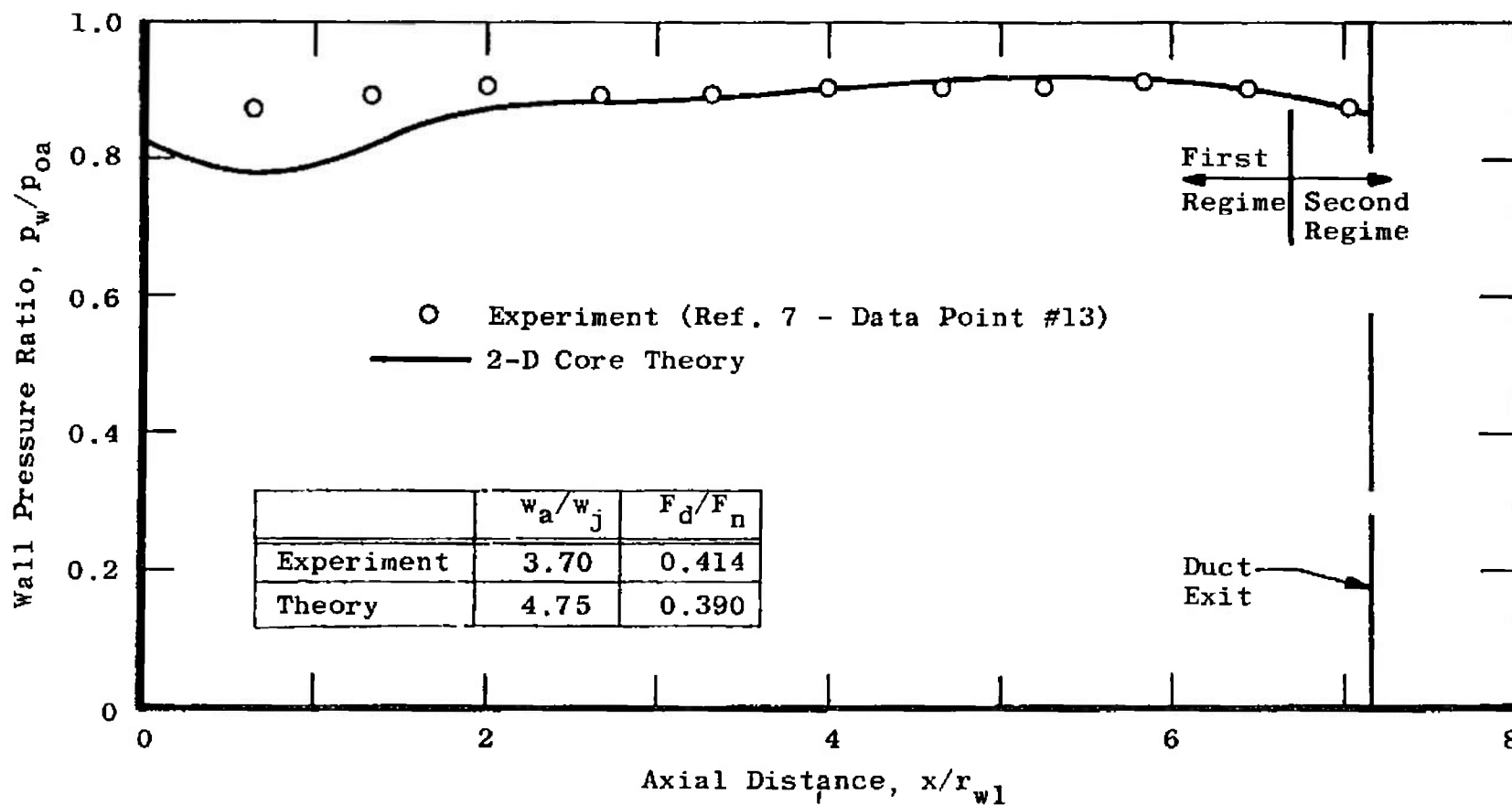
b. $p_{oa}/p_{oi} = 0.0333$

Fig. 36 Concluded

SECTION XVIII

CONCLUSIONS

An analytical model has been presented for the
turbulent mixing of coaxial streams inside a duct of arbi-
trary shape. The influences of nonuniform inviscid core flow
and of equilibrium chemical reactions have been included in
the analysis. Even though the current detailed knowledge
about turbulent flows with chemical reactions is meager, the
use of integral methods permits reasonably accurate compu-
tations of the flow in complex mixing systems. An important
point in the analytical model is the technique used to couple
the integral solution for the mixing layer and secondary flow
with the solution for the nonuniform inviscid core flow
(treated with the method of characteristics). This technique
should be applicable to other supersonic viscous interaction
problems in which integral methods can be applied to the
viscous layer.

The analytical and experimental results which were
discussed in Section XVII clearly show that viscous effects
are predominant in certain types of ducted mixing systems.
In some cases, the viscous effects completely change the
character of the flow from that predicted by inviscid theories.
Consequently, it is essential that the viscous and inviscid
portions of the flow be computed simultaneously for such
mixing systems.

The main emphasis of this investigation has been
placed on predicting the performance of ducted mixing systems
which are strongly influenced by viscous effects. Of course,
the theoretical model is also applicable to flows which are
weakly influenced by mixing, such as supersonic air-air
ejectors operating in the upstream choking mode. The present
theory accurately predicts the experimental performance of

such air-air ejectors, but the theory offers no quantitative improvement over the superposition technique of Chow and Addy (Ref. 5).

Many assumptions have been made in the development of the present analytical model. Extensive correlations of the theory with experiments, however, have shown that the various assumptions are acceptable, or at least not prohibitively inaccurate. The method of treating the flow in the mixing layer appears to be satisfactory considering the current state of knowledge about free turbulent mixing in the regime of interest. There is no point in discarding the assumptions of mixing zone profile similarity and of unity Prandtl and Lewis numbers until detailed and precise experimental results are available for mixing with large density gradients and chemical reactions. The assumption of equilibrium mixing zone chemistry yields good results for the rocket-air mixing systems considered in this investigation. However, the theory should be applied with caution to mixing systems for which there is no experimental verification for the assumption of equilibrium chemistry.

The weakest aspects of the present theory are (1) the model for the eddy viscosity, and (2) the assumption that the inviscid core flow is irrotational (without shocks). The eddy viscosity model is based on the Prandtl incompressible model, which is known to be inadequate when the secondary velocity is larger than about 0.3 times the primary velocity. Although the correction used to account for the influence of density gradients gives satisfactory results for the cases considered in this investigation, the correction needs to be checked against a broad range of experiments. It is hoped that the current research on free turbulent mixing will result in an improved semi-empirical model for the eddy

viscosity; such an improved eddy viscosity model could easily be incorporated into the present ducted mixing theory.

It is thought that the major source of quantitative disagreement between the present theory and ducted rocket—air mixing experiments is the neglect of shock waves in the inviscid core flow. There is no conceptual problem in incorporating the rotational method of characteristics (with shock waves) into the present theory. The method of computing the inviscid core flow (Section XIII) would be the only change required in the existing computer program; the system of differential—integral equations for the mixing layer and the inviscid secondary flow would be unchanged.

In spite of the deficiencies in the theoretical model developed during this investigation, the results are certainly qualitatively correct. In addition, the theoretical results are sufficiently accurate so that the theory may be considered a useful tool for the engineering analysis of ducted mixing systems.

REFERENCES

1. Perini, L., Wilson, W. E., Walker, R. E., and Dugger, G. L. "Preliminary Study of Air Augmentation of Rocket Thrust." Journal of Spacecraft and Rockets, Vol. 1, No. 6, November–December 1964, pp. 626–634.

2. Staff Report. "Composite Engines." Space/Aeronautics, Vol. 48, No. 3, August 1967, pp. 83–90.

3. Fabri, J. and Paulon, J. "Théorie et Expérimentation des Ejecteurs Supersoniques Air–Air." ONERA Note Technique No. 36, 1956. (English translation – NACA TM1410, September 1958).

4. Kochendorfer, F. D. and Rousso, M. D. "Performance Characteristics of Aircraft Cooling Ejectors Having Short Cylindrical Shrouds." NACA RM E51E01, May 1951.

5. Chow, W. L. and Addy, A. L. "Interaction Between Primary and Secondary Streams of Supersonic Ejector Systems and Their Performance Characteristics." AIAA Journal, Vol. 2, No. 4, April 1964, pp. 686–695.

6. Peters, C. E., Peters, T. and Billings, R. B. "Mixing and Burning of Bounded Coaxial Streams." AEDC-TR-65-4, March 1965 (AD 458348).

7. Cunningham, T. H. M. and Peters, C. E. "Further Experiments on Mixing and Burning of Bounded Coaxial Streams." AEDC-TR-68-136 (AD676646), October 1968.

8. Abramovich, G. N. The Theory of Turbulent Jets. MIT Press, Cambridge, Massachusetts, 1963.

9. Schlichting, H. Boundary Layer Theory. McGraw–Hill, New York, 1960.

10. Hinze, J. O. _Turbulence_. McGraw-Hill, New York, 1959.

11. Pai, S. I. _Fluid Dynamics of Jets_. Van Nostrand, New York, 1954.

12. Tollmein, W. "Berechnung Turbulenter Ausbreitungs – vorgänge." _ZAMM._, Vol. 6, pp. 468–478, 1926. (English translation – NACA TM 1085, 1945).

13. Goertler, H. "Berechnung von Aufgaben der freien Turbulenz auf Grund eines neuen Näherungsansatzes." _ZAMM._, Vol. 22, pp. 244–254, October 1942.

14. Reichardt, H. "Gesetzmässigkeiten der freien Turbulenz." _VDI – Forschungsheft_, 414, 1st ed., Berlin, 1942.

15. Kuethe, A. M. "Investigation of the Turbulent Regions Formed by Jets." _Journal of Applied Mechanics_, Vol. 2, No. 3, September 1935, pp. A-87–95.

16. Squire, H. B. and Trouncer, J. "Round Jets in a General Stream." ARC TR R & M No. 1974, 1944.

17. Fejer, A. A., Torda, T. P., Boehman, L. I., Ghia, K. N. and Herman, W. G. "Research on Mixing of Coaxial Streams." ARL 67-0058, March 1967 (AD654014).

18. Forstall, W. and Shapiro, A. H. "Momentum and Mass Transfer in Coaxial Jets." _Journal of Applied Mechanics_, Vol. 17, No. 12, December 1950, pp. 399–408.

19. Vasiliu, J. "Determination of Temperature, Velocity and Concentration Profiles in the Mixing Layer Between a Rocket Exhaust Jet and the Surrounding Supersonic Air Stream." Convair-Astronautics Report ERR-AN-005, March 1960.

20. Mager, A. "Transformation of the Compressible Turbulent Boundary Layer." _Journal of the Aeronautical Sciences_, Vol. 25, No. 5, May 1958, pp. 305–311.

21. Ting, L. and Libby, P. A. "Remarks on the Eddy Viscosity in Compressible Mixing Flows." _Journal of the Aerospace Sciences_, Vol. 27, No. 10, October 1960, pp. 797–798.

22. Libby, P. A. "Theoretical Analysis of Turbulent Mixing of Reactive Gases with Application to Supersonic Combustion of Hydrogen." _ARS Journal_, Vol. 32, No. 3, March 1962, pp. 388–396.

23. Hill, J. A. F., and Nicholson, J. E. "Compressibility Effects on Fluid Entrainment by Turbulent Mixing Layers." NASA-CR-131, November 1964.

24. Peters, C. E. "A Model for the Free Turbulent Eddy Viscosity." AEDC-TR-65-209, November 1965 (AD473663).

25. Kleinstein, G. "Mixing in Turbulent Axially Symmetric Free Jets." _Journal of Spacecraft and Rockets_, Vol. 1, No. 4, July–August 1964, pp. 403–408.

26. Korst, H. H., Chow, W. L. and Zumwalt, G. W. "Research on Transonic and Supersonic Flow of a Real Fluid at Abrupt Increases in Cross Section." University of Illinois ME-TR-392-5, (OSR TR-60-74), December 1959.

27. Warren, W. R. "An Analytical and Experimental Study of Compressible Free Jets." Princeton University Department of Aeronautical Engineering Report No. 381, 1957.

28. Donaldson, C. duP., and Gray, K. E. "Theoretical and Experimental Investigation of the Compressible Free Mixing of Two Dissimilar Gases." _AIAA Journal_, Vol. 4, No. 11, November 1966, pp. 2017–2025.

29. Alpinieri, L. J. "Turbulent Mixing of Coaxial Jets." _AIAA Journal_, Vol. 2, No. 9, September 1964, pp. 1560–1567.

30. Zakkay, V., Krause, E. and Woo, S. D. L. "Turbulent Transport Properties for Axisymmetric Heterogeneous Mixing." AIAA Journal, Vol. 2, No. 11, November 1964, pp. 1939-1947.

31. Mikhail, S. "Mixing of Coaxial Streams Inside a Closed Conduit." Journal of Mechanical Engineering Science, Vol. 2, No. 1, March 1960, pp. 59-68.

32. Emmons, D. L. "Analysis of the Turbulent Mixing Between a Reactive Gas – Particle Rocket Exhaust and a Confined Airstream." AIAA Paper No. 65-609, June 1965.

33. Abramovich, G. N. "Mixing Turbulent Jets of Different Density." Izvestiya Akademii Nauk SSSR, Otdeleniye Tekhnicheskikh Nauk (English translation – Wright-Patterson Air Force Base FTD-63-222).

34. Addy, A. L. "On the Steady State and Transient Operating Characteristics of Long Cylindrical Shroud Supersonic Ejectors (with Emphasis on the Viscous Interaction Between the Primary and Secondary Streams)." Ph.D. Thesis, University of Illinois, Department of Mechanical Engineering, June 1963.

35. Korst, H. H. and Chow, W. L. "Compressible Non-isoenergetic Turbulent (P_{rt} = 1) Jet Mixing Between Two Compressible Streams at Constant Pressure." NASA-CR-419, April 1966.

36. Kaplan, W. Advanced Calculus. Addison-Wesley, Reading, Massachusetts, 1959.

37. Browne, W. G. and Warlick, D. L. "Properties of Combustion Gases – System H_2 – Air." General Electric Company, Cincinnati, Ohio, R62FPD-366, November 1962.

38. Freemont, H. A., et al. "Properties of Combustion Gases – System C_nH_{2n} – Air." General Electric Company, Cincinnati, Ohio, 1955 (2 volumes).

39. Keenan, J. H. and Kaye, J. _Gas Tables_. Wiley, New York, 1956.

40. Phares, W. J. and Loper, F. C. "A Technique for Solving Integro-Differential Equations with Application to Turbulent Mixing." AEDC-TDR-64-209, November 1964 (AD450730).

41. Ralston, A. _A First Course in Numerical Analysis_. McGraw-Hill, New York, 1965.

42. Corrsin, S. and Uberoi, M. S. "Further Experiments on the Flow and Heat Transfer in a Heated Air Jet." NACA TN998, 1950.

43. Shapiro, A. H. _The Dynamics and Thermodynamics of Compressible Fluid Flow_. Ronald Press, New York, 1953.

44. Loper, F. C. and Lightsey, M. B. "Characteristic Equations for a Supersonic Flow Problem with Magneto-hydrodynamic Effects." AEDC-TR-66-206, January 1967 (AD645107).

45. Chow, W. L. and Yeh, P. S. "Characteristics of Supersonic Ejector Systems with Nonconstant Area Shroud." _AIAA Journal_, Vol. 3, No. 3, March 1965, pp. 525-527.

46. Herpfer, E. "Choking of Non-uniform Flow." von Kármán Institute for Fluid Dynamics, Project Report 66-155, June 1966.

47. Edelman, R. and Fortune, O. "An Analysis of Mixing and Combustion in Ducted Flows." AIAA Paper No. 68-114, January 1968.

APPENDIX I
AUXILIARY FUNCTIONS FOR 1-D CORE THEORY

In Section VII, the basic differential-integral equations for the ducted mixing problem were transformed into a system of linear first order differential equations which is amenable to numerical solution. The numerous auxiliary equations needed to evaluate the coefficients F, G and H are presented in this appendix.

The following equations are developed in logical order in that all the parameters in a particular equation are developed prior to use in that equation. All of the equations for the parameters which appear directly in the coefficients F, G and H are denoted by an asterisk at the equation number, for example eq. (A-11)*.

Note that in the evaluation of the terms for the coefficients the independent variables are considered to be (x, p_w, r_i, b) in the first regime, (x, p_w, u_c, b) in the second regime and (x, p_w, u_c, u_w) in the third regime.

1. Isentropic Stream Equations

A number of relations which are used in all three regimes are obtained from the assumption that the inviscid streams are isentropic. The following parameters are assumed to be prescribed: p_{oa}, p_{oj}, T_{oa}, T_{oj}, R_a, R_j, c_{pa}, c_{pj}.

From the definition of the ratio of specific heats:

$$\gamma_a = \frac{c_{pa}}{c_{pa} - R_a} \tag{A-1}$$

$$\gamma_j = \frac{c_{pj}}{c_{pj} - R_j} \tag{A-2}$$

From the isentropic pressure ratio equation:

$$M_a = \left\{ \frac{2}{\gamma_a - 1} \left[\left(\frac{P_{oa}}{P_w} \right)^{\frac{\gamma_a - 1}{\gamma_a}} - 1 \right] \right\}^{1/2} \tag{A-3}$$

$$M_j = \left\{ \frac{2}{\gamma_j - 1} \left[\left(\frac{P_{oj}}{P_w} \right)^{\frac{\gamma_j - 1}{\gamma_j}} - 1 \right] \right\}^{1/2} \tag{A-4}$$

Differentiating eqs. (A-3) and (A-4) with respect to p_w:

$$\frac{dM_a}{dP_w} = - \frac{1}{\gamma_a} \frac{\left(\frac{P_{oa}}{P_w} \right)^{\frac{\gamma_a - 1}{\gamma_a}}}{P_w M_a} \tag{A-5}$$

$$\frac{dM_j}{dP_w} = - \frac{1}{\gamma_j} \frac{\left(\frac{P_{oj}}{P_w} \right)^{\frac{\gamma_j - 1}{\gamma_j}}}{P_w M_j} \tag{A-6}$$

From the energy equation[*]:

$$T_a = T_{oa} \Big/ \left(1 + \frac{\gamma_a - 1}{2} M_a^2 \right) \tag{A-7}$$

---

[*] Use of the energy equation (and eqs. A-3 and A-4) in this form implies that the specific heats are invariant over the range of temperature from 0 to T_o, whereas in Section V the total temperature was defined by assuming that c_p is constant from T to T_o. For rocket-air mixing, no error is involved in the secondary stream which is relatively low temperature. For the rocket-air mixing experiments of Refs. 6 and 7, $T_j \approx 1100°K$, and the error in T_j caused by using eq. (A-8) is less than 1%.

$$T_j = T_{oj} \Big/ \Big(1 + \tfrac{\gamma_j - 1}{2} M_j^2\Big) \tag{A-8}$$

Differentiating eqs. (A-7) and (A-8) with respect to p_w:

$$\frac{dT_a}{dP_w} = \frac{(1 - \gamma_a) M_a T_a^2}{T_{oa}} \frac{dM_a}{dP_w} \tag{A-9}$$

$$\frac{dT_j}{dP_w} = \frac{(1 - \gamma_j) M_j T_j^2}{T_{oj}} \frac{dM_j}{dP_w} \tag{A-10}$$

From the definition of the Mach number:

$$u_a = M_a \big(\gamma_a R_a T_a\big)^{1/2} \tag{A-11}*$$

$$u_j = M_j \big(\gamma_j R_j T_j\big)^{1/2} \tag{A-12}*$$

Differentiating eqs. (A-11) and (A-12) with respect to p_w:

$$\frac{du_a}{dP_w} = \frac{u_a}{M_a} \frac{dM_a}{dP_w} + \frac{1}{2} \frac{M_a^2}{u_a} \gamma_a R_a \frac{dT_a}{dP_w} \tag{A-13}*$$

$$\frac{du_j}{dP_w} = \frac{u_j}{M_j} \frac{dM_j}{dP_w} + \frac{1}{2} \frac{M_j^2}{u_j} \gamma_j R_j \frac{dT_j}{dP_w} \tag{A-14}*$$

From the perfect gas law:

$$\rho_a = P_W \big/ R_a T_a \qquad \text{(A-15)}^*$$

$$\rho_j = P_W \big/ R_j T_j \qquad \text{(A-16)}^*$$

Differentiating eqs. (A-15) and (A-16) with respect to p_W:

$$\frac{d\rho_a}{dP_W} = -\frac{\rho_a}{T_a}\frac{dT_a}{dP_W} + \frac{1}{R_a T_a} \qquad \text{(A-17)}^*$$

$$\frac{d\rho_j}{dP_W} = -\frac{\rho_j}{T_j}\frac{dT_j}{dP_W} + \frac{1}{R_j T_j} \qquad \text{(A-18)}^*$$

2. Duct Wall Equations

The duct wall is assumed to be represented by the following pair of equations, where the constants $C_1 - C_7$ and x_e are specified:

$$r_W = C_1 + C_2 x + C_3 x^2 + C_4 x^3 + C_5 x^4 ,$$
$$x \leq x_e \qquad \text{(A-19a)}^*$$

$$r_W = C_6 + C_7 x , \qquad\qquad x > x_e \qquad \text{(A-19b)}^*$$

Differentiating eqs. (A-19a) and (A-19b) with respect to x:

$$\frac{dr_W}{dx} = C_2 + 2C_3 x + 3C_4 x^2 + 4C_5 x^3 , x \leq x_e$$
$$\text{(A-20a)}^*$$

$$\frac{dr_W}{dx} = C_7 , \quad x > x_e \qquad \text{(A-20b)}^*$$

3. Mixing Zone Property Equations

The mixing zone total temperatures, specific heats and gas constants are prescribed (Section V):

$$T_0 = T_0(\bar{C}) \tag{A-21}$$

$$c_P = c_P(\bar{C}) \tag{A-22}$$

$$R = R(\bar{C}) \tag{A-23}$$

These equations are also differentiated with respect to $\bar{C}$ to provide $dT_0/d\bar{C}$, $dc_p/d\bar{C}$ and $dR/d\bar{C}$.

4. First Regime Equations

From Section V, the equations for the mixing zone velocity and composition are:

$$u = u_a + \frac{1}{2}\left(1 + \cos\pi\,\frac{r-r_i}{b}\right)\left(u_j - u_a\right) \tag{A-24}*$$

$$\bar{C} = \frac{1}{2}\left(1 + \cos\pi\,\frac{r-r_i}{b}\right) \tag{A-25}*$$

Differentiating eqs. (A-24) and (A-25):

$$\frac{\partial \bar{u}}{\partial x} = 0 \tag{A-26}*$$

$$\frac{\partial \bar{u}}{\partial P_w} = \frac{1}{2}\left(1 + \cos\pi\,\frac{r-r_i}{b}\right)\left(\frac{du_j}{dP_w} - \frac{du_a}{dP_w}\right) + \frac{du_a}{dP_w} \tag{A-27}*$$

$$\frac{\partial \bar{u}}{\partial r_i} = \frac{\pi}{2b}\left(u_j - u_a\right)\sin\left(\pi\,\frac{r-r_i}{b}\right) \tag{A-28}*$$

.

$$\frac{\partial \bar{u}}{\partial b} = \frac{1}{2}\left(u_j - u_a\right)\left(\pi \frac{r - r_i}{b^2}\right)\sin\left(\pi \frac{r - r_i}{b}\right) \qquad \text{(A-29)}^*$$

$$\frac{\partial \bar{C}}{\partial x} = 0 \qquad \text{(A-30)}$$

$$\frac{\partial \bar{C}}{\partial P_w} = 0 \qquad \text{(A-31)}$$

$$\frac{\partial \bar{C}}{\partial r_i} = \frac{1}{2}\frac{\pi}{b}\sin\left(\pi \frac{r - r_i}{b}\right) \qquad \text{(A-32)}$$

$$\frac{\partial \bar{C}}{\partial b} = \frac{\pi}{2}\left(\frac{r - r_i}{b^2}\right)\sin\left(\pi \frac{r - r_i}{b}\right) \qquad \text{(A-33)}$$

From eqs. (A-21) – (A-23) one obtains $dT_0/d\bar{C}$, $dc_p/d\bar{C}$, and $dR/d\bar{C}$, and

$$\frac{\partial T_0}{\partial x} = \frac{\partial c_p}{\partial x} = \frac{\partial R}{\partial x} = 0 \qquad \text{(A-34)}$$

$$\frac{\partial T_0}{\partial P_w} = \frac{\partial c_p}{\partial P_w} = \frac{\partial R}{\partial P_w} = 0 \qquad \text{(A-35)}$$

$$\frac{\partial T_0}{\partial r_i} = \frac{\partial \bar{C}}{\partial r_i}\frac{dT_0}{d\bar{C}} \qquad \text{(A-36)}$$

$$\frac{\partial c_p}{\partial r_i} = \frac{\partial \bar{C}}{\partial r_i}\frac{dc_p}{d\bar{C}} \qquad \text{(A-37)}$$

$$\frac{\partial R}{\partial r_i} = \frac{\partial \bar{C}}{\partial r_i}\frac{dR}{d\bar{C}} \qquad \text{(A-38)}$$

$$\frac{\partial T_0}{\partial b} = \frac{\partial \overline{C}}{\partial b} \frac{dT_0}{d\overline{C}} \tag{A-39}$$

$$\frac{\partial c_p}{\partial b} = \frac{\partial \overline{C}}{\partial b} \frac{dc_p}{d\overline{C}} \tag{A-40}$$

$$\frac{\partial R}{\partial b} = \frac{\partial \overline{C}}{\partial b} \frac{dR}{d\overline{C}} \tag{A-41}$$

The mixing zone temperature, T, is given by the energy equation:

$$T = T_0 - u^2/2c_p \tag{A-42}$$

Differentiating eq. (A-42), one obtains

$$\frac{\partial T}{\partial x} = \frac{\partial T_0}{\partial x} - \frac{1}{2c_p^2}\left(2uc_p\frac{\partial \overline{u}}{\partial x} - u^2\frac{\partial c_p}{\partial x}\right) = 0 \tag{A-43}$$

$$\frac{\partial T}{\partial P_W} = \frac{\partial T_0}{\partial P_W} - \frac{1}{2c_p^2}\left(2uc_p\frac{\partial \overline{u}}{\partial P_W} - u^2\frac{\partial c_p}{\partial P_W}\right)$$

$$= -\frac{u}{c_p}\frac{\partial \overline{u}}{\partial P_W} \tag{A-44}$$

$$\frac{\partial T}{\partial r_i} = \frac{\partial T_0}{\partial r_i} - \frac{1}{2c_p^2}\left(2uc_p\frac{\partial \overline{u}}{\partial r_i} - u^2\frac{\partial c_p}{\partial r_i}\right) \tag{A-45}$$

168

$$\frac{\partial T}{\partial b} = \frac{\partial T_o}{\partial b} - \frac{1}{2c_p^2}\left(2uc_p\frac{\partial \bar{u}}{\partial b} - u^2\frac{\partial c_p}{\partial b}\right) \qquad \text{(A-46)}$$

The mixing zone density is given by

$$\rho = P_w / RT \qquad \text{(A-47)}^*$$

Differentiating eq. (A-47), one obtains

$$\frac{\partial \bar{\rho}}{\partial x} = -\frac{\rho}{RT}\left(R\frac{\partial T}{\partial x} + T\frac{\partial R}{\partial x}\right) = 0 \qquad \text{(A-48)}^*$$

$$\frac{\partial \bar{\rho}}{\partial P_w} = -\frac{\rho}{RT}\left(R\frac{\partial T}{\partial P_w} + T\frac{\partial R}{\partial P_w}\right) = -\frac{\rho}{T}\frac{\partial T}{\partial P_w} \qquad \text{(A-49)}^*$$

$$\frac{\partial \bar{\rho}}{\partial r_i} = -\frac{\rho}{RT}\left(R\frac{\partial T}{\partial r_i} + T\frac{\partial R}{\partial r_i}\right) \qquad \text{(A-50)}^*$$

$$\frac{\partial \bar{\rho}}{\partial b} = -\frac{\rho}{RT}\left(R\frac{\partial T}{\partial b} + T\frac{\partial R}{\partial b}\right) \qquad \text{(A-51)}^*$$

Equations (A-24) — (A-51) completely specify the terms which appear in the mixing zone integrals of the coefficients F, G and H.

The mixing zone shear stress, τ_m, is given by eq. (44a) of Section VI:

$$\tau_m = \frac{\pi}{2}k_I\rho_m(u_a - u_j)\left|(u_a - u_j)\right| \qquad \text{(44a)}^*$$

where the half-radius density, ρ_m, is evaluated from eq. (A-47) at $\overline{C} = \frac{1}{2}$ and $u_m = \frac{1}{2}(u_j + u_a)$. The first regime mixing zone constant, k_I, is given by the modified Donaldson and Gray equation (eq. 42, Section VI),

$$k_I = 0.007\left[0.66 + 0.34 \exp\left(-3.42\, M_m^2\right)\right] \qquad \text{(A-52)}$$

where M_m is the Mach number corresponding to u_m and $\overline{C} = \frac{1}{2}$. In calculating M_m, the variables T_m, R_m and c_{pm} are determined by eqs. (A-21) – (A-23) and (A-42). The definition for γ_m $(\gamma_m = c_{pm}/(c_{pm} - R_m))$ then permits determination of M_m from:

$$M_m = u_m\left(\gamma_m\, R_m\, T_m\right)^{-\frac{1}{2}} \qquad \text{(A-53)}$$

5. Second Regime Equations

The mixing zone velocity is given by (Section V):

$$u = u_a + \frac{1}{2}(u_c - u_a)\left(1 + \cos \pi\, \frac{r}{b}\right) \qquad \text{(A-54)}^*$$

The mixing zone composition, $\overline{C}$, is given by

$$\overline{C} = \frac{1}{2}\overline{C}_c\left(1 + \cos \pi\, \frac{r}{b}\right) \qquad \text{(A-55)}$$

where $\overline{C}_c$ is determined by eq. (25a) (Section V):

$$\overline{C}_c = \frac{u_c - u_a}{u_j - u_a} \qquad \text{(A-56)}$$

The velocities u_a and u_j are given by eqs. (A-11) and (A-12). Differentiating eq. (A-54):

$$\frac{\partial \overline{u}}{\partial x} = 0 \qquad \text{(A-57)}^*$$

$$\frac{\partial \bar{u}}{\partial P_w} = \left[1 - \frac{1}{2}\left(1 + \cos \pi \frac{r}{b}\right)\right] \frac{d u_a}{d P_w} \qquad \text{(A-58)}^*$$

$$\frac{\partial \bar{u}}{\partial u_c} = \frac{1}{2}\left(1 + \cos \pi \frac{r}{b}\right) \qquad \text{(A-59)}^*$$

$$\frac{\partial \bar{u}}{\partial b} = \frac{1}{2}\left(u_c - u_a\right)\left(\pi \frac{r}{b^2}\right) \sin\left(\pi \frac{r}{b}\right) \qquad \text{(A-60)}^*$$

Differentiating eq. (A-56), one obtains

$$\frac{\partial \bar{C}_c}{\partial x} = \frac{\partial \bar{C}_c}{\partial b} = 0 \qquad \text{(A-61)}$$

$$\frac{\partial \bar{C}_c}{\partial P_w} = \frac{1}{(u_a - u_j)}\left[\bar{C}_c \frac{d u_j}{d P_w} + \left(1 - \bar{C}_c\right)\frac{d u_a}{d P_w}\right] \qquad \text{(A-62)}$$

$$\frac{\partial \bar{C}_c}{\partial u_c} = \frac{1}{(u_j - u_a)} \qquad \text{(A-63)}$$

Differentiating eq. (A-55), one obtains

$$\frac{\partial \bar{C}}{\partial x} = 0 \qquad \text{(A-64)}$$

$$\frac{\partial \bar{C}}{\partial P_w} = \frac{1}{2}\left(1 + \cos \pi \frac{r}{b}\right) \frac{\partial \bar{C}_c}{\partial P_w} \qquad \text{(A-65)}$$

$$\frac{\partial \overline{C}}{\partial u_c} = \frac{1}{2}\left(1 + \cos \pi \frac{r}{b}\right) \frac{\partial \overline{C}_c}{\partial u_c} \qquad \text{(A-66)}$$

$$\frac{\partial \overline{C}}{\partial b} = \frac{\overline{C}_c}{2}\left(\pi \frac{r}{b^2}\right) \sin\left(\pi \frac{r}{b}\right) \qquad \text{(A-67)}$$

Equations (A-21) – (A-23), (A-34) and (A-39) – (A-41) are applicable in this regime. In addition,

$$\frac{\partial T_o}{\partial P_w} = \frac{\partial \overline{C}}{\partial P_w} \frac{d T_o}{d \overline{C}} \qquad \text{(A-68)}$$

$$\frac{\partial c_p}{\partial P_w} = \frac{\partial \overline{C}}{\partial P_w} \frac{d c_p}{d \overline{C}} \qquad \text{(A-69)}$$

$$\frac{\partial R}{\partial P_w} = \frac{\partial \overline{C}}{\partial P_w} \frac{d R}{d \overline{C}} \qquad \text{(A-70)}$$

$$\frac{\partial T_o}{\partial u_c} = \frac{\partial \overline{C}}{\partial u_c} \frac{d T_o}{d \overline{C}} \qquad \text{(A-71)}$$

$$\frac{\partial c_p}{\partial u_c} = \frac{\partial \overline{C}}{\partial u_c} \frac{d c_p}{d \overline{C}} \qquad \text{(A-72)}$$

$$\frac{\partial R}{\partial u_c} = \frac{\partial \overline{C}}{\partial u_c} \frac{d R}{d \overline{C}} \qquad \text{(A-73)}$$

The mixing zone temperature is given by eq. (A-42).
Differentiating eq. (A-42), one obtains eq. (A-46) and

$$\frac{\partial T}{\partial x} = 0 \tag{A-74}$$

$$\frac{\partial T}{\partial P_W} = \frac{\partial T_0}{\partial P_W} - \frac{1}{2 c_P^2} \left(2 u c_P \frac{\partial \bar{u}}{\partial P_W} - u^2 \frac{\partial c_P}{\partial P_W} \right) \tag{A-75}$$

$$\frac{\partial T}{\partial u_c} = \frac{\partial T_0}{\partial u_c} - \frac{1}{2 c_P^2} \left(2 u c_P \frac{\partial \bar{u}}{\partial u_c} - u^2 \frac{\partial c_P}{\partial u_c} \right) \tag{A-76}$$

The mixing zone density is given by eq. (A-47).
Differentiating eq. (A-47), one obtains eqs. (A-48) and
(A-51) and

$$\frac{\partial \bar{\rho}}{\partial P_W} = -\frac{\rho}{RT} \left(R \frac{\partial T}{\partial P_W} + T \frac{\partial R}{\partial P_W} \right) \tag{A-77}*$$

$$\frac{\partial \bar{\rho}}{\partial u_c} = -\frac{\rho}{RT} \left(R \frac{\partial T}{\partial u_c} + T \frac{\partial R}{\partial u_c} \right) \tag{A-78}*$$

The mixing zone shear stress is given by eq. (44b)
of Section VI:

$$\tau_m = \frac{\pi}{2} k_{II} \rho_m \left(u_a - u_c \right) \left| \left(u_a - u_c \right) \right| \tag{44b}*$$

The density, ρ_m, is calculated at $u_m = \frac{1}{2}(u_c + u_a)$ and
$\bar{C}_m = 1/2 \, \bar{C}_c$.
The second regime mixing constant, k_{II}, is given by

$$k_{II} = 0.011 \left[0.66 + 0.34 \exp\left(-3.42 \, M_m^2\right) \right] \qquad \text{(A--79)}$$

where M_m is calculated with eq. (A--53).

6. Third Regime Equations

The mixing zone velocity is given by (Section V):

$$u = u_w + \tfrac{1}{2} \left(u_c - u_w\right)\left(1 + \cos \pi \, \frac{r}{r_w}\right) \qquad \text{(A--80)}^*$$

The mixing zone composition is

$$\overline{C} = \overline{C}_w + \tfrac{1}{2} \left(\overline{C}_c - \overline{C}_w\right)\left(1 + \cos \pi \, \frac{r}{r_w}\right) \qquad \text{(A--81)}$$

where

$$\overline{C}_c = \frac{u_c - u_a}{u_j - u_a} \qquad \text{(A--56)}$$

and

$$\overline{C}_w = \frac{u_w - u_a}{u_j - u_a} \qquad \text{(A--82)}$$

The velocities u_a and u_j are given by eqs. (A--11) and (A--12). Differentiating eq. (A--80):

$$\frac{\partial \overline{u}}{\partial x} = \frac{\partial \overline{u}}{\partial r_w} \frac{d r_w}{d x} = \frac{1}{2}\left(u_c - u_w\right)\left(\pi \, \frac{r}{r_w^2}\right) \sin\left(\pi \, \frac{r}{r_w}\right) \frac{d r_w}{d x} \qquad \text{(A--83)}^*$$

$$\frac{\partial \overline{u}}{\partial P_w} = 0 \qquad \text{(A--84)}^*$$

$$\frac{\partial \bar{u}}{\partial u_c} = \frac{1}{2}\left(1 + \cos \pi \frac{r}{r_w}\right) \qquad \text{(A–85)}^*$$

$$\frac{\partial \bar{u}}{\partial u_w} = \frac{1}{2}\left(1 - \cos \pi \frac{r}{r_w}\right) \qquad \text{(A–86)}^*$$

Differentiating eq. (A–56), one obtains

$$\frac{\partial \bar{C}_c}{\partial x} = \frac{\partial \bar{C}_c}{\partial u_w} = 0 \qquad \text{(A–87)}$$

$$\frac{\partial \bar{C}_c}{\partial P_w} = \frac{1}{(u_a - u_j)}\left[(1 - \bar{C}_c)\frac{d u_a}{d P_w} + \bar{C}_c \frac{d u_j}{d P_w}\right] \qquad \text{(A–88)}$$

$$\frac{\partial \bar{C}_c}{\partial u_c} = \frac{1}{(u_j - u_a)} \qquad \text{(A–89)}$$

Differentiating eq. (A–82), one obtains

$$\frac{\partial \bar{C}_w}{\partial x} = \frac{\partial \bar{C}_w}{\partial u_c} = 0 \qquad \text{(A–90)}$$

$$\frac{\partial \bar{C}_w}{\partial P_w} = \frac{1}{(u_a - u_j)}\left[\bar{C}_w \frac{d u_j}{d P_w} + (1 - \bar{C}_w)\frac{d u_a}{d P_w}\right] \qquad \text{(A–91)}$$

$$\frac{\partial \bar{C}_w}{\partial u_w} = \frac{1}{(u_j - u_a)} \qquad \text{(A–92)}$$

175

Differentiating eq. (A-81), one obtains

$$\frac{\partial \bar{C}}{\partial x} = \frac{\partial \bar{C}}{\partial r_W}\frac{dr_W}{dx} = \frac{1}{2}\left(\bar{C}_c - \bar{C}_W\right)\left(\pi\frac{r}{r_W^2}\right)\sin\left(\pi\frac{r}{r_W}\right)\frac{dr_W}{dx} \qquad \text{(A-93)}$$

$$\frac{\partial \bar{C}}{\partial P_W} = \frac{1}{2}\left(1+\cos\pi\frac{r}{r_W}\right)\left(\frac{\partial \bar{C}_c}{\partial P_W} - \frac{\partial \bar{C}_W}{\partial P_W}\right) + \frac{\partial \bar{C}_W}{\partial P_W} \qquad \text{(A-94)}$$

$$\frac{\partial \bar{C}}{\partial u_c} = \frac{1}{2}\left(1+\cos\pi\frac{r}{r_W}\right)\frac{\partial \bar{C}_c}{\partial u_c} \qquad \text{(A-95)}$$

$$\frac{\partial \bar{C}}{\partial u_W} = \frac{1}{2}\left(1-\cos\pi\frac{r}{r_W}\right)\frac{\partial \bar{C}_W}{\partial u_W} \qquad \text{(A-96)}$$

Equations (A-21) — (A-23) are applicable to the third regime. The derivatives of the mixing zone gas properties are:

$$\frac{\partial T_o}{\partial x} = \frac{\partial \bar{C}}{\partial x}\frac{dT_o}{d\bar{C}} \qquad \text{(A-97)}$$

$$\frac{\partial T_o}{\partial P_W} = \frac{\partial \bar{C}}{\partial P_W}\frac{dT_o}{d\bar{C}} \qquad \text{(A-98)}$$

$$\frac{\partial T_o}{\partial u_c} = \frac{\partial \bar{C}}{\partial u_c}\frac{dT_o}{d\bar{C}} \qquad \text{(A-99)}$$

$$\frac{\partial c_p}{\partial x} = \frac{\partial \bar{C}}{\partial x}\frac{dc_p}{d\bar{C}} \qquad \text{(A-100)}$$

$$\frac{\partial c_p}{\partial P_W} = \frac{\partial \bar{C}}{\partial P_W}\frac{dc_p}{d\bar{C}} \qquad \text{(A-101)}$$

$$\frac{\partial c_P}{\partial u_c} = \frac{\partial \bar{C}}{\partial u_c} \frac{d c_P}{d \bar{C}} \tag{A-102}$$

$$\frac{\partial c_P}{\partial u_w} = \frac{\partial \bar{C}}{\partial u_w} \frac{d c_P}{d \bar{C}} \tag{A-103}$$

$$\frac{\partial R}{\partial x} = \frac{\partial \bar{C}}{\partial x} \frac{d R}{d \bar{C}} \tag{A-104}$$

$$\frac{\partial R}{\partial P_w} = \frac{\partial \bar{C}}{\partial P_w} \frac{d R}{d \bar{C}} \tag{A-105}$$

$$\frac{\partial R}{\partial u_c} = \frac{\partial \bar{C}}{\partial u_c} \frac{d R}{d \bar{C}} \tag{A-106}$$

$$\frac{\partial R}{\partial u_w} = \frac{\partial \bar{C}}{\partial u_w} \frac{d R}{d \bar{C}} \tag{A-107}$$

The mixing zone temperature is given by the energy equation (eq. A-42). Differentiating eq. (A-42) one obtains eqs. (A-75) and (A-76) and

$$\frac{\partial T}{\partial x} = \frac{\partial T_o}{\partial x} - \frac{1}{2 c_P^2}\left(2 u c_P \frac{\partial \bar{u}}{\partial x} - u^2 \frac{\partial c_P}{\partial x}\right) \tag{A-108}$$

$$\frac{\partial T}{\partial u_w} = \frac{\partial T_o}{\partial u_w} - \frac{1}{2 c_P^2}\left(2 u c_P \frac{\partial \bar{u}}{\partial u_w} - u^2 \frac{\partial c_P}{\partial u_w}\right) \tag{A-109}$$

The mixing zone density is given by eq. (A-47). Differentiating eq. (A-47), one obtains eqs. (A-77) and (A-78) and

$$\frac{\partial \bar{P}}{\partial x} = -\frac{P}{RT}\left(R \frac{\partial T}{\partial x} + T \frac{\partial R}{\partial x}\right) \tag{A-110}[*]$$

$$\frac{\partial \bar{\rho}}{\partial u_w} = -\frac{\rho}{RT}\left(R\frac{\partial T}{\partial u_w} + T\frac{\partial R}{\partial u_w}\right) \tag{A-111}^*$$

The mixing zone shear stress is given by eq. (44c) of Section VI,

$$\tau_m = \frac{\pi}{2} k_{III} \rho_m (u_w - u_c)\left|(u_w - u_c)\right| \tag{44c}^*$$

The density, ρ_m, is calculated at $u_m = \frac{1}{2}(u_c + u_w)$ and $\bar{C}_m = \frac{1}{2}(\bar{C}_c + \bar{C}_w)$. The third regime mixing constant, k_{III}, is the same as k_{II} and is calculated with eq. (A-79).

APPENDIX II
AUXILIARY FUNCTIONS FOR 2-D CORE THEORY

In this appendix the auxiliary functions required for evaluation of the coefficients F, G and H (Section XII) are presented. Most of the auxiliary functions are the same as those for the 1-D Core Theory (Appendix I). Consequently, only those functions which differ from the 1-D Core Theory are presented here. As in Appendix I, the equations for the parameters which appear directly in the coefficients F, G and H are denoted by an asterisk at the equation number.

As was the case in evaluating the auxiliary functions for the first regime of the 1-D Core Theory, the variables (x, p_w, r_i, b) are considered to be independent.

1. Isentropic Stream Equations

The secondary stream velocity, u_a, is calculated from eq. (A-11). The inviscid core velocity at r_i, V_i, is computed from eq. (A-12) by replacing u_j by V_i. Similarly, dV_i/dp_w is calculated with eq. (A-14). The density at r_i, ρ_i, is obtained from eq. (A-16) by replacing ρ_j by ρ_i. Similarly, $d\rho_i/dp_w$ is calculated from eq. (A-18).

2. Velocity Profile Equation

The mixing zone velocity is calculated from

$$u = u_a + \tfrac{1}{2}\left(1 + \cos \pi \, \frac{r - r_i}{b}\right)\left(u_i - u_a\right) \qquad \text{(A-24a)}^*$$

where

$$u_i = V_i \cos \theta_i \qquad \text{(A-112)}^*$$

The normal velocity component at r_1 is given by

$$\sigma_i = V_i \, \sin \, \theta_i \qquad \text{(A-113)}^*$$

Differentiating eq. (A-24a), one obtains

$$\frac{\partial \bar{u}}{\partial x} = \frac{1}{2}\left(1 + \cos \pi \, \frac{r - r_i}{b}\right) \frac{\partial u_i}{\partial x} \qquad \text{(A-114)}^*$$

$$\frac{\partial \bar{u}}{\partial P_w} = \frac{1}{2}\left(1 + \cos \pi \, \frac{r - r_i}{b}\right)\left(\frac{\partial u_i}{\partial P_w} - \frac{d u_a}{d P_w}\right) + \frac{d u_a}{d P_w} \qquad \text{(A-115)}^*$$

$$\frac{\partial \bar{u}}{\partial r_i} = \frac{1}{2}\left(u_i - u_a\right)\left(\frac{\pi}{b} \sin \pi \, \frac{r - r_i}{b}\right)$$
$$+ \frac{1}{2}\left(1 + \cos \pi \, \frac{r - r_i}{b}\right) \frac{\partial u_i}{\partial r_i} \qquad \text{(A-116)}^*$$

$$\frac{\partial \bar{u}}{\partial b} = \frac{1}{2}\left(u_i - u_a\right)\left(\pi \, \frac{r - r_i}{b^2}\right) \sin\left(\pi \, \frac{r - r_i}{b}\right) \qquad \text{(A-117)}^*$$

Equations (A-114) – (A-116) contain partial derivatives $\partial u_i/\partial x$, $\partial u_i/\partial p_w$, and $\partial u_i/\partial r_1$ which must be obtained from the method of characteristics solution of the inviscid core flow (Section XIII). These derivatives are presented in the next section.

3. Partial Derivatives at Inner Mixing Zone Boundary

One obtains from the method of characteristics solution (Section XIII) the partial derivatives $\partial u/\partial x$, $\partial u/\partial r$, $\partial p/\partial x$, and $\partial p/\partial r$. It is important to recognize that these derivatives are obtained from a system in which the

independent variables are x and r. Thus, these derivatives will be denoted by $\frac{\partial u}{\partial x}\big|_r$, $\frac{\partial u}{\partial r}\big|_x$, $\frac{\partial P}{\partial x}\big|_r$ and $\frac{\partial P}{\partial r}\big|_x$ with the subscript denoting the variable held constant during the differentiation.

The derivatives appearing in eqs. (A-114) — (A-116) are used in a system where the independent variables are (x, p_w, r_i), thus

$$\frac{\partial u_i}{\partial x}\bigg|_{P_w, r_i} \qquad \frac{\partial u_i}{\partial P_w}\bigg|_{x, r_i} \qquad \frac{\partial u_i}{\partial r_i}\bigg|_{x, P_w}$$

One can write, in general

$$\frac{\partial u}{\partial r}\bigg|_x = \frac{\partial u}{\partial r}\bigg|_{x, P} + \frac{\partial u}{\partial P}\bigg|_{x, r} \frac{\partial P}{\partial r}\bigg|_x$$

and

$$\frac{\partial u}{\partial x}\bigg|_r = \frac{\partial u}{\partial x}\bigg|_{r, P} + \frac{\partial u}{\partial P}\bigg|_{x, r} \frac{\partial P}{\partial x}\bigg|_r$$

Thus one can compute the necessary derivatives from

$$\frac{\partial u_i}{\partial x}\bigg|_{r_i, P_w} = \frac{\partial u}{\partial x}\bigg|_r - \frac{\partial u_i}{\partial P_w}\bigg|_{x, r_i} \frac{\partial P}{\partial x}\bigg|_r \qquad (A-118)$$

and

$$\frac{\partial u_i}{\partial r_i}\bigg|_{x, P_w} = \frac{\partial u}{\partial r}\bigg|_x - \frac{\partial u_i}{\partial P_w}\bigg|_{x, r_i} \frac{\partial P}{\partial r}\bigg|_x \qquad (A-119)$$

The derivative $\partial u_i / \partial P_w\big|_{x, r_i}$ must now be evaluated to solve eqs. (A-118) and (A-119). Differentiating eq. (A-112):

$$\frac{\partial u_i}{\partial P_W}\bigg|_{x,r_i} = -V_i \sin \Theta_i \frac{\partial \Theta_i}{\partial P_W}\bigg|_{x,r_i} + \cos \Theta_i \frac{\partial V_i}{\partial P_W}\bigg|_{x,r_i} \quad \text{(A-120)}$$

From the Bernoulli equation,

$$\frac{\partial V_i}{\partial P_W}\bigg|_{x,r_i} = \frac{d V_i}{d P_W} = -\frac{1}{\rho_i V_i} \quad \text{(A-120a)}$$

The derivative $\partial \Theta_i / \partial P_W\big|_{x,r_i}$ is given by

$$\frac{\partial \Theta_i}{\partial P_W}\bigg|_{x,r_i} = -\frac{\sqrt{M_i^2 - 1}}{\rho_i V_i^2} \quad \text{(A-120b)}$$

The results of eqs. (A-118) — (A-120) allow the solution of eqs. (A-114) — (A-116) for the necessary derivatives.

4. Mixing Zone Temperature

The mixing zone temperature is assumed to be given by eq. (A-42). To be correct, the kinetic energy should be represented by V^2 rather than u^2; therefore, use of eq. (A-42) implies that the flow angles in the mixing zone are not large, i.e., $\cos \Theta \approx 1$. As discussed in Section X, the system of differential-integral equations was derived on the basis that $\cos \theta \approx 1$; therefore, use of eq. (A-42) does not further limit the validity of the 2-D Core Theory.

All of the derivatives of the temperature are the same as in Appendix I, with the following exception:

$$\frac{\partial T}{\partial x} = -\frac{u}{c_P} \frac{\partial \bar{u}}{\partial x} \quad \text{(A-121)}$$

5. Mixing Zone Shear Stress

The shear stress, τ_m, is given by

$$\tau_m = \frac{\pi}{2} k_I \rho_m (u_a - u_i)|(u_a - u_i)| \qquad \text{(A-122)}$$

where ρ_m is evaluated at u_m, and

$$u_m = \frac{1}{2}(u_i + u_a) \qquad \text{(A-123)}$$

APPENDIX III
INPUT AND PRINTOUT PARAMETERS FOR COMPUTER PROGRAMS

This appendix lists the parameters which must be prescribed for operation of both the 1-D Core Theory and 2-D Core Theory computer programs. The flow field variables which are printed out are also listed.

1. 1-D Core Theory Program

Input parameters — The following parameters must be prescribed:

1. Incompressible mixing zone constants, k_{oI}, k_{oII}, and k_{oIII}.

2. Integration step size, Δx, and maximum x (L).

3. Primary nozzle radius, r_n.

4. Initial static pressure, p_{w1}.

5. Constants in duct wall equation, $C_1 - C_7$, x_e.

6. Inviscid stream stagnation conditions, p_{oa}, p_{oj}, T_{oa}, T_{oj}.

7. Inviscid stream gas properties, c_{pa}, c_{pj}, R_a, R_j.

8. Mixing zone property functions: $T_o(\overline{C})$, $c_p(\overline{C})$, $R(\overline{C})$ (an array of 20 values from $\overline{C} = 0$ to $\overline{C} = 1$).

Printout parameters — The following parameters are printed out at each axial station in the first regime computation:

1. Wall pressure, p_w.

2. Secondary stream Mach number, M_a.

3. Primary stream Mach number, M_j.

4. Width of mixing zone, b.

5. Radius of inner mixing zone boundary, r_i.

6. Mixing zone growth rate, db/dx.

7. Total stream thrust.

8. $(r_i + b)/r_w$.

9. Species conservation parameter, Q.

10. Coefficient determinant, $|D|$.

The following parameters are printed out at each axial station in the second regime computation:

1. Wall pressure, p_w.

2. Secondary stream Mach number, M_a.

3. Width of mixing zone, b.

4. Growth rate of mixing zone, db/dx.

5. Centerline velocity ratio, u_c/u_j.

6. Centerline composition, $\overline{C}_c$.

7. b/r_w.

8. Total stream thrust.

9. Species conservation parameter, Q.

10. Coefficient determinant, $|D|$.

11. Choking parameter, Ch.

The following parameters are printed out at each axial station in the third regime computation:

1. Wall pressure, p_w.

2. Centerline velocity ratio, u_c/u_j.

3. Centerline composition, $\overline{C}_c$.

4. Wall velocity ratio, u_w/u_a.

5. Wall composition, $\overline{C}_w$.

6. Centerline Mach number, M_c.

7. Wall Mach number, M_w.

8. Total stream thrust.

9. Species conservation parameter, Q.

10. Coefficient determinant, $|D|$.

11. Choking parameter, Ch.

2. 2-D Core Theory Program

Input parameters — The input parameters are the same as for the 1-D Core Theory program, with the addition that the flow conditions across the primary nozzle exit plane must be prescribed. An array (typically 11 points) of $(p/p_{oj}, \theta)$ vs. r is used (for $0 \leq r \leq r_n$).

Printout parameters — The following parameters are printed out at each axial station in the first regime computation:

1. Wall pressure, p_w.

2. Secondary stream Mach number, M_a.

3. Mach number at inner boundary of mixing zone, M_i.

4. Width of mixing zone, b.

5. Radius of inner mixing zone boundary, r_i.

6. Mixing zone growth rate, db/dx.

7. Total stream thrust.

8. $(r_i + b)/r_w$.

9. Species conservation parameter, Q.

10. Coefficient determinant, $|D|$.

11. Flow angle at inner mixing zone boundary, θ_i.

One also has the option of printing out a radial array of $(p/p_{oj}, \theta)$ across the inviscid core flow.

The printout parameters in the second and third mixing regimes are the same as for the 1-D Core Theory program.

DOCUMENT CONTROL DATA - R & D		
(Security classification of title, body of abstract and indexing annotation must be entered when the overall report is classified)		

1. ORIGINATING ACTIVITY *(Corporate author)*	2a. REPORT SECURITY CLASSIFICATION
Arnold Engineering Development Center ARO, Inc., Operating Contractor Arnold Air Force Station, Tennessee	UNCLASSIFIED
	2b. GROUP N/A

3. REPORT TITLE

TURBULENT MIXING AND BURNING OF COAXIAL STREAMS INSIDE A
DUCT OF ARBITRARY SHAPE

4. DESCRIPTIVE NOTES *(Type of report and inclusive dates)*
Final Report

5. AUTHOR(S) *(First name, middle initial, last name)*

C. E. Peters, ARO, Inc.

6. REPORT DATE	7a. TOTAL NO. OF PAGES	7b. NO. OF REFS
January 1969	202	47

8a. CONTRACT OR GRANT NO	9a. ORIGINATOR'S REPORT NUMBER(S)
F40600-69-C-0001 b. PROJECT NO 6952	AEDC-TR-68-270
c. Program Element Nos. 65402234 and 6144501F	9b. OTHER REPORT NO(S) *(Any other numbers that may be assigned this report)*
d Task 695202	N/A

10. DISTRIBUTION STATEMENT

This document has been approved for public release and sale; its
distribution is unlimited.

11. SUPPLEMENTARY NOTES	12. SPONSORING MILITARY ACTIVITY
Available in DDC	Arnold Engineering Development Center, Air Force Systems Command, Arnold Air Force Station, Tennessee

13. ABSTRACT

A theoretical investigation of the ducted turbulent mixing of co-axial streams is presented. The effects of equilibrium chemical reactions in the mixing layer are included in the analysis. In Part I, the theory is developed for ducted mixing systems in which the inviscid portions of the flow are assumed to be one-dimensional. The integral method is used, and the mixing zone velocity profiles are assumed to be similar. Turbulent Prandtl and Lewis numbers are assumed to be unity, and the turbulent shear stress along one control surface in the mixing layer is computed by use of a semi-empirical model for the eddy viscosity. The theory is formulated to include the downstream regime where the mixing layer extends across the entire duct. The system of integral equations is transformed into a form suitable for numerical solution by standard methods. In Part II, the theory is extended to include the influence of a nonuniform supersonic inviscid core flow. A technique is developed for coupling the numerical solution of the inviscid core flow (from the method of characteristics) with the solution of the integral equations for the mixing layer. The theory is correlated with low speed experiments, with supersonic air-air ejector experiments and with experiments on ducted rocket-air mixing. The correlations show that the theory gives satisfactory results for the performance of ducted rocket-air mixing systems which are representative of air augmented rockets.

DD FORM 1473

14. KEY WORDS	LINK A		LINK B		LINK C	
	ROLE	WT	ROLE	WT	ROLE	WT
jet mixing flow						
ducts						
combustion						
turbulent flow						
chemical reactions						
theory						
jet pumps						
rockets						